Dynamic Model Construction and Optimization of Hanging Truss Structural System Having Shape Memory Alloy Wires

Zhang, Xuan

(Degree)
博士（工学）

(Date of Degree)
2018-03-25

(Date of Publication)
2019-03-01

(Resource Type)
doctoral thesis

(Report Number)
甲第7200号

(URL)
https://hdl.handle.net/20.500.14094/D1007200

博　士　論　文

Dynamic Model Construction and Optimization of Hanging Truss Structural System Having Shape Memory Alloy Wires

（形状記憶合金ワイヤを用いた吊下げトラス構造の数理モデルの構築と最適化）

平成30年1月

神戸大学大学院システム情報学研究科

張　鉉

Contents

Abstract

There are two viewpoints for reducing the influence of environmental vibration. One is the vibration isolation that aims to cut off the transmission of vibration motion to the target object in consideration. The other is the vibration suppression that aims to reduce or attenuate the vibration itself. The former is well demonstrated by a pendulum; its behavior is not immediately affected by horizontal vibration motion of its support due to inertia. The latter is a typical effect usually achieved by means of a damping device.

A truss structure in hanging configuration with an apparatus at the peripheral end of the truss is expected to possess the capability of vibration isolation resembles the behavior of pendulum. Owing to the gravitational force, stability of the truss structure in this type can be guaranteed in many situations.

Hanging truss structural system having SMA wires is able to attenuate the vibration energy exerted by the support ceiling due to the hysteretic loop of the SMA wires in relatively high temperature working conditions and is able to isolate the vibration from the support ceiling to the peripheral end due to the effect of pendulum.

In the case that the SMA wires are in compression or in small strain state, such kind of SMA wires can be replaceable to ordinary wires. In addition, characteristics of zero compressive stiffness of wire members contribute to variation of natural frequency of the truss structural system due to the variable stiffness behavior of the truss structural system itself.

This dissertation deals with the dynamic characteristics of a type of truss structural system having SMA wires in hanging configuration. The main contribution of this dissertation is composed of two parts. One is the development of the physical model for the dynamic problems. The numerical integration process in order to tackle the material and geometric nonlinear dynamic problem is introduced. Adequacy of the developed dynamic model is confirmed from the energy conservation point of view. On the basis of numerical calculation, vibration isolation and attenuation capabilities of this kind of structures are confirmed. The constitutive model of the SMA material considering the sub-loop behavior is developed. This model reflects the vibration attenuation capability better than the constitutive model without the sub-loop behavior. The other one is the construction of the optimization algorithms for obtaining the optimal place-

ments or sectional area of the SMA wires from the vibration isolation and attenuation points of view. The fact that the number and the placement of the SMA wires are significant factors on the effects of vibration isolation and attenuation has been attained. Besides, the optimization results of the placement and the sectional area show the same tendency of distribution of the SMA wires. In the case of the placement optimization, there are few SMA wires in the stages near the support ceiling or apparatus in the optimal configurations. The placements of SMA wires in optimal configurations show a tendency of decentralization in the case of emphasis on vibration isolation. In the case of sectional area optimization, the values of the sectional area of the SMA wires near the support ceiling or apparatus are extremely small in the optimal solutions.

Acknowlegements

I would like thank my supervisor, Professor Yukio Tada, for his kindness guidance, encouragement and support throughout the research. Without his advice and comments, this thesis would never be completed.

I also would like to express my special gratitude to Professor Kazuyuki Hanahara, because without his instructions and discussions, I could not complete the graduation task in such a smooth way.

I would like to thank Professor Toshiya Kaihara, Professor Zhiwei Luo and Professor Takateru Urakubo, for their valuable advice and suggestions in the recent review meetings.

I would like to thank all the members of the laboratory for providing a quiet and friendly environment to work in. Especially, I am grateful to my seniors and classmates for their help in the laboratory life and study materials in the past years. Without these, research work may not become so smooth.

Lastly, I am grateful to my families for their support and warm encouragement.

Chapter 1

Introduction

1.1. Background

There are a large number of studies on dealing with the environmental vibration. For example, in order to isolate the substructure beam from vibration, variable stiffness damped absorbers are used [1]. A damper with porous anisotropic outer ring and the compressed oily layer is put forward for the purpose of reducing the vibration impact [2].

There are two ways for reducing the influence of environmental vibration. One is the vibration isolation that aims to cut off the transmission of vibration motion to the target object in consideration. The other is the vibration suppression that aims to reduce or attenuate the vibration itself. Several studies on vibration isolation taking advantage of the behavior of the pendulum have been conducted in recent years. Seismic isolation systems using translational pendulum are free from influence of the weight of the structure they bear and functionally stable [3]. The results obtained by Sanap et al. show that the friction pendulum system works effectively in limiting the building responses during excitation due to earthquakes [4]. The multi-suspended pendulum isolation system developed by Narita et al. works well concerning vibration isolation [5]. By changing the design parameters of the pendulum type structures, the natural period of the structure can be large enough than the environmental excitation periods. Therefore, vibration isolation by such kind of structure can be expected. In the research of Fallah and Zamiri, the genetic algorithm is used to find the optimal values of the isolator [6]. A variable frequency pendulum isolator has been developed [7]. The effect of horizontal and vertical component of seismic load was studied by a kind of pendulum type structure [8].

Recently, SMA material has been researched in the area of structural engineering extensively due to the conspicuous characteristics of the shape memory effect and the pseudo-elasticity. Shape memory effect is the property that in the relatively low temperature environmental condition, this metallic alloy can experience large shape change, but it can return to the original

configuration upon the supply of heat. The characteristic of pseudo-elasticity demonstrates a hysteretic loop under a specific temperature condition, which can be altered by adjusting the constituents of the material in the process of manufacture. Thus, the percentage of the chemical element can be studied and determined on the basis of the working temperature of the SMA material. Therefore, pseudo-elasticity of SMA material attracts great attention for researches in the structural vibration control area. For the purpose of dealing with active vibration control, the shape memory effect plays an important role, and for the purpose of dealing with vibration isolation or passive vibration control, the pseudo-elasticity plays a significant role.

The first research on the application to seismic area using SMAs traces back to the work of Graesser and Cozzarelli [9]. The main achievement of their work is the influence of frequency and history on the energy dissipation characteristics of SMA wires. This result also tells us that the arrangement of different states of SMA materials in structures attains better performance. Except for the pseudo-elasticity and the shape memory effect, the family of SMA material also shows high-fatigue properties and the ability to provide hysteretic damping [10]. A suitable pseudo-elastic constitutive mathematical model is developed considering residual martensite strain effect and the behavior of the simulation result agrees with the experiment data. Omar [11] has compared nonlinear seismic performance of braced steel frames with two different bracing systems by means of nonlinear time history analyses, and examined the effectiveness of these two systems. Some research results according to experimental and theoretical studies have recently shown that SMA-based structures and devices are practically applicable [12-15].

There are a wealth of researches concerning passive vibration control using SMA material. For instance, in the case of dealing with environmental vibration attenuation by means of a structural system, the effect is not remarkably significant based only on the hysteretic characteristic of the SMA material. Combinations of the SMA material and viscoelastic material demonstrate noticeable result of vibration attenuation [16]. For the purpose of obtaining the maximum energy dissipation capability, the optimal configurations of the combination of SMA wires and energy-absorbing struts of the structures are attained [17]. A multi-linear hysteretic constitutive model of pseudo-elasticity of SMA incorporating residual martensite strain effect has been developed [18]. This model is implemented on a SDOF system and the comparison of the result of experiment and the numerical response has been made. Pseudo-elastic SMA dampers are effective in mitigating the structural response of building structures subjected to strong earthquakes [19]. The study of Fosdick and Ketema contributes to the understanding of the general macroscopic dynamic characteristics of SMA and its use in vibration damping [20]. In addition, there are many studies on energy dissipation by civil engineering structures having SMA materials [21-27].

However, the pseudo-elastic constitutive models of the above-mentioned studies have not considered the sub-loop behavior of the SMA material. Thus, the vibration energy can not be

attenuated totally by the SMA materials and such kind of constitutive models can not reflect the mechanical behaviors of pseudo-elastic SMA material suitably. Therefore, it is necessary to apply pseudo-elastic constitutive model considering the sub-loop behavior of SMA to the structure for reflecting the damping capability of this material better. Pseudo-elastic constitutive models considering the sub-loop behaviors have been developed in a number of studies. In the research of Müller, the fact that the hysteretic loop contains metastable states has been proposed. It tells us that both of the austenite phase and the martensite phase loose their (meta-)stability on a line defining phase equilibrium [28]. This phenomenon is shown by an experiment on an alloy of nickel and titanium also known as NiTi, namely, a kind of SMA material. In addition, with different constituents of the material or owing to other influence factors, there are maybe two trigger lines in the hysteretic loop [29]. On the basis of the work of Müller, some open problems concerning the states inside the hysteretic loop and the formation of interfaces are discussed [30]. The stress-strain-temperature hysteretic loops due to the incomplete transformation are analyzed from phenomenological point of view [31]. A nonlinear thermomechanical behavior of SMA by finite element method is presented [32]. This research is the same as the research of Müller, that is to say, there exists a trigger line in the major loop of the hysteretic loop of pseudo-elasticity. To consider the inner hysteretic loops of a stress-strain-temperature relationship, a shift and skip model is proposed [33]. A numerical investigation of the phenomenological description of the thermomechanical behavior of SMA is carried out. The model shows the capability describing the sub-loop behaviors. Comparisons between the numerical and experimental results show that they are in close agreement [34].

For the purpose of application, the process of optimization design is necessary and significant because the optimal results bring us excellent structural properties and material saving. In the research of Zhao and Wang, in order to deal with the two difficulties of time-dependent responses and sensitivity analysis for the dynamics, the authors proposed a method in which there is a one-parameter functional to approximate the extreme value of time-dependent response [35]. A FRP-bracing-based optimal seismic retrofit method for reinforced concrete frames with infill walls has been proposed [36]. In their study, a reinforced structure with the optimal solution shows improved results in terms of both strength and deformation capacity. In order to alleviate the calculation complexity of the optimization of large-scale structures having complicated mathematical models, an efficient approach has been proposed, which is suitable for linear and nonlinear response, static and dynamic response, direct and gradient optimization methods [37]. For the purpose of reducing the vibration while the variable geometry trusses moves a target payload from one point to another as a space manipulator, an optimization of motion plans has been studied [38]. A dynamic response topology optimization problem is dealt with in the time domain. In that research, authors refer that when the natural frequency of a structure is low, the dynamic characteristics (inertia effect) should be considered [39].

1.2. Motivation and Objective

In the current study, we deal with a truss structural system in hanging type that consists of rigid and wire members; part of the wire members are of SMA. The physical models [40] are adopted for the dynamics calculation. We discuss about the dynamic characteristics of the hanging truss structures. This type of truss structure becomes a mechanism in the case of less stiff members required to maintain the statical determinacy, due to the compressive force on wires and/or due to the removal of wires. However, owing to the influence of the gravitational force, stability of this mechanism can be guaranteed in many situations. Vibration isolation effect of the hanging truss is expected. The energy dissipation and performance of structures at the time of vibration of basement is highly dependent on the nonlinearity of elements [41]. The SMA material is applied to the hanging truss structure for the conspicuous pseudo-elastic characteristic for the purpose of attenuating the vibration energy. Thus, this hanging truss structural system have the capabilities of vibration isolation and attenuation.

We develop a mathematical model of the dynamic problem in consideration. For the purpose of dealing with the nonlinearities of this dynamic problem, a time integration method coupled with nonlinear iterative method is introduced. The effect of hanging configuration of the truss, as well as the effects of mechanical properties of SMA and ordinary wires are demonstrated respectively. We confirm the following characteristic benefits in dynamic behavior of the hanging truss: the vibration isolation capability taking advantage of the pendulum characteristic and the vibration attenuation ability due to hysteretic loop of the SMA wires. It should be noted in addition that the ordinary wires have constant tensile stiffness while the stiffness of SMA wires changes in accordance with their stress and histories of the routes of the corresponding constitutive models. Adequate combinations of these factors are expected to exhibit excellent vibration isolation and attenuation effects from the deformation point of view.

According to the above-mentioned contents, we have examined the vibration attenuation capability of SMA truss structural systems. However, subsequent to the motion of the support ceiling, the exerted energy is not attenuated thoroughly. Therefore, the utilized constitutive model dose not reflect the mechanical property of the pseudo-elastic SMA appropriately. For the purpose of dealing with the residual vibration, a piecewise linear pseudo-elastic constitutive model considering the sub-loop behavior is developed based on the theory of Müller [28]. On the basis of numerical calculation, we have confirmed that this model is able to deal with the residual vibration. The exerted energy by the support ceiling can be attenuated thoroughly due to the constitutive model of SMA considering the sub-loop behavior. From the result of phase plot of the dynamic behavior of the truss structural system having SMA wire members considering the sub-loop behavior, we understand that, subsequent to the motion of the support ceiling,

all of the energy exerted by the support ceiling has been attenuated and the truss structure gets back to its original configuration just as the behavior in the phase plot moves toward the center of the graph.

Optimization problems are conducted from three aspects: combination of truss unit having SMA wire members and truss unit without bracing wire members; combination of SMA wire and ordinary wire; sectional area of the SMA wire members.

In terms of the first case, placements of SMA wires in hanging truss are calculated from the viewpoints of vibration isolation and attenuation under the constraint condition of the number of the SMA wires. The evolutionary process of NSGA-based method which contains the elite preservation strategy is demonstrated [42]. In order to reduce the calculation time, a method coupled with the evolutionary optimal algorithm is proposed. The crossover operator and mutation operator due to the constraint condition of the number of the SMA wires are proposed. The relationships between the placements of the SMA wire members and the objective functions are discussed. The appropriateness of the proposed optimal calculation algorithm has been confirmed by the simulated examples.

In terms of the second case, we conduct the optimization problem that combines the SMA wire and ordinary wire members. Since the SMA wires in slack state or small strain state condition do not play a significant role in energy absorption, such SMA wires can be replaceable to ordinary wires from this point of view. On the basis of this consideration, we are able to suppress the number of SMA wires of the truss structure with due consideration to the effect of vibration isolation and absorption. In addition, the relatively high stiffness property of the ordinary wires contributes to the relative stability of the behaviors of the truss structural system from the deformation point of view. We combine the two kinds of wires with different mechanical properties in order to obtain the optimal solutions of configuration considering both of the effects of vibration isolation and attenuation in case of being evaluated in the light of displacement criterion.

In terms of the third case, the optimal problem concerning the sectional area of the SMA wire members is conducted. The trade-off relationship of sectional area of bracing SMA wire members exists. The hanging truss with thin SMA wires demonstrates more sufficient vibration isolation capability due to insufficient vibration transmission from the support ceiling to the peripheral end and energy consumption by the hysteretic loop of SMA wire members; however, vibration attenuation efficiency is low in such cases. The hanging truss with thick SMA wires demonstrates sufficient vibration attenuation capability and stability from the deformation point of view; however, vibration transmitted significantly from the support ceiling to the peripheral end. On the basis of this consideration, the optimal values of sectional area of SMA wires are obtained in order to improve the capabilities of vibration isolation and attenuation.

1.3. Organization of This Dissertation

This dissertation is composed of six chapters. Chapter 1 is the research background introduction. In Chapter 2, several pseudo-elastic constitutive models of the SMA material are reviewed or developed. The first one is a piecewise model developed from the viewpoint of linearization of evolutionary function [43]; the second one is a piecewise linear function developed based on the theory of a meta-stable characteristic of the austenite phase and martensite phase in the major hysteretic loop. The sub-loop behavior is considered in this model. The dynamic equation of motion of the hanging truss structural system having SMA wires is developed on the basis of finite element method. Numerical calculation process is constructed taking consideration of the material nonlinearity and geometric nonlinearity. Adequacy for this dynamic model is confirmed from the viewpoint of energy confirmation.

In Chapter 3, the dynamic behavior of hanging truss structural system having SMA wire members, ordinary wire members and rigid members are discussed. The typical influences on the dynamic behaviors of the SMA wire, the ordinary wire and the hanging configuration are demonstrated. The influences of the number of the truss units of the column-type hanging truss are displayed. Vibration isolation and attenuation capabilities of this kind of truss structure are confirmed from the displacement criterion. In addition, the dynamic behaviors of the hanging truss having the truss units with and without SMA wire members are discussed. The vibration isolation and vibration attenuation effects are demonstrated from the acceleration viewpoint.

In Chapter 4, the optimization problems are formulated and are solved by a multi-objective genetic algorithm from three aspects. The first one is the combination of the truss units with SMA wire members and truss units without SMA wire members. The second one is the combination of the SMA wire members and the ordinary wire members. The third one concerns the sectional area of the SMA wires. The optimal solutions of the hanging truss structures are obtained by a NSGA-based approach under the constraint condition of the number of the SMA wires in the former two problems; crossover and mutation operators in order to deal with the constraint condition of the number of the SMA wires are proposed. The non-dominated Pareto fronts are obtained in the case of different numbers of SMA wire members. On the basis of the calculation process, the fact that the number and the configuration of the SMA wire members are significant factors on the effects of vibration isolation and attenuation has been confirmed. The results of the first and the third optimization problems show a consistent distribution tendency of the SMA wires.

In Chapter 5, several other dynamic cases of the hanging truss structural system having SMA wires are discussed. Dynamic behaviors of hanging truss structural system in three dimension are calculated. The dynamic behavior of a three-dimension truss having SMA wire members

considering the sub-loop behavior is demonstrated. The differences of the two constitutive models on the influences of the dynamic characteristics are compared. The results manifest that the constitutive model considering the sub-loop reflects the attenuation capability more effectively. Dynamic behaviors of hanging truss structural system with topologies besides the column-type are displayed. Influence of the damping force has also been shown.

Chapter 6 closes the dissertation by presenting our main conclusions.

Chapter 2

Physical Model for the Dynamic Problem

2.1. Introduction

In this chapter, fundamental behaviors of SMA material are introduced. Several constitutive models are reviewed or developed. Dynamic equation of motion of the hanging truss structure having SMA wires are developed on the basis of finite element method. Numerical calculation process in order to deal with the material nonlinearity and the geometric nonlinearity of this kind of structural dynamic problems are constructed. The numerical integration algorithm is shown.

2.2. Introduction of SMA

Because the effects of rhombohedral phase transformation are negligible [44], we assume that SMA material has only two typical phases, namely, the austenite phase in high temperature condition and the martensite phase in low temperature condition. The phase transformation between these two phases is a solid-solid phase transformation and is different from most of the other metal alloys. This solid-solid phase transformation from one crystalline structure to the other does not occur by diffusion of atoms, but rather by shear lattice distortion [45]. Therefore, behaviors of SMA material assume the martensite fraction to depend on the current value of stress and temperature only, and do not incorporate any rate dependence [46]. Such a transformation is known as the martensitic transformation. It occurs instantaneously when a change in temperature causes a change in driving force.

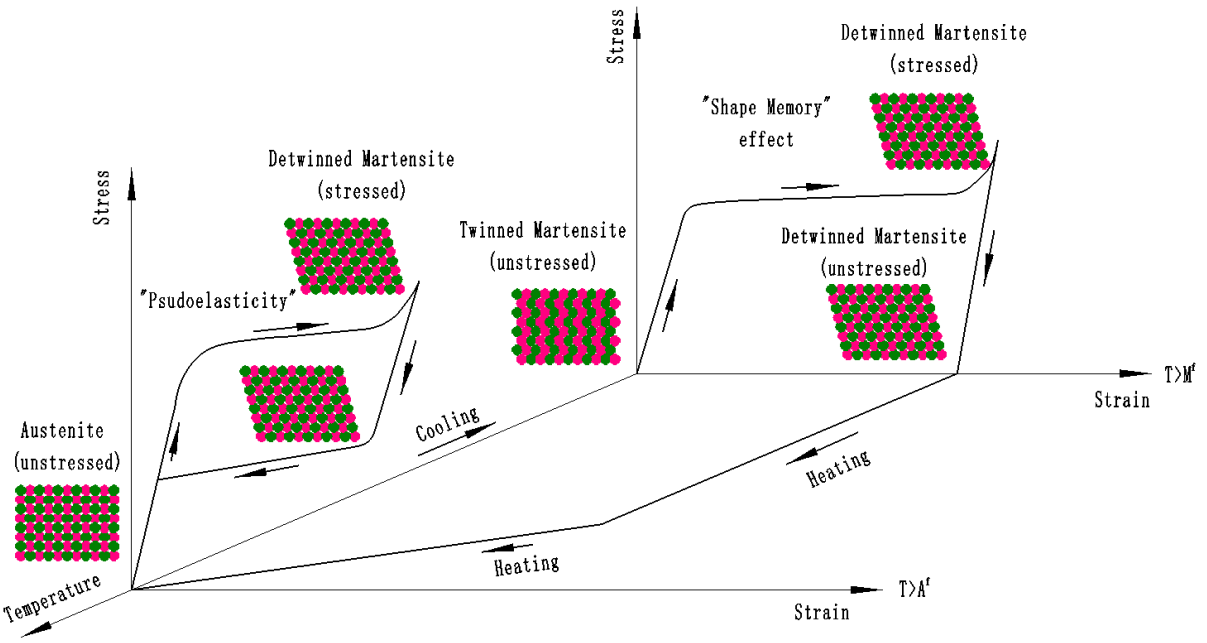

Figure 2.1: Characteristics of SMA

2.2.1 Fundamental Behaviors of SMA

In the relatively low temperature and stress-free condition, the martensite phase is called the twinned martensite, the crystal structure of which is an orthorhombic structure. If apply a load to the material, when the stress reaches a critical value, the crystal structure begins to change from the orthorhombic structure to monoclinic structure, the form of which is called the detwinned martensite. This process is known as detwinning. If remove the load to stress-free condition, the residual strain is remained. On the supply of heat, the crystal structure is altered gradually from monoclinic structure to body-centered cubic structure, which is named as the austenite phase. Upon decreasing the temperature of the material, the crystal structure transforms from the body-centered cubic structure to the orthorhombic structure. This process is referred to as self-accommodating and the material gets back to its original configuration in the end. It seems that the material is able to remember its original shape. We term this transformation process as the shape memory effect. It should be noted that, in the process of supply of heat, the transformation could take place slowly earlier than the critical transformation start temperature and remain unfinished after the critical transformation finish temperature [47].

In the relatively high temperature condition, this material can experience large deformation on raising the stress and return to the original austenite phase on reducing the stress. This is the conspicuous behavior of pseudo-elasticity. Description of the characteristics of shape memory effect and pseudo-elasticity considering the crystalline structures are shown in Figure

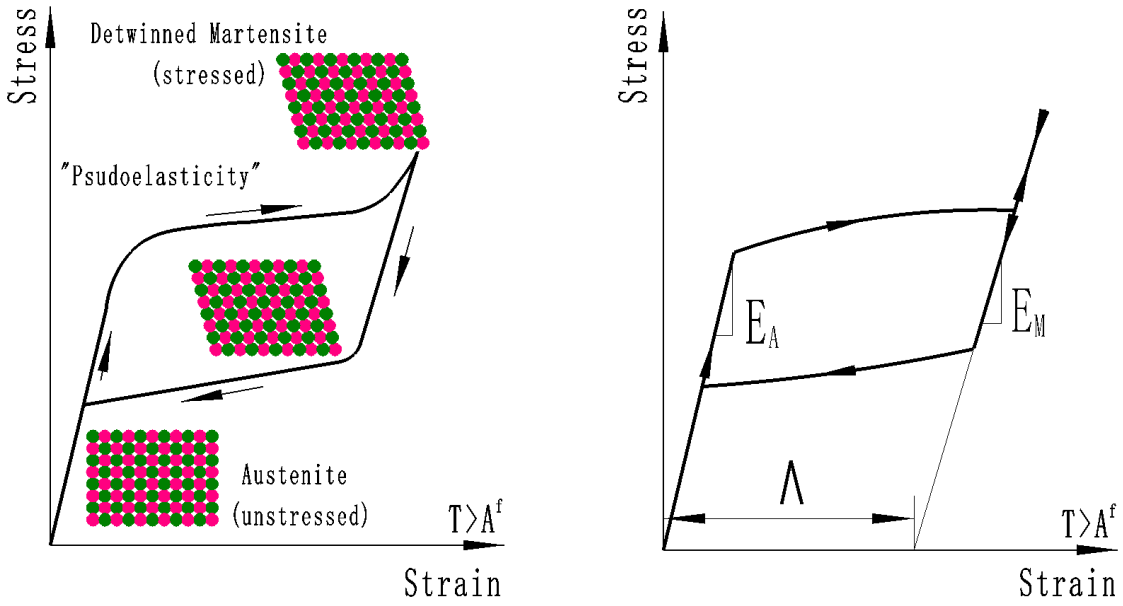

(a) Conceptual illustration (b) Introduced model

Figure 2.2: Pseudo-elasticity of SMA

2.1. In the following subsections, we introduce some piecewise constitutive models of the pseudo-elasticity. Even though nonlinear stress-strain relation and numerical integration can be used to get more accurate results, the piecewise model gives acceptable results for studying the strain energy absorption of SMA, since it captures the physical essence of energy absorption capability of SMA [48].

2.2.2 Piecewise Model of Pseudo-Elasticity

The pseudo-elasticity for the dynamic problems are introduced. The original mechanical characteristic in accordance with the experimental observation for the pseudo-elasticity is shown in Figure 2.2(a); however, it is difficult to perform numerical calculations in such a manner. The piecewise model as in Figure 2.2(b) is introduced for dynamic calculations. The fundamental constitutive model of SMA is on the basis of [43]. We modify the pseudo-elastic constitutive model for the purpose of dealing with the current dynamic problems. In addition, the Young's modulus changes with different martensitic volume fractions. Owing to the wire members of SMA, the uniaxial model is enough for predicting the mechanical behaviors of SMA [49]. Owing to the property of zero stiffness in compression of the wire members, the pseudo-elastic constitutive model with minus strain value is not taken into account.

The condition for phase transformation from the austenite phase to the martensite phase,

namely, the forward phase transformation is as follows:

$$\epsilon_s^{AM} < \epsilon < \epsilon_f^{AM} \text{ and } \dot{\epsilon} > 0$$

where parameter ϵ denotes the strain, parameter ϵ_s^{AM} is the martensite phase transformation start strain and ϵ_f^{AM} is the martensite phase transformation finish strain. The corresponding evolution function is:

$$\dot{\xi} = -(1-\xi)\frac{\dot{\sigma}}{\sigma - \sigma_f^{AM}} \tag{2.1}$$

where parameter ξ is the martensitic volume fraction and σ is the stress. The condition for the transformation from martensite phase to austenite phase, namely, the reverse phase transformation is as follows:

$$\epsilon_f^{MA} < \epsilon < \epsilon_s^{MA} \text{ and } \dot{\epsilon} < 0$$

where parameter ϵ_s^{MA} is the reverse phase transformation start strain and ϵ_f^{MA} is the reverse phase transformation finish strain. The corresponding evolution function is:

$$\dot{\xi} = \xi\frac{\dot{\sigma}}{\sigma - \sigma_f^{MA}} \tag{2.2}$$

Experiments indicate that the phase transformation strain is directly proportional to ξ, that is, $\epsilon^t = \Lambda\xi$, where parameter Λ is a constant value called the maximum phase transformation strain [50]. Total strain ϵ can be decomposed as the elastic strain ϵ^e and the phase transformation strain ϵ^t in the following form:

$$\epsilon = \epsilon^e + \epsilon^t = \epsilon^e + \Lambda\xi \tag{2.3}$$

The constitutive relation between the stress and the elastic strain is:

$$\sigma = E\epsilon^e \tag{2.4}$$

with a Young's modulus E attained by the interpolation of Young's moduli at pure austenite phase E_A and martensite phase E_M [51] as:

$$E = \frac{E_M E_A}{\xi(E_A - E_M) + E_M} \tag{2.5}$$

The time-continuous Equations 2.1 and 2.2 are linearized and written as the corresponding incremental equations as:

$$(1-\xi_t)\Delta\sigma + \Delta\xi(\sigma_t - \sigma_f^{AM}) = 0 \tag{2.6}$$

$$-\xi_t\Delta\sigma + \Delta\xi(\sigma_t - \sigma_f^{MA}) = 0 \tag{2.7}$$

In the above equations, the subscripts t denotes the time point. The next time point is $t + \Delta t$. Parameter Δ means the corresponding incrementation values from t to $t + \Delta t$. $\Delta\xi$ is obtained from:

$$\Delta\xi = \int_t^{t+\Delta t} \dot{\xi}\mathrm{d}t = \xi(t+\Delta t) - \xi(t) \tag{2.8}$$

The linearized constitutive relation is attained from Equation 2.4 as:

$$\Delta\sigma = E(\Delta\epsilon - \Lambda\Delta\xi) \tag{2.9}$$

Assuming the linear relationship between the incrementation of martensite volume fraction and the incrementation of the total strain, we have the following equation:

$$\Delta\xi = H\Delta\epsilon \tag{2.10}$$

with a proportion coefficient H. On the basis of this assumption, the incrementation of the constitutive equation becomes:

$$\Delta\sigma = \hat{E}\Delta\epsilon, \quad \hat{E} = E(1 - H\Lambda) \tag{2.11}$$

We can see that at the stages of phase transformation, the tangent elastic coefficient $\hat{E}$ changes with the martensitic phase volume fraction. Substituting Equation 2.11 into Equations 2.6 and 2.7 respectively, the proportion coefficient H at $t + \Delta t$ can be given as:

$$H = H^{AM}_{t+\Delta t} = \frac{E(\xi_t - 1)}{\sigma_t - \sigma^{AM}_f + E\Lambda(\xi_t - 1)} \tag{2.12}$$

$$H = H^{MA}_{t+\Delta t} = \frac{E\xi_t}{\sigma_t - \sigma^{MA}_f + \xi_t E\Lambda} \tag{2.13}$$

By substituting Equation 2.4 into Equations 2.6 and 2.7 respectively, the martensitic volume fraction at $t + \Delta t$ can be calculated during the deformation time history as the following equations:

$$\xi = \xi^{AM}_{t+\Delta t} = \frac{E\epsilon_{t+\Delta t} - \sigma_t - \xi_t E\epsilon_{t+\Delta t} + \xi_t\sigma^{AM}_f}{E\Lambda - E\Lambda\xi_t - \sigma_t + \sigma^{AM}_f} \tag{2.14}$$

$$\xi = \xi^{MA}_{t+\Delta t} = \frac{\xi_t E\epsilon_{t+\Delta t} - \xi_t\sigma^{MA}_f}{-\sigma^{MA}_f + \xi_t E\Lambda + \sigma_t} \tag{2.15}$$

For the purpose of dealing with dynamic problems using the introduced pseudo-elastic constitutive model, the algorithms are shown in the following tables. This model is considered as a stain-driven type. That is to say, before determining the internal variables in the time history of deformation, the strain value should be given in the current state of the material.

Table 2.1: Algorithm for overall strain-driven solution

1. Detect loading or unloading
If $\epsilon_{t+\Delta t} - \epsilon_t > 0 \Rightarrow$ Loading
If $\epsilon_{t+\Delta t} - \epsilon_t < 0 \Rightarrow$ Unloading
2. Check phase transformations
If loading then check A $\rightarrow$ M phase transformation (Table 2.2)
else if unloading then check M $\rightarrow$ A phase transformation (Table 2.3)
end if

Table 2.2: Algorithm for forward phase transformation

Determine the range of the strain in the major loop

(1). $0 < \epsilon_{t+\Delta t} < \epsilon_s^{AM}$

$$\xi_{t+\Delta t} = \xi_{min}$$

$$E_{t+\Delta t} = \frac{E_M E_A}{\xi_{min}(E_A - E_M) + E_M}$$

$$\sigma_{t+\Delta t} = \sigma_{min} + E_{t+\Delta t}(\epsilon_{t+\Delta t} - \epsilon_{min})$$

(2). $\epsilon_s^{AM} < \epsilon_{t+\Delta t} < \epsilon_f^{AM}$

Determine the range of strain in the inner loop

1). $\epsilon_{min} < \epsilon_{t+\Delta t} < \epsilon_{tp1}$

$$\xi_{t+\Delta t} = \xi_{min}$$

$$E_{t+\Delta t} = \frac{E_M E_A}{\xi_{min}(E_A - E_M) + E_M}$$

$$\sigma_{t+\Delta t} = \sigma_{min} + E_{t+\Delta t}(\epsilon_{t+\Delta t} - \epsilon_{min})$$

2). $\epsilon_{tp1} < \epsilon_{t+\Delta t} < \epsilon_f^{AM}$

$$H_{t+\Delta t}^{AM} = \frac{E_t(\xi_t - 1)}{\sigma_t - \sigma_f^{AM} + E_t\Lambda(\xi_t - 1)}$$

$$\xi_{t+\Delta t}^{AM} = \frac{E_t\epsilon_{t+\Delta t} - \sigma_t - \xi_t E_t\epsilon_{t+\Delta t} + \xi_t\sigma_f^{AM}}{E_t\Lambda - E_t\Lambda\xi_t - \sigma_t + \sigma_f^{AM}}$$

$$E_{t+\Delta t} = \frac{E_M E_A}{\xi_{t+\Delta t}(E_A - E_M) + E_M}$$

$$\sigma_{t+\Delta t} = E_{t+\Delta t}(1 - H_{t+\Delta t}\Lambda)(\epsilon_{t+\Delta t} - \epsilon_t) + \sigma_t$$

(3). $\epsilon_f^{AM} < \epsilon_{t+\Delta t}$

$$\xi_{t+\Delta t} = 1$$

$$\sigma_{t+\Delta t} = \sigma_f^{AM} + E_M(\epsilon_{t+\Delta t} - \epsilon_f^{AM})$$

Table 2.3: Algorithm for reverse phase transformation

Determine the range of the strain

(1). $\epsilon_{tp3} < \epsilon_{t+\Delta t} < \epsilon_{max}$

$$\xi_{t+\Delta t} = \xi_{max}$$

$$E_{t+\Delta t} = \frac{E_M E_A}{\xi_{max}(E_A - E_M) + E_M}$$

$$\sigma_{t+\Delta t} = \sigma_{max} + E_{t+\Delta t}(\epsilon_{t+\Delta t} - \epsilon_{max})$$

(2). $\epsilon_f^{MA} < \epsilon_{t+\Delta t} < \epsilon_{tp3}$

$$H_{t+\Delta t}^{MA} = \frac{E_t \xi_t}{\sigma_t - \sigma_f^{MA} + \xi_t E_t \Lambda}$$

$$\xi_{t+\Delta t}^{MA} = \frac{\xi_t E_t \epsilon_{t+\Delta t} - \xi_t \sigma_f^{MA}}{-\sigma_f^{MA} + \xi_t E_t \Lambda + \sigma_t}$$

$$E_{t+\Delta t} = \frac{E_M E_A}{\xi_{t+\Delta t}(E_A - E_M) + E_M}$$

$$\sigma_{t+\Delta t} = E_{t+\Delta t}(1 - H_{t+\Delta t}\Lambda)(\epsilon_{t+\Delta t} - \epsilon_t) + \sigma_t$$

(3). $\epsilon_{max} < \epsilon_{t+\Delta t}$

$$\xi_{t+\Delta t} = 1$$

$$\sigma_{t+\Delta t} = \sigma_f^{MA} + E_M(\epsilon_{t+\Delta t} - \epsilon_f^{MA})$$

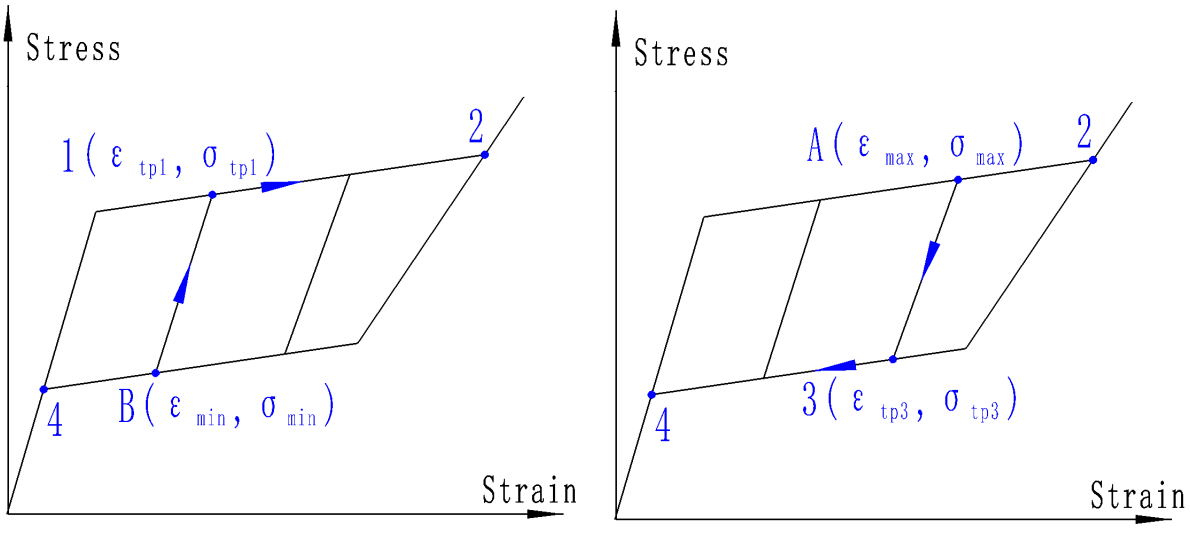

(a) Strain increase (b) Strain decrease

Figure 2.3: Inner loop explanation

The unknown parameters in the Tables 2.1-2.3 are denoted in Figure 2.3 and explained in the following two paragraphs.

The point B in Figure 2.3(a) is the point with the minimum strain value in the former process of strain decrease. The martensitic volume fraction at this point is ξ_{min}. From point B to point 1, there is no phase transformation and the relationship between the stress and the strain is linear elastic. If the strain is larger than ϵ_{tp1}, the relationship between the stress and the strain steps into the forward phase transformation in the major loop.

The point A in Figure 2.3(b) is the point with the maximum strain value in the former process of strain increase. The martensitic volume fraction at this point is ξ_{max}. From point A to point 3, there is no phase transformation and the relationship between the stress and the strain is linear elastic. If the strain becomes smaller than ϵ_{tp3}, the relationship between the stress and the strain steps into the reverse phase transformation in the major loop.

2.2.3 Pseudo-Elasticity Considering Sub-Loop Behavior

The constitutive model of the SMA material considering the sub-loop behavior is developed. The diagonals in all the four schematic figures in Figure 2.4 are called the trigger line. In the case that the stress-strain relation inside the major loop encounters the trigger line, moving direction will change from the inner elastic process to the inner phase transformation process according to the theory of [28]. There are four situations considering the variation history of strain and the positional relations between the start point inside the major loop and the trigger line.

Situation 1 in Case of Strain Increase

In Figure 2.4(a), turning point is denoted as $(\epsilon_{min}, \sigma_{min})$, where $'min'$ means the minimum value of the stress in the previous decreasing process. Utilizing line 1 and the trigger line in Figure 2.4(a), coordinate of the point (ϵ_T, σ_T) on the trigger line is determined. The slope of line 1 is the interpolation of the Young's moduli at the pure austenite phase E_A and the pure martensite phase E_M as:

$$k_1 = \frac{E_M E_A}{\frac{\epsilon^t_{min}}{\Lambda}(E_A - E_M) + E_M} \tag{2.16}$$

where parameter ϵ^t_{min} is the phase transformation strain at the turning point. The slope of line 2 is the interpolation of the slopes of the forward phase transformation stage k_f and the reverse phase transformation stage k_r in the major loop. The slope of line 2 is determined as:

$$k_2 = k_f + \frac{d_1}{d_0}(k_r - k_f) \tag{2.17}$$

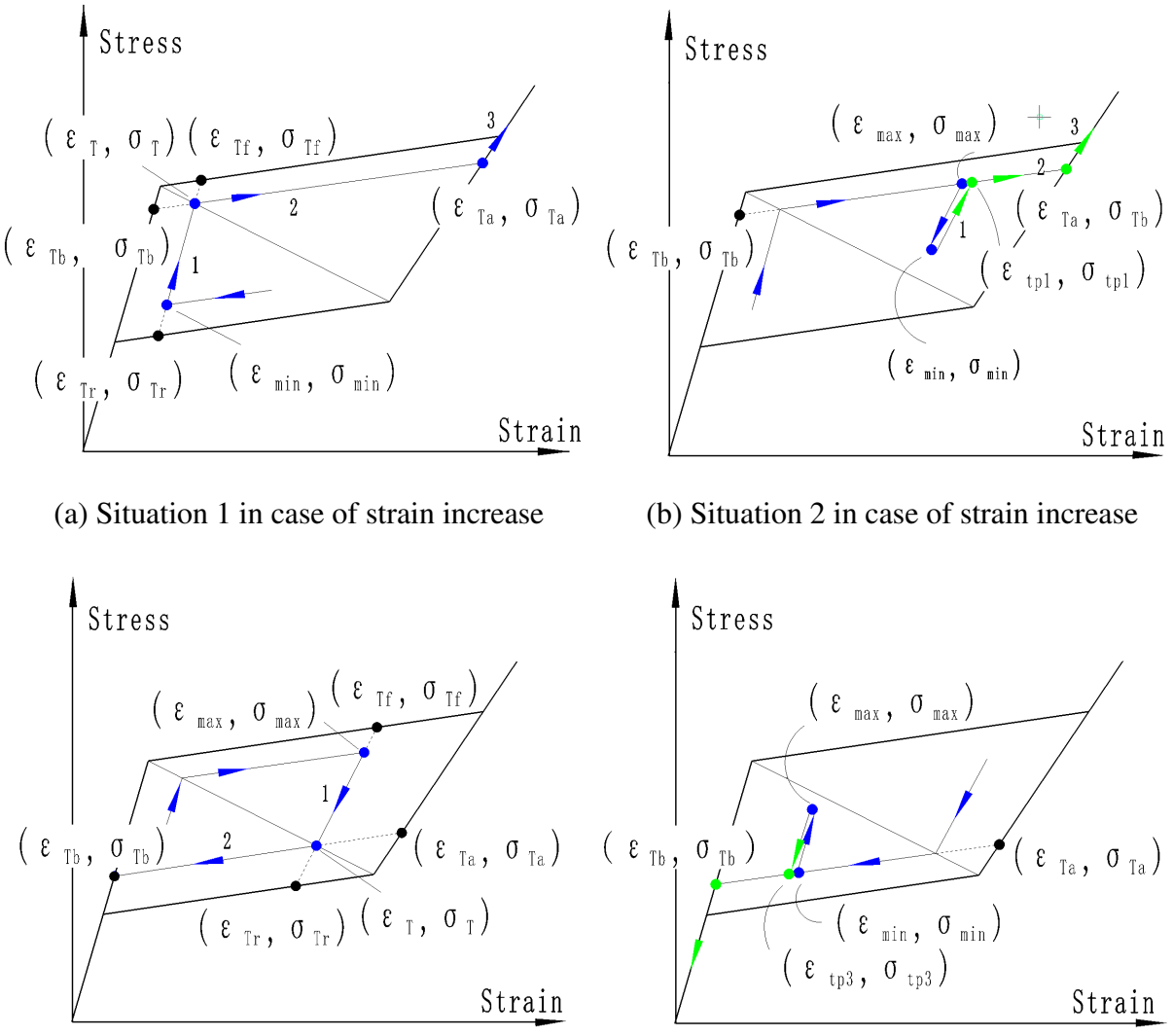

(a) Situation 1 in case of strain increase

(b) Situation 2 in case of strain increase

(c) Situation 1 in case of strain decrease

(d) Situation 2 in case of strain decrease

Figure 2.4: Pseudo-elasticity of SMA with sub-loop behavior

where parameter d_0 is the distance between the points of $(\epsilon_{Tf}, \sigma_{Tf})$ and $(\epsilon_{Tr}, \sigma_{Tr})$; parameter d_1 is the distance between the points of $(\epsilon_{Tf}, \sigma_{Tf})$ and (ϵ_T, σ_T). Coordinates of points $(\epsilon_{Ta}, \sigma_{Ta})$ and $(\epsilon_{Tb}, \sigma_{Tb})$ are easily determined as shown in Figure 2.4(a). Phase transformation strain along the line 2 can be calculated as [52]:

$$\epsilon^t = \Lambda \frac{\epsilon - \epsilon_{Tb}}{\epsilon_{Ta} - \epsilon_{Tb}} \tag{2.18}$$

Situation 2 in Case of Strain Increase

In Figure 2.4(b), point $(\epsilon_{max}, \sigma_{max})$ is the maximum stress value point in the previous increasing process and point $(\epsilon_{min}, \sigma_{min})$ is the minimum stress point in the previous decreasing process. Utilizing line 1 and line 2 to determine the coordinate of point $(\epsilon_{tp1}, \sigma_{tp1})$. In the case that the strain value becomes larger than ϵ_{tp1}, the behavior steps into line 2. In fact, points $(\epsilon_{max}, \sigma_{max})$ and $(\epsilon_{tp1}, \sigma_{tp1})$ are the same; however, owing to the different route histories between these two points, different symbols are used. The slopes of line 1 and line 2 in Figure 2.4(b) are easily determined as the former equations.

Situation 1 in Case of Strain Decrease

In Figure 2.4(c), the strain decreases from the point $(\epsilon_{max}, \sigma_{max})$. By using the line 1 in Figure 2.4(c) and the trigger line, coordinate of the point (ϵ_T, σ_T) is attained. Resembles the method in the former contents, coordinates of the other points are easily determined. Slope of line 1 is determined as:

$$k_1 = \frac{E_M E_A}{\frac{\epsilon^t_{max}}{\Lambda}(E_A - E_M) + E_M} \tag{2.19}$$

where parameter ϵ^t_{max} is the phase transformation strain value at the point $(\epsilon_{max}, \sigma_{max})$. Slope of line 2 in Figure 2.4(c) is calculated as the former contents. Phase transformation strain along the line 2 in this figure is obtained as:

$$\epsilon^t = \Lambda - \Lambda \frac{\epsilon_{Ta} - \epsilon}{\epsilon_{Ta} - \epsilon_{Tb}} \tag{2.20}$$

Situation 2 in Case of Strain Decrease

This case is shown as in Figure 2.4(d). Behaviors and the fundamental formulations are the same as the above-mentioned approaches.

2.2.4 Review of a Cosine Model of SMA

The early work conducted by Tanaka [53] assumes that the harding function in the process of phase transformation are exponential curves. Afterwards, modification are performed by Liang and Rogers [49]. In the modified model, the exponential curves are replaced by cosine functions and the modified model suits the experiment observation well.

On the basis of the theory of thermal-mechanics, the stress is the function of strain, temperature and the martensite phase volume fraction. The rate form of the constitutive equation

derived by Tanaka [53] is expressed as:

$$\dot{\sigma} = \frac{\partial \sigma}{\partial \epsilon}\dot{\epsilon} + \frac{\partial \sigma}{\partial T}\dot{T} + \frac{\partial \sigma}{\partial \xi}\dot{\xi} = E\dot{\epsilon} + \Theta\dot{T} + \Omega\dot{\xi} \tag{2.21}$$

where parameter E is the Young's modulus (In this model, $E = E_A = E_M$), Θ is the thermoelastic tensor and Ω is the phase transformation tensor. The following constitutive equation is derived by integrating the above equation with time:

$$\sigma - \sigma_0 = E(\epsilon - \epsilon_0) + \Theta(T - T_0) + \Omega(\xi - \xi_0) \tag{2.22}$$

where the parameters σ_0, ϵ_0, T_0 and ξ_0 are the corresponding initial variables. Martensite volume fraction in the reverse phase transformation ($M \rightarrow A$) and the forward phase transformation ($A \rightarrow M$) processes are as follows:

$$\xi = \begin{cases} \dfrac{\xi_M}{2}\{\cos[a_A(T - A_s) + b_A\sigma] + 1\} & (M \rightarrow A) \\ \dfrac{1 - \xi_A}{2}\cos[a_M(T - M_f) + b_M\sigma] + \dfrac{1 + \xi_A}{2} & (A \rightarrow M) \end{cases} \tag{2.23}$$

Constant parameters a_A and a_M are determined by the following equations:

$$a_A = \frac{\pi}{A_f - A_s}, \quad a_M = \frac{\pi}{M_s - M_f} \tag{2.24}$$

where M_s, M_f, A_s and A_f are martensite phase transformation start temperature, martensite phase transformation finish temperature, austenite phase transformation start temperature and austenite phase transformation finish temperature, respectively. ξ_A is the initial martensite volume fraction in the forward phase transformation process and ξ_M is the initial martensite volume fraction in the reverse phase transformation process. Material constants b_A and b_M are determined by the following equations:

$$b_A = -\frac{a_A}{C_A}, \quad b_M = -\frac{a_M}{C_M} \tag{2.25}$$

In the above equations, parameters C_A and C_M are obtained based on experimental identification.

The harding function is not explicit. Since the strain-driven type is considered, for a certain strain, iteration is necessary for the time consuming convergence in order to determine the corresponding stress value. In this research, Newton-Raphson iterative method is utilized for solving the implicit nonlinear equations in the phase transformation stages. It should be noted that, the selection of the initial stress values of the nonlinear iteration should be performed by trial and error because that convergence can not be attained by using inappropriate initial stress values. The initial stress values in forward phase transformation stage is different from the reverse phase transformation stage.

2.3. Dynamic Equation

The kinematic relations are formulated on the basis of the geometric relations of the truss structure having wire members [40]. The mass of the members are supposed to be distributed at the nodes of the members. The gravitational forces of the members are assumed to be acted on the nodes of the truss members. Energy definition of this kind of dynamic problems is conducted. Based on the energy formulations, the dynamic equation of motion of the hanging truss structural system having SMA wire members is derived according to the Hamilton Principle.

2.3.1 Geometric Relations

The kinematic relation of the hanging truss structural system having wire members is formulated according to the geometrical relationship. The length of the ith member l_i can be calculated based on the distance between the two connected nodes, $\alpha(i)$ and $\beta(i)$, of the member. For the two nodal positions vectors $\boldsymbol{p}_{\alpha(i)}$ and $\boldsymbol{p}_{\beta(i)}$, the geometrical relation is expressed as:

$$l_i = [(\boldsymbol{p}_{\alpha(i)} - \boldsymbol{p}_{\beta(i)})^T(\boldsymbol{p}_{\alpha(i)} - \boldsymbol{p}_{\beta(i)})]^{(1/2)} \tag{2.26}$$

Pick up all the truss members, the geometrical relation can be written in vector form as:

$$\boldsymbol{l} = \boldsymbol{l}(\boldsymbol{P}) \tag{2.27}$$

where $\boldsymbol{l} = [l_1, ..., l_M]^T$ is the total member lengths vector and $\boldsymbol{P} = [\boldsymbol{p}_1^T, ..., \boldsymbol{p}_N^T]^T$ is the total nodal positions vector. Perform total differential of the above equation, we can obtain the following equation:

$$\mathrm{d}\boldsymbol{l} = \frac{\partial \boldsymbol{l}}{\partial \boldsymbol{P}}\mathrm{d}\boldsymbol{P} \tag{2.28}$$

The Jacobian matrix is expressed as:

$$\boldsymbol{J} = \frac{\partial \boldsymbol{l}}{\partial \boldsymbol{P}} = \left[\frac{\partial l_i}{\partial \boldsymbol{p}_n}\right] \quad (i = 1, ..., M,\ n = 1, ..., N) \tag{2.29}$$

where

$$\frac{\partial l_i}{\partial \boldsymbol{p}_n} = \begin{cases} \dfrac{1}{l_i}(\boldsymbol{p}_{\alpha(i)} - \boldsymbol{p}_{\beta(i)})^T & (n = \alpha(i)) \\ \dfrac{1}{l_i}(\boldsymbol{p}_{\beta(i)} - \boldsymbol{p}_{\alpha(i)})^T & (n = \beta(i)) \\ 0 & \text{(other)} \end{cases} \tag{2.30}$$

2.3.2 Energy Definition

Taking the constitutive relations of the SMA wire members into consideration, the elastic strain of the ith member is expressed as:

$$\epsilon_i^e = \begin{cases} \epsilon_i & \text{Rigid or austenite SMA} \\ \epsilon_i - \epsilon_i^t & \text{Phase transformed SMA} \end{cases} \tag{2.31}$$

The elastic deformation of the ith member is:

$$R_i = \begin{cases} r_i & \text{Rigid or austenite SMA} \\ r_i - \rho_i \epsilon_i^t & \text{Phase transformed SMA} \end{cases} \tag{2.32}$$

where ρ_i is the natural length of member i. Elastic energy is defined as:

$$U = \frac{1}{2}(\boldsymbol{r} - \boldsymbol{\epsilon}^t\boldsymbol{\rho})^T \boldsymbol{K}_L(\boldsymbol{r} - \boldsymbol{\epsilon}^t\boldsymbol{\rho}) = \frac{1}{2}\boldsymbol{R}^T\boldsymbol{K}_L\boldsymbol{R} \tag{2.33}$$

where vector $\boldsymbol{r} = [r_1, ..., r_M]^T$ is the total deformation vector. Vector $\boldsymbol{\rho} = [\rho_1, ..., \rho_M]^T$ is the natural length vector. Matrix $\boldsymbol{K}_L = \text{diag}[E_1A_1/\rho_1, ..., E_MA_M/\rho_M]$ is a diagonal matrix contains the stiffness of all the truss members. Vector $\boldsymbol{R}$ is the elastic deformation of the members. Parameters E_i and A_i are the Young's modulus and the cross-sectional area of the ith member. Matrix $\boldsymbol{\epsilon}^t = \text{diag}[\epsilon_1^t, ..., \epsilon_M^t]$ and ϵ_i^t is expressed as:

$$\epsilon_i^t \begin{cases} = 0 & \text{Rigid or austenite SMA} \\ \neq 0 & \text{Phase transformed SMA} \end{cases} \tag{2.34}$$

The kinetic energy, the work done by the gravitational force and the work done by the support ceiling can be defined as:

$$\begin{aligned} Q &= \frac{1}{2}\dot{\boldsymbol{X}}^T\boldsymbol{M}\dot{\boldsymbol{X}} \\ P_1 &= \boldsymbol{G}^T\boldsymbol{X} \\ P_2 &= \boldsymbol{f}^T\boldsymbol{D}' \end{aligned} \tag{2.35}$$

where $\boldsymbol{M}$ is the mass matrix of the truss structural system and $\boldsymbol{G}$ is the gravitational force vector. $\boldsymbol{f}$ is the support ceiling force vector. As shown in Figure 2.5, $\boldsymbol{X}$ is the absolute displacement vector of the truss nodes and $\boldsymbol{D}'$ is the displacement of the truss nodes due to motion of the support ceiling. The relationship between $\boldsymbol{X}$ and $\boldsymbol{D}'$ is as follows:

$$\boldsymbol{X} = \boldsymbol{D} + \boldsymbol{D}' \quad \Rightarrow \quad \delta\boldsymbol{X} = \delta\boldsymbol{D} + \delta\boldsymbol{D}' \tag{2.36}$$

where $\boldsymbol{D}$ is the relative displacement of the truss nodes due to the deformation of members. Symbol $'\delta'$ means variation.

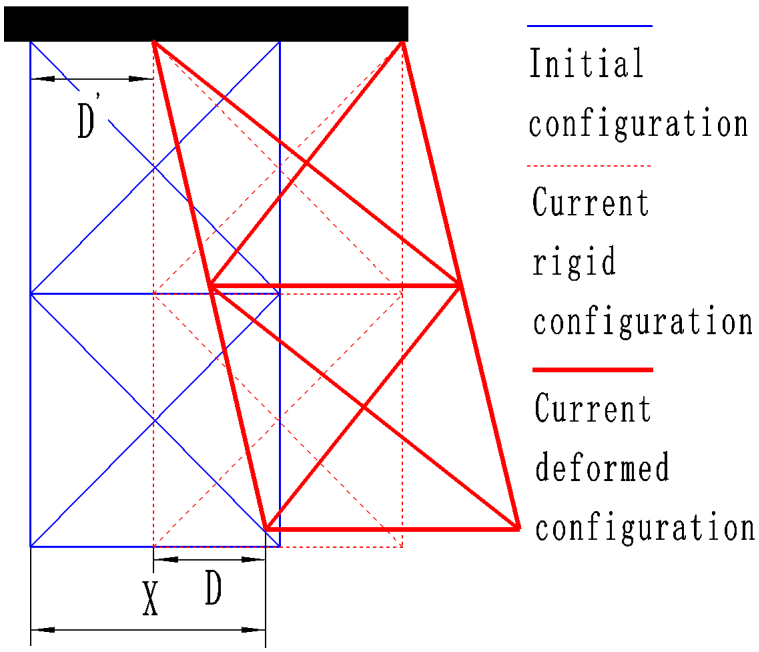

Figure 2.5: Relationship of the displacements

2.3.3 Derivation of Dynamic Equation

Equation of Hamilton Principle is expressed as:

$$\delta I = \delta \int_t^{t+\Delta t} (Q - U + P_1 + P_2)\mathrm{dt} = 0 \tag{2.37}$$

It should be noticed that t and $t + \Delta t$ are two specified time points. By substituting the energy terms, the following equation is obtained:

$$\delta I = \int_t^{t+\Delta t} (\dot{\boldsymbol{X}}^T \boldsymbol{M} \delta \dot{\boldsymbol{X}} - \boldsymbol{R}^T \boldsymbol{K}_L \delta \boldsymbol{R} + \boldsymbol{G}^T \delta \boldsymbol{X} + \boldsymbol{f}^T \delta \boldsymbol{D}')\mathrm{dt} = 0 \tag{2.38}$$

Elastic deformation vector is given as:

$$\boldsymbol{R}(\boldsymbol{D}) = \boldsymbol{r} - \boldsymbol{\epsilon}^t \boldsymbol{\rho} = \boldsymbol{l}(\boldsymbol{P}) - \boldsymbol{l}(\boldsymbol{O}) - \boldsymbol{\epsilon}^t \boldsymbol{\rho} \tag{2.39}$$

where vector $\boldsymbol{P} = \boldsymbol{D} + \boldsymbol{D}' + \boldsymbol{O}$ is the current coordinate vector of the truss nodes and vector $\boldsymbol{O}$ is the initial coordinate vector of the truss nodes. We can derive the following equations from Equation 2.39 as:

$$\delta \boldsymbol{R} = \frac{\partial \boldsymbol{l}}{\partial \boldsymbol{P}} \delta \boldsymbol{P}, \quad \frac{\partial \boldsymbol{R}}{\partial \boldsymbol{D}} = \frac{\partial \boldsymbol{l}}{\partial \boldsymbol{P}} = \boldsymbol{J} \tag{2.40}$$

Jacobian matrix $\boldsymbol{J}$ transforms the member values to the corresponding nodal values. Thus, we have $\boldsymbol{r} = \boldsymbol{J}\boldsymbol{D}$. The derivation of the first term in Equation 2.38 can be performed as:

$$\int_t^{t+\Delta t} (\dot{\boldsymbol{X}}^T \boldsymbol{M} \delta \dot{\boldsymbol{X}}) \mathrm{dt} = \dot{\boldsymbol{X}}^T \boldsymbol{M} \delta \boldsymbol{X} \Big|_t^{t+\Delta t} - \int_t^{t+\Delta t} (\ddot{\boldsymbol{X}}^T \boldsymbol{M} \delta \boldsymbol{X}) \mathrm{dt} \tag{2.41}$$

Paying attention to $\delta \boldsymbol{X}(t) = \delta \boldsymbol{X}(t + \Delta t) = 0$,

$$\int_t^{t+\Delta t} (\dot{\boldsymbol{X}}^T \boldsymbol{M} \delta \dot{\boldsymbol{X}}) \mathrm{dt} = - \int_t^{t+\Delta t} (\ddot{\boldsymbol{X}}^T \boldsymbol{M} \delta \boldsymbol{X}) \mathrm{dt} \tag{2.42}$$

The second term in Equation 2.38 is calculated as:

$$- \int_t^{t+\Delta t} (\boldsymbol{R}^T \boldsymbol{K}_L \delta \boldsymbol{R}) \mathrm{dt} = - \int_t^{t+\Delta t} [\boldsymbol{R}^T \boldsymbol{K}_L \frac{\partial \boldsymbol{R}(\boldsymbol{D})}{\partial \boldsymbol{D}} \delta \boldsymbol{D}] \mathrm{dt} \tag{2.43}$$

Substituting Equations 2.42, 2.43 into 2.38 obtains:

$$\begin{aligned} &\delta I = 0 \\ &= \int_t^{t+\Delta t} [-\ddot{\boldsymbol{X}}^T \boldsymbol{M} \delta \boldsymbol{D} - \boldsymbol{R}^T \boldsymbol{K}_L \frac{\partial \boldsymbol{R}(\boldsymbol{D})}{\partial \boldsymbol{D}} \delta \boldsymbol{D} + \boldsymbol{G}^T \delta \boldsymbol{D} + \boldsymbol{G}^T \delta \boldsymbol{D}' + \boldsymbol{f}^T \delta \boldsymbol{D}' - \ddot{\boldsymbol{X}}^T \boldsymbol{M} \delta \boldsymbol{D}'] \mathrm{dt} \end{aligned} \tag{2.44}$$

For arbitrary $\delta \boldsymbol{D}$ and $\delta \boldsymbol{D}'$, we can derive the dynamic equation of motion in the following form:

$$\boldsymbol{M} \ddot{\boldsymbol{X}} + (\frac{\partial \boldsymbol{R}}{\partial \boldsymbol{D}})^T \boldsymbol{K}_L \boldsymbol{R} = \boldsymbol{G} \tag{2.45}$$

By substituting Equations 2.39 and 2.40, we attain:

$$\boldsymbol{M} \ddot{\boldsymbol{X}} + (\frac{\partial \boldsymbol{l}}{\partial \boldsymbol{P}})^T \boldsymbol{K}_L (\boldsymbol{r} - \boldsymbol{\epsilon}^t \boldsymbol{\rho}) = \boldsymbol{G} \tag{2.46}$$

To arrange the above dynamic equation of motion in the conventional form, the final type of the equation is obtained.

$$\boldsymbol{M} \ddot{\boldsymbol{X}} + \boldsymbol{K} \boldsymbol{D} = \boldsymbol{G} + \boldsymbol{J}^T \boldsymbol{q} \tag{2.47}$$

where $\boldsymbol{K} = \boldsymbol{J}^T \boldsymbol{K}_L \boldsymbol{J}$, $\boldsymbol{q} = \boldsymbol{K}_L \boldsymbol{\epsilon}^t \boldsymbol{\rho}$.

Substituting $\ddot{\boldsymbol{X}} = \ddot{\boldsymbol{D}} + \ddot{\boldsymbol{D}}'$ into the above equation, the dynamic equation of motion is derived as:

$$\boldsymbol{M} \ddot{\boldsymbol{D}} + \boldsymbol{K} \boldsymbol{D} = -\boldsymbol{M} \ddot{\boldsymbol{D}}' + \boldsymbol{G} + \boldsymbol{J}^T \boldsymbol{q} \tag{2.48}$$

The hanging truss structure is assumed to be supported by the ceiling. The motion of the support ceiling nodes and the external force on the other nodes are assumed to be given. Nodal deformation displacement vector $\boldsymbol{D}$ can be represented as $\boldsymbol{D} = [\boldsymbol{D}_U^T, \ \boldsymbol{D}_C^T]^T$, where $\boldsymbol{D}_U$ and $\boldsymbol{D}_C$ correspond to the unconfined or confined nodal elements, respectively. On the basis of this representation, the above equation is rewritten as:

$$\boldsymbol{M}_{UU} \ddot{\boldsymbol{D}}_U + \boldsymbol{M}_{UC} \ddot{\boldsymbol{D}}_C + \boldsymbol{K}_{UU} \boldsymbol{D}_U + \boldsymbol{K}_{UC} \boldsymbol{D}_C = -\boldsymbol{M}_{UU} \ddot{\boldsymbol{D}}'_U - \boldsymbol{M}_{UC} \ddot{\boldsymbol{D}}'_C + \boldsymbol{J}_U^T \boldsymbol{q} + \boldsymbol{G}_U \tag{2.49}$$

$$\boldsymbol{M}_{CU}\ddot{\boldsymbol{D}}_U + \boldsymbol{M}_{CC}\ddot{\boldsymbol{D}}_C + \boldsymbol{K}_{CU}\boldsymbol{D}_U + \boldsymbol{K}_{CC}\boldsymbol{D}_C = -\boldsymbol{M}_{CU}\ddot{\boldsymbol{D}}'_U - \boldsymbol{M}_{CC}\ddot{\boldsymbol{D}}'_C + \boldsymbol{J}_C^T\boldsymbol{q} + \boldsymbol{G}_C \tag{2.50}$$

We pay attention to Equation 2.49 that deals with the motion of the free nodal elements. It should be noted that $\boldsymbol{D}_C = \boldsymbol{0}$, $\ddot{\boldsymbol{D}}_C = \boldsymbol{0}$; thus, the dynamic equation of motion reduces to:

$$\boldsymbol{M}_{UU}\ddot{\boldsymbol{D}}_U + \boldsymbol{K}_{UU}\boldsymbol{D}_U = -\boldsymbol{M}_{UU}\ddot{\boldsymbol{D}}'_U + \boldsymbol{G}_U + \boldsymbol{J}_U^T\boldsymbol{q} \tag{2.51}$$

For the purpose of simplification, we denote $\boldsymbol{F}_U = -\boldsymbol{M}_{UU}\ddot{\boldsymbol{D}}'_U + \boldsymbol{G}_U$. The dynamic equation becomes:

$$\boldsymbol{M}_{UU}\ddot{\boldsymbol{D}}_U + \boldsymbol{K}_{UU}\boldsymbol{D}_U = \boldsymbol{F}_U + \boldsymbol{J}_U^T\boldsymbol{q} \tag{2.52}$$

2.3.4 Natural Frequency

In the case that the stiffness matrix $\boldsymbol{K}_{UU}$ is nonsingular, modal analysis of the truss structural system is conducted by the following equation:

$$\boldsymbol{K}_{UU} - \omega_h^2\boldsymbol{M}_{UU} = \boldsymbol{0} \tag{2.53}$$

In the above equation, ω_h denotes the hth angular natural frequency of the truss structural system; the corresponding natural frequency is obtained as $f_h = \omega_h/2\pi$. Owing to the material nonlinearity of the SMA wire members and the geometric nonlinearity of the truss structural system itself, the stiffness matrix $\boldsymbol{K}_{UU}$ is time dependent and so do the natural frequencies. In this research, the first natural frequency f_1 is calculated and evaluated.

It should be noted that, when the unstable truss structure is in hanging configuration, the unstable truss becomes a stable structure; however, the modal analysis can not be performed. Only the natural frequencies of the static determinate or indeterminate truss structures can be determined.

2.4. Numerical Integration

In order to deal with the nonlinearity of this kind of dynamic problem, the nonlinear iterative method is introduced. The fundamental equations for the numerical integration are derived in the following subsections.

2.4.1 Newmark β Method Considering Nonlinear Iteration

In dynamic Equation 2.52, as the coordinate transformation matrix $\boldsymbol{J}_U$ contains the geometric nonlinear characteristic and the member force vector $\boldsymbol{q}$ depends on the nodal displacement as well as the nonlinear characteristics of SMA members, the nodal force vector $\boldsymbol{J}_U^T\boldsymbol{q}$ has to be

examined in accordance with the dynamics calculation. We introduce the following iterative approach to calculate the state at time $t + \Delta t$ based on the state at time t. The equation of motion to be satisfied at $t + \Delta t$ is approximated by using the stiffness matrix $\boldsymbol{K}_U^{(t)}$ and force vector $(\boldsymbol{J}_U^{(t)})^T \boldsymbol{q}^{(t)}$ at t as:

$$\boldsymbol{M}_{UU} \ddot{\boldsymbol{D}}_U^{(t+\Delta t)} + \boldsymbol{K}_{UU}^{(t)} \boldsymbol{D}_U^{(t+\Delta t)} = \boldsymbol{F}_U^{(t+\Delta t)} + (\boldsymbol{J}_U^{(t)})^T \boldsymbol{q}^{(t)} \tag{2.54}$$

On the basis of the Newmark β method, the nodal displacement $\boldsymbol{D}_U^{(t+\Delta t)}$ and its velocity $\dot{\boldsymbol{D}}_U^{(t+\Delta t)}$ at $t+\Delta t$ are represented in terms of the acceleration $\ddot{\boldsymbol{D}}_U^{(t+\Delta t)}$. By substituting these representations into Equation 2.54 and solving the obtained linear equation, $\ddot{\boldsymbol{D}}_U^{(t+\Delta t)}$ is calculated. Once $\ddot{\boldsymbol{D}}_U^{(t+\Delta t)}$ is known, $\boldsymbol{D}_U^{(t+\Delta t)}$ and $\dot{\boldsymbol{D}}_U^{(t+\Delta t)}$ are calculated based on the representations of the fundamental equations of the Newmark β method. The matrix and vector at $t + \Delta t$, $\boldsymbol{K}_{UU}^{(t+\Delta t)}$ and $(\boldsymbol{J}_U^{(t+\Delta t)})^T \boldsymbol{q}^{(t+\Delta t)}$ are accordingly updated based on $\boldsymbol{D}_U^{(t+\Delta t)}$. Force error vector due to the approximation at this moment can be evaluated as:

$$\boldsymbol{F}_{err}^{(t+\Delta t)} = \boldsymbol{F}_U^{(t+\Delta t)} + (\boldsymbol{J}_U^{(t+\Delta t)})^T \boldsymbol{q}^{(t+\Delta t)} - (\boldsymbol{M}_{UU} \ddot{\boldsymbol{D}}_U^{(t+\Delta t)} + \boldsymbol{K}_{UU}^{(t+\Delta t)} \boldsymbol{D}_U^{(t+\Delta t)}) \tag{2.55}$$

For the purpose of dealing with the nonlinearity of this kind of dynamic problem, it is necessary to update $\boldsymbol{D}_U^{(t+\Delta t)}$, $\boldsymbol{K}_{UU}^{(t+\Delta t)}$ and $(\boldsymbol{J}_U^{(t+\Delta t)})^T \boldsymbol{q}^{(t+\Delta t)}$ several times to suppress the force error vector by introducing the corresponding incremental vectors as follows:

$$\boldsymbol{M}_{UU}(\ddot{\boldsymbol{D}}_U^{(t+\Delta t)} + \mathrm{d}\ddot{\boldsymbol{D}}_U) + \boldsymbol{K}_{UU}^{(t+\Delta t)}(\boldsymbol{D}_U^{(t+\Delta t)} + \mathrm{d}\boldsymbol{D}_U) = \boldsymbol{F}_U^{(t+\Delta t)} + (\boldsymbol{J}_U^{(t+\Delta t)})^T(\boldsymbol{q}^{(t+\Delta t)} + \mathrm{d}\boldsymbol{q}) \tag{2.56}$$

Re-arranging the above equation by taking Equation 2.55 into consideration, we obtain the following equation:

$$\boldsymbol{M}_{UU}\mathrm{d}\ddot{\boldsymbol{D}}_U + \boldsymbol{K}_{UU}^{(t+\Delta t)}\mathrm{d}\boldsymbol{D}_U - (\boldsymbol{J}_U^{(t+\Delta t)})^T \mathrm{d}\boldsymbol{q} = \boldsymbol{F}_{err}^{(t+\Delta t)} \tag{2.57}$$

To denote the update time as μ, the fundamental equations of displacement of Newmark β method at update times μ and $\mu - 1$ can be written as follows respectively.

$$\begin{aligned} \boldsymbol{D}_U^{(t+\Delta t,\mu)} &= \boldsymbol{D}_U^{(t)} + \Delta t \dot{\boldsymbol{D}}_U^{(t)} + \Delta t^2[(\frac{1}{2} - \beta)\ddot{\boldsymbol{D}}_U^{(t)} + \beta \ddot{\boldsymbol{D}}_U^{(t+\Delta t,\mu)}] \\ \boldsymbol{D}_U^{(t+\Delta t,\mu-1)} &= \boldsymbol{D}_U^{(t)} + \Delta t \dot{\boldsymbol{D}}_U^{(t)} + \Delta t^2[(\frac{1}{2} - \beta)\ddot{\boldsymbol{D}}_U^{(t)} + \beta \ddot{\boldsymbol{D}}_U^{(t+\Delta t,\mu-1)}] \end{aligned} \tag{2.58}$$

According to the above two equations, the relationship between $\mathrm{d}\ddot{\boldsymbol{D}}_U$ and $\mathrm{d}\boldsymbol{D}_U$ can be derived as:

$$\mathrm{d}\ddot{\boldsymbol{D}}_U = \frac{1}{\beta \Delta t^2} \mathrm{d}\boldsymbol{D}_U \tag{2.59}$$

Different from the original Newmark β method, we choose the displacement as the primary variable. On the basis of Equation 2.59 and the linear relation in Equation 2.66 between the

correction in member force $\mathrm{d}\boldsymbol{q}$ and the correction in nodal displacement $\mathrm{d}\boldsymbol{D}_U$ that is to be described in 2.4.2, Equation 2.57 is rewritten as:

$$\left(\frac{1}{\beta\Delta t^2}\boldsymbol{M}_{UU} + \boldsymbol{K}_{UU}^{(t+\Delta t)} - (\boldsymbol{J}_U^{(t+\Delta t)})^T\boldsymbol{H}\right)\mathrm{d}\boldsymbol{D}_U = \boldsymbol{F}_{err}^{(t+\Delta t)} \tag{2.60}$$

Solving this equation, we obtain $\mathrm{d}\boldsymbol{D}_U$ and accordingly $\mathrm{d}\ddot{\boldsymbol{D}}_U$ and $\mathrm{d}\boldsymbol{q}$. The values corresponding to the equation of motion at time $t + \Delta t$ are then corrected based on the following relations:

$$\begin{aligned}
\boldsymbol{D}_U^{(t+\Delta t)} &\leftarrow \boldsymbol{D}_U^{(t+\Delta t)} + \mathrm{d}\boldsymbol{D}_U \\
\ddot{\boldsymbol{D}}_U^{(t+\Delta t)} &\leftarrow \ddot{\boldsymbol{D}}_U^{(t+\Delta t)} + \mathrm{d}\ddot{\boldsymbol{D}}_U \\
\boldsymbol{q}^{(t+\Delta t)} &\leftarrow \boldsymbol{q}^{(t+\Delta t)} + \mathrm{d}\boldsymbol{q}
\end{aligned} \tag{2.61}$$

On the basis of the updated displacement vector $\boldsymbol{D}_U^{(t+\Delta t)}$, the current system stiffness matrix $\boldsymbol{K}_{UU}^{(t+\Delta t)}$ is updated. The force error vector is updated accordingly, and the convergence condition is evaluated by means of the following criterion [55]:

$$\frac{\mathrm{d}\boldsymbol{D}_U^{(\mu)} \,.\, \boldsymbol{F}_{err}^{(t+\Delta t,\mu)}}{\mathrm{d}\boldsymbol{D}_U^{(1)} \,.\, \boldsymbol{F}_{err}^{(t+\Delta t,1)}} < \text{tolerance}$$

where the 'tolerance' is a extremely small value that is set in advance by trial and error for different nonlinear dynamic problems. The iterative process between the time steps t and $t + \Delta t$ continues until the above condition is satisfied.

2.4.2 Compatibility Condition

The relationship between $\mathrm{d}\boldsymbol{q}$ and $\mathrm{d}\boldsymbol{D}_U$ is developed in this subsection. On the basis of the constitutive equation of SMA, the component of the ith SMA member in vector $\mathrm{d}\boldsymbol{q}$ is denoted as $\mathrm{d}q_i = E_i A_i \mathrm{d}\epsilon_i^t$. As shown in Figure 2.6, the phase transformation strain of SMA is expressed as a piecewise linear function of total strain ϵ_i as:

$$\epsilon_i^t = f(\epsilon_i) = \begin{cases} 0 & \text{Part 1} \\ \Lambda\dfrac{\epsilon_i - \epsilon_s^{MA}}{\epsilon_f^{MA} - \epsilon_s^{MA}} & \text{Part 2} \\ \Lambda & \text{Part 3} \\ \epsilon_{max}^t - \epsilon_{max}^t\dfrac{\epsilon_C - \epsilon_i}{\epsilon_C - \epsilon_s^{AM}} & \text{Part 4} \\ \epsilon_{max}^t \quad \text{or} \quad \epsilon_{min}^t & \text{Part 5} \end{cases} \tag{2.62}$$

where parameter ϵ_C is the total strain of point C.

The incrementation of ϵ_i^t can be derived as:

$$\mathrm{d}\epsilon_i^t = \frac{\partial f(\epsilon_i)}{\partial \epsilon_i}\mathrm{d}\epsilon_i = \begin{cases} \dfrac{\Lambda}{\epsilon_f^{MA} - \epsilon_s^{MA}}\mathrm{d}\epsilon_i & \text{Part 2} \\ \dfrac{\epsilon_{max}^t}{\epsilon_C - \epsilon_f^{AM}}\mathrm{d}\epsilon_i & \text{Part 4} \\ 0 & \text{Others} \end{cases} \tag{2.63}$$

By denoting the deformation, the Jacobian matrix and the nodal displacement vector of the ith SMA member as r_i, $\hat{\boldsymbol{J}}$ and $\hat{\boldsymbol{D}}$ respectively, the incrementation of the total strain of the ith SMA member is attained as $\mathrm{d}\epsilon_i = \dfrac{\mathrm{d}r_i}{l_i} = \dfrac{\hat{\boldsymbol{J}} \cdot \mathrm{d}\hat{\boldsymbol{D}}}{l_i}$. By substituting $\mathrm{d}\epsilon_i$ into Equation 2.63, we can obtain the relationship between the incrementation of phase transformation strain and the incrementation of nodal displacement vector of the ith SMA member:

$$\mathrm{d}\epsilon_i^t = \frac{\partial f(\epsilon_i)}{\partial \epsilon_i}\mathrm{d}\epsilon_i = \begin{cases} \dfrac{\Lambda}{\epsilon_f^{MA} - \epsilon_s^{MA}}\dfrac{\hat{\boldsymbol{J}} \cdot \mathrm{d}\hat{\boldsymbol{D}}}{l_i} \\ \dfrac{\epsilon_{max}^t}{\epsilon_C - \epsilon_f^{AM}}\dfrac{\hat{\boldsymbol{J}} \cdot \mathrm{d}\hat{\boldsymbol{D}}}{l_i} \\ 0 \end{cases} = \begin{cases} c_i^{(2)}\hat{\boldsymbol{J}} \cdot \mathrm{d}\hat{\boldsymbol{D}} & \text{Part 2} \\ c_i^{(4)}\hat{\boldsymbol{J}} \cdot \mathrm{d}\hat{\boldsymbol{D}} & \text{Part 4} \\ 0 & \text{Others} \end{cases} \tag{2.64}$$

where coefficients $c_i^{(2)}$ and $c_i^{(4)}$ can be denoted as one parameter c_i. Based on the above equations,

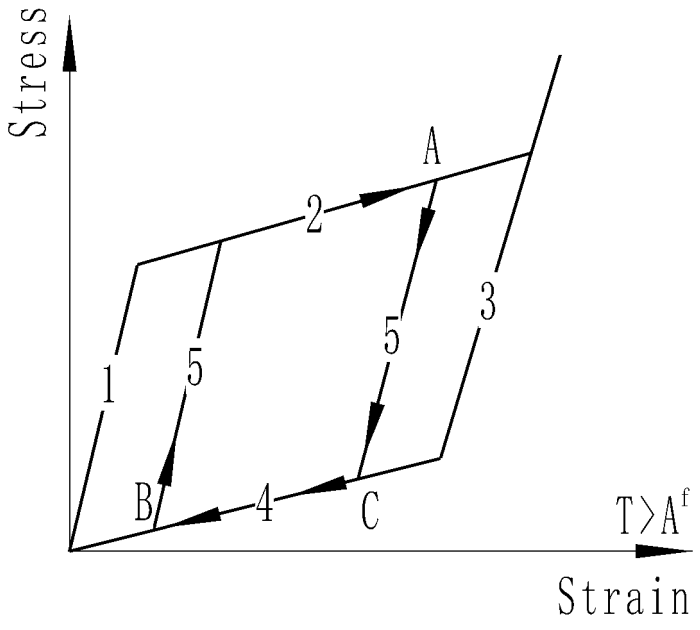

Figure 2.6: Piecewise analysis for phase transformation strain

we can express the ith component in $\mathrm{d}\boldsymbol{q}$ as:

$$\mathrm{d}q_i = \begin{cases} E_i A_i \mathrm{d}\epsilon_i^t & \text{SMA members} \\ 0 & \text{Others} \end{cases} \tag{2.65}$$

On the basis of Equations 2.64 and 2.65, the following linear relation between $\mathrm{d}\boldsymbol{q}$ and $\mathrm{d}\boldsymbol{D}_U$ is achieved:

$$\mathrm{d}\boldsymbol{q} = \boldsymbol{H}\mathrm{d}\boldsymbol{D}_U \tag{2.66}$$

where $\boldsymbol{H}$ is the corresponding coefficient matrix obtained based on these equations. The derivation process for the compatibility condition can refer to Appendix 2.A.

2.4.3 Numerical Integration Algorithm

The numerical integration algorithm in order to deal with the dynamics of such kind of truss structure problem is carried out. This kind of dynamic problem is nonlinear due to the material nonlinearity of the SMA wires and geometric nonlinearity of the truss structure itself. This nonlinear iterative method is introduced in order to reduce the calculation time. It should be noted that, as the term $(\boldsymbol{J}^{(t+\Delta t)})^T \mathrm{d}\boldsymbol{q}$ is tremendously small, in the numerical calculation process, this term can be ignored, and there is little influence on the results.

The numerical integration procedure is:

step 0: Initialization.

step 1: Calculate $\mathrm{d}\boldsymbol{D}^{(\mu)}$. Update $\boldsymbol{D}^{(t+\Delta t,\mu)} = \boldsymbol{D}^{(t+\Delta t,0)} + \mathrm{d}\boldsymbol{D}^{(1)} + ... + \mathrm{d}\boldsymbol{D}^{(\mu)}$, $\dot{\boldsymbol{D}}^{(t+\Delta t,\mu)}$ and $\ddot{\boldsymbol{D}}^{(t+\Delta t,\mu)}$.

step 2: Determine $\boldsymbol{P}$ on the basis of $\boldsymbol{D}^{(t+\Delta t,\mu)}$. Update $\boldsymbol{l} = \boldsymbol{l}(\boldsymbol{P})$.

step 3: Calculate SMA constitutive model to obtain $\boldsymbol{\epsilon}^t$ and the Young's moduli.

step 4: Determine $\boldsymbol{J}$. Update $\boldsymbol{K}^{(t+\Delta t,\mu)}$.

step 5: If convergence is obtained, then terminate. if not, get back to step 1.

It should be noted that the convergence condition in case of $\mu = 1$ is different from $\mu > 1$ because the convergence condition can not be utilized with $\mu = 1$. For the purpose of improving calculation accuracy, the convergence in the first iteration is set to be extremely rigorous, and it should iterate several times to suppress the unbalanced force due to nonlinearities.

2.5. Model Adequacy Confirmation

The balance equation in terms of force is rewritten as a balance equation in terms of energy during the time period of numerical calculation in the following form:

$$\int_0^T \dot{\boldsymbol{D}}_U^T \boldsymbol{M}_{UU} \ddot{\boldsymbol{D}}_U \mathrm{d}t + \int_0^T \dot{\boldsymbol{D}}_U^T \boldsymbol{K}_{UU} \boldsymbol{D}_U \mathrm{d}t = -\int_0^T \dot{\boldsymbol{D}}_U^T \boldsymbol{M}_{UU} \ddot{\boldsymbol{D}}'_U \mathrm{d}t + \int_0^T \dot{\boldsymbol{D}}_U^T \boldsymbol{J}_U^T \boldsymbol{q} \mathrm{d}t + \int_0^T \dot{\boldsymbol{D}}_U^T \boldsymbol{G}_U \mathrm{d}t \tag{2.67}$$

where parameter T is the time of numerical calculation. The input energy by the support ceiling $E_I = -\int_0^T \dot{\boldsymbol{D}}_U^T \boldsymbol{M}_{UU} \ddot{\boldsymbol{D}}'_U \mathrm{d}t$ equals the summation (denoted as E_O) of kinetic energy E_k of the truss members, the potential energy E_p of the truss members at the end of numerical calculation, the elastic energy E_e of the bracing SMA wire members in pure austenite at the end of numerical calculation and the consumed energy E_c by the hysteretic loops of SMA wire members as follows:

$$E_I = E_O = E_k + E_p + E_e + E_c \tag{2.68}$$

In this study, mass of the truss structure is assumed at the truss nodes. The kinetic energy E_k and the potential energy E_p of the truss members are attained by calculating the corresponding kinetic energy and the potential energy of the truss nodes. The elastic energy of a SMA wire member i in pure austenite at the end of numerical calculation is determined as $A_i l_i S_i$, where S_i is the area of the triangle $O_1O_2O_3$ shown in Figure 2.7(a) at the end of numerical calculation. The consumed energy by the ith SMA wire member is attained as $A_i l_i S'_i$, where S'_i is the summation of the experienced area values inside the major loop of the constitutive relationship between stress and strain of the ith SMA wire member during the time period of numerical calculation.

Algorithm for determining the area inside the major loop of constitutive relationship in the time history of numerical calculation is shown in Table 2.4. Parameter t is the time point for numerical calculation. ϵ_A and ϵ_B are labeled as in Figure 2.7(b). Area value of quadrangle $ABCD$ is utilized for determining the consumed energy in the current cycle on the basis of line segment AB on the forward phase transformation line. Owing to the assumption of piecewise linear relationship of the constitutive model, coordinates of points C and D are easily attained.

Simulation example is conducted on the truss structure shown in Figure 2.8(a). The black rectangle represents the support ceiling and the red rectangle represents an apparatus. Mass of the apparatus is 5kg and mass of the hanging truss is 19.26kg. Motion trajectory of support ceiling is a sinusoidal wave, frequency of which is assumed to be 5Hz and the amplitude is assumed to vary from 0.01m to 0.1m with interval of 0.01m.

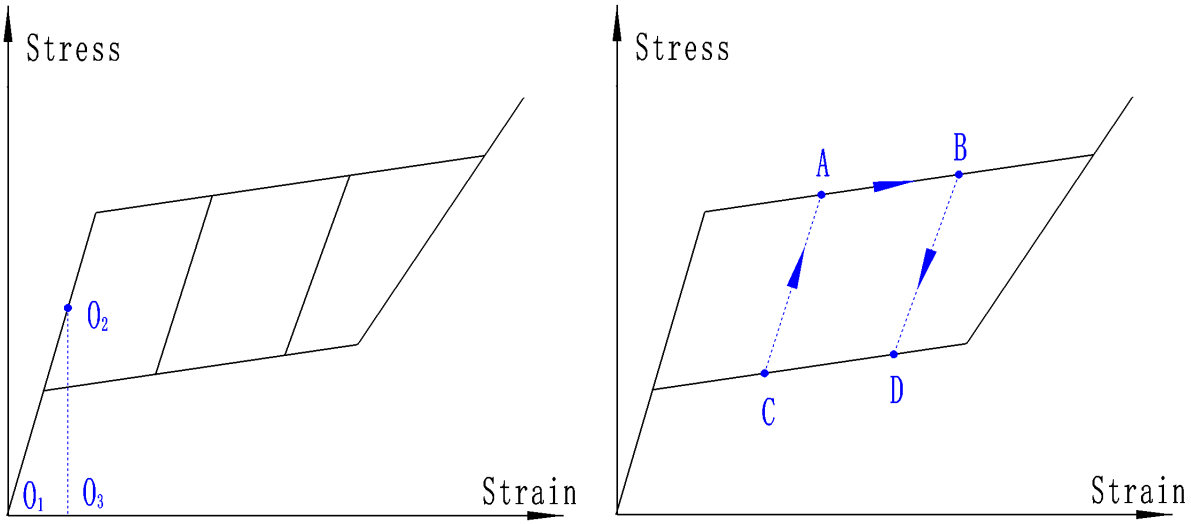

(a) Section for elastic energy (b) Section for consumed energy

Figure 2.7: Constitutive relations for explaining the value of energy

Table 2.4: Algorithm for obtaining area value in the constitutive relationship

(1). Detect forward phase transformation

If $\epsilon_{t+1} > \epsilon_t$ & $\epsilon_{t+1} > \epsilon_A$ (energy consumption is detected)

Memorize values of point A

End if

(2). Detect termination of forward transformation

If $\epsilon_{t+1} < \epsilon_t$ & $\epsilon_{t+1} < \epsilon_B$ (consumed energy is obtained in this cycle)

Memorize values of point B

End if

(3). Calculate area of quadrangle $ABCD$ shown in Figure 2.6(b)

Relationships of the input energy and the output energy with the variation of vibration amplitude are shown in Figure 2.8(b). As can be seen in this result, with a fixed value of vibration amplitude, the difference between the input energy and the output energy is tremendously small. The developed dynamic model is adequacy. However, the differences of the input energy and the output energy produce errors that are calculated as $e = (E_I - E_O)/E_I$. Variation between error and vibration amplitude is shown in Figure 2.8(c). Variation range of error is from -4% to 6%. It is considered that the error is due to two aspects. The first one is the simplification of mass matrix because in this dynamic model, mass of the truss members are assumed at the truss nodes. The second one is the real area of constitutive model in dynamic calculation is

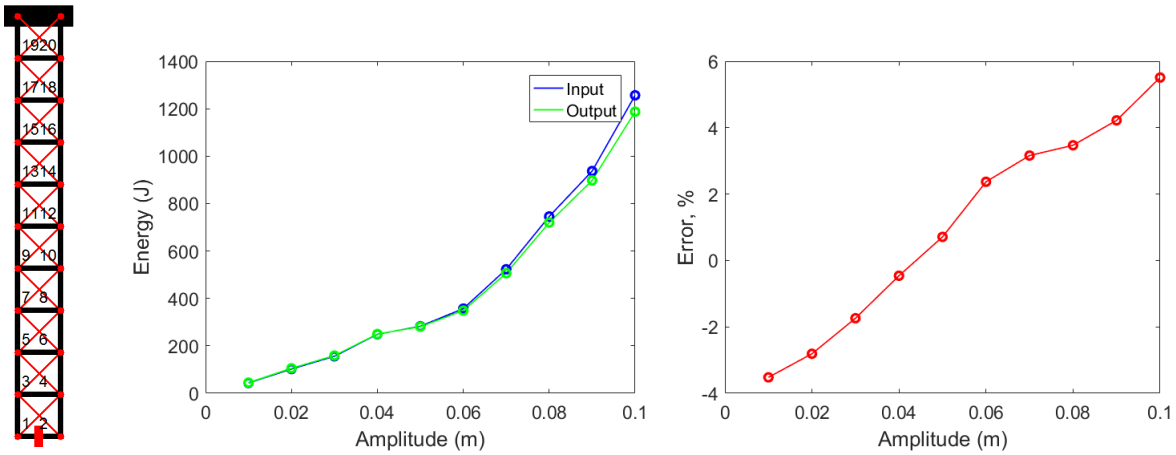

(a) Truss (b) Input and output energy (c) Error

Figure 2.8: Truss configuration and results for demonstrating energy conservation

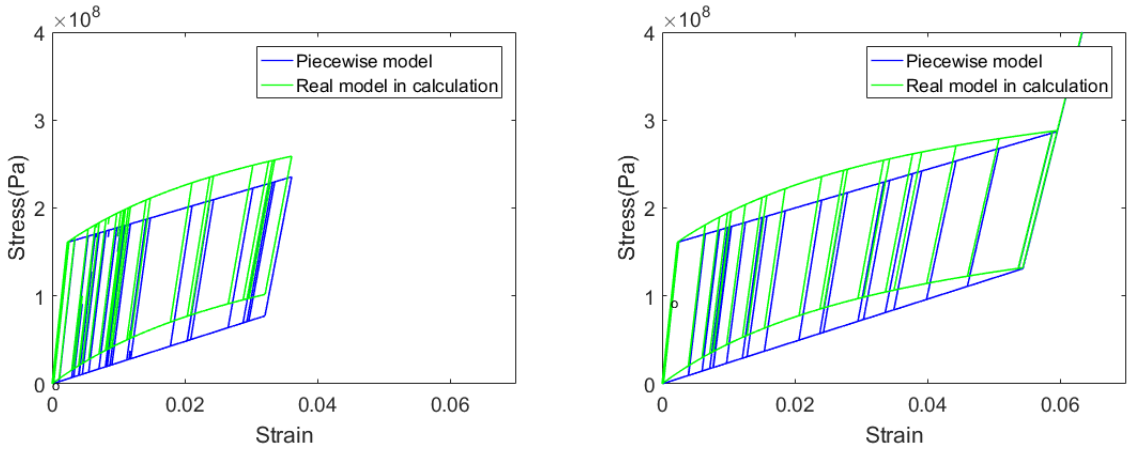

(a) The 17th SMA wire member (b) The 20th SMA wire member

Figure 2.9: The piecewise model and the real model in the dynamic calculation

different from the area obtained by piecewise linear constitutive model. For example, in the case of vibration amplitude of support ceiling is 0.05m, constitutive relationships of the 17th and the 20th SMA wire members are shown in Figure 2.9. Blue line is the piecewise model and green line is the real model experienced in the dynamic calculation due to the process of dynamic model construction. The difference of the area enclosed by green line and blue line produces error between the input energy and the output energy. On the basis of the contents mentioned above, under the circumstance of some error, the input energy and the output energy is equal. Therefore, the developed dynamic model is adequacy.

2.6. Summary

In this chapter, characteristics of SMA material are introduced. Several constitutive physical models of pseudo-elasticity of SMA material have been given. The first constitutive model is a piecewise model that does not consider the sub-loop behavior; the second constitutive model is a piecewise linear model that considers the sub-loop behavior. The geometric relation of the truss structural system is introduced. Based on this geometric relationship, the dynamic equation of motion of the truss structural system having SMA wire members are derived. The numerical integration algorithm is shown. Adequacy of the dynamic model is confirmed from the viewpoint of energy conservation.

Appendix 2.A Compatibility Condition Derivation

Equation 2.60 is expressed as follows:

$$\hat{\boldsymbol{K}}_{UU}^{(t+\Delta t)}\mathrm{d}\boldsymbol{D}_U - (\boldsymbol{J}_U^{(t+\Delta t)})^T\mathrm{d}\boldsymbol{q} = \boldsymbol{F}_{err}^{(t+\Delta t)} \tag{2.69}$$

where $\hat{\boldsymbol{K}}_{UU}^{(t+\Delta t)} = \dfrac{1}{\beta\Delta t^2}\boldsymbol{M}_{UU} + \boldsymbol{K}_{UU}^{(t+\Delta t)}$. Taking Figure 2.9 as an example to demonstrate the approach for solving Equation 2.69. The left side of Equation 2.69 is expressed as follows by ignoring the confined nodes at the support ceiling.

$$\begin{aligned}
&\begin{bmatrix} \hat{K}_{11} & \hat{K}_{12} & \cdots & \hat{K}_{18} \\ \hat{K}_{21} & \ddots & \ddots & \vdots \\ \vdots & \ddots & \ddots & \hat{K}_{78} \\ \hat{K}_{81} & \cdots & \hat{K}_{87} & \hat{K}_{88} \end{bmatrix}\begin{bmatrix} \mathrm{d}D_1 \\ \mathrm{d}D_2 \\ \vdots \\ \mathrm{d}D_8 \end{bmatrix} \\
-&\begin{bmatrix} J_{11} & J_{21} & \cdots & J_{10-1} \\ J_{12} & \ddots & \ddots & J_{10-2} \\ \vdots & \ddots & \ddots & \vdots \\ J_{18} & \cdots & J_{98} & J_{10-8} \end{bmatrix}\begin{bmatrix} c_1[\hat{J}_1^1\ \hat{J}_2^1\ \hat{J}_3^1\ \hat{J}_4^1][\mathrm{d}D_3\ \mathrm{d}D_4\ \mathrm{d}D_5\ \mathrm{d}D_6]^T \\ c_2[\hat{J}_1^2\ \hat{J}_2^2\ \hat{J}_3^2\ \hat{J}_4^2][\mathrm{d}D_1\ \mathrm{d}D_2\ \mathrm{d}D_7\ \mathrm{d}D_8]^T \\ \vdots \\ c_{10}[\hat{J}_1^{10}\ \hat{J}_2^{10}\ \hat{J}_3^{10}\ \hat{J}_4^{10}][\mathrm{d}D_7\ \mathrm{d}D_8\ \mathrm{d}D_{11}\ \mathrm{d}D_{12}]^T \end{bmatrix}
\end{aligned} \tag{2.70}$$

As can be seen in Figure 2.10, the degrees of freedom 9, 10, 11 and 12 are confined at the support ceiling. Therefore, $\mathrm{d}D_9 = 0$, $\mathrm{d}D_{10} = 0$, $\mathrm{d}D_{11} = 0$, $\mathrm{d}D_{12} = 0$. This formulation can be arranged as a 8×1 vector. $m = 1, 2, ..., 8$ is used to denote the sequence number of term in this

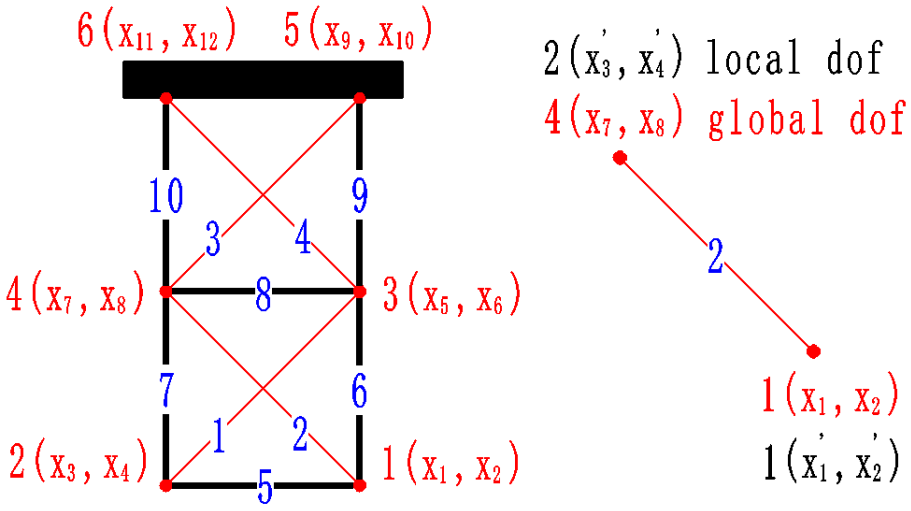

Figure 2.10: Conceptual analysis for finite element method of the truss

vector. The first term ($m = 1$) is derived as follows:

$$\begin{aligned}
&(\hat{K}_{11} - J_{21}c_2\hat{J}_1^2 - J_{51}c_5\hat{J}_1^5 - J_{61}c_6\hat{J}_1^6)\mathrm{d}D_1 \\
+&(\hat{K}_{12} - J_{21}c_2\hat{J}_2^2 - J_{51}c_5\hat{J}_2^5 - J_{61}c_6\hat{J}_2^6)\mathrm{d}D_2 \\
+&(\hat{K}_{13} - J_{11}c_1\hat{J}_1^1 - J_{51}c_5\hat{J}_3^5 - J_{71}c_7\hat{J}_1^7)\mathrm{d}D_3 \\
+&(\hat{K}_{14} - J_{11}c_1\hat{J}_2^1 - J_{51}c_5\hat{J}_4^5 - J_{71}c_7\hat{J}_2^7)\mathrm{d}D_4 \\
+&(\hat{K}_{15} - J_{11}c_1\hat{J}_3^1 - J_{41}c_4\hat{J}_1^4 - J_{61}c_6\hat{J}_3^6 - J_{81}c_8\hat{J}_1^8 - J_{91}c_9\hat{J}_1^9)\mathrm{d}D_5 \\
+&(\hat{K}_{16} - J_{11}c_1\hat{J}_4^1 - J_{41}c_4\hat{J}_2^4 - J_{61}c_6\hat{J}_4^6 - J_{81}c_8\hat{J}_2^8 - J_{91}c_9\hat{J}_2^9)\mathrm{d}D_6 \\
+&(\hat{K}_{17} - J_{21}c_2\hat{J}_3^2 - J_{31}c_3\hat{J}_1^3 - J_{71}c_7\hat{J}_3^7 - J_{81}c_8\hat{J}_3^8 - J_{10-1}c_{10}\hat{J}_1^{10})\mathrm{d}D_7 \\
+&(\hat{K}_{18} - J_{21}c_2\hat{J}_4^2 - J_{31}c_3\hat{J}_2^3 - J_{71}c_7\hat{J}_4^7 - J_{81}c_8\hat{J}_4^8 - J_{10-1}c_{10}\hat{J}_2^{10})\mathrm{d}D_8
\end{aligned} \tag{2.71}$$

In the first term ($m = 1$), $j = 1, 2, ..., 8$ is used to denote the sequence number of degree of freedom of the truss structural system (the subscript of $\mathrm{d}D$). Regular patterns on the scripts of coefficients of $\mathrm{d}D_j$ of the above formulation are summarized as follows:

- $\hat{K}$: In the term of number m, $\hat{K}_{mj}$ is a coefficient of $\mathrm{d}D_j$. (For example, in case of $m = 1$, $\hat{K}_{11}$ is a coefficient of $\mathrm{d}D_1$; $\hat{K}_{12}$ is a coefficient of $\mathrm{d}D_2$)

- c: The subscript g of c corresponds to the number of truss members having the node with the degree of freedom j. (For example, In Figure 2.10, truss members $g = 2$, $g = 5$ and $g = 6$ have the first node and the degrees of freedom of the first node are $j = 1$ and $j = 2$. Therefore, c_2, c_5 and c_6 appear in the coefficients of $\mathrm{d}D_1$ and $\mathrm{d}D_2$)

- J: In the term of number m, $J_{gm}c_g$ appear. (For example, in term $m = 1$, $J_{21}c_2$, $J_{51}c_5$ and $J_{61}c_6$ appear in the coefficients of $\mathrm{d}D_1$)

- $\hat{J}$: $c_g\hat{J}_u^g$ appear. u is the local degree of freedom of the truss member. (The local degree of freedom $u = 1, 2, 3, 4$ of truss member $g = 2$ are considered as $j = 1, 2, 7, 8$ in the global system. For example, $c_2\hat{J}_1^2$ appears in the coefficients of $\mathrm{d}D_1$; $c_2\hat{J}_2^2$ appears in the coefficients of $\mathrm{d}D_2$; $c_2\hat{J}_3^2$ appears in the coefficients of $\mathrm{d}D_7$; $c_2\hat{J}_4^2$ appears in the coefficients of $\mathrm{d}D_8$)

We can examine the correctness of the above-mentioned regular patterns by the second term

($m = 2$) of the aforementioned vector:

$$\begin{aligned}
&(\hat{K}_{21} - J_{22}c_2\hat{J}_1^2 - J_{52}c_5\hat{J}_1^5 - J_{62}c_6\hat{J}_1^6)\mathrm{d}D_1 \\
+&(\hat{K}_{22} - J_{22}c_2\hat{J}_2^2 - J_{52}c_5\hat{J}_2^5 - J_{62}c_6\hat{J}_2^6)\mathrm{d}D_2 \\
+&(\hat{K}_{23} - J_{12}c_1\hat{J}_1^1 - J_{52}c_5\hat{J}_3^5 - J_{72}c_7\hat{J}_1^7)\mathrm{d}D_3 \\
+&(\hat{K}_{24} - J_{12}c_1\hat{J}_2^1 - J_{52}c_5\hat{J}_4^5 - J_{72}c_7\hat{J}_2^7)\mathrm{d}D_4 \\
+&(\hat{K}_{25} - J_{12}c_1\hat{J}_3^1 - J_{42}c_4\hat{J}_1^4 - J_{62}c_6\hat{J}_3^6 - J_{82}c_8\hat{J}_1^8 - J_{92}c_9\hat{J}_1^9)\mathrm{d}D_5 \\
+&(\hat{K}_{26} - J_{12}c_1\hat{J}_4^1 - J_{42}c_4\hat{J}_2^4 - J_{62}c_6\hat{J}_4^6 - J_{82}c_8\hat{J}_2^8 - J_{92}c_9\hat{J}_2^9)\mathrm{d}D_6 \\
+&(\hat{K}_{27} - J_{22}c_2\hat{J}_3^2 - J_{32}c_3\hat{J}_1^3 - J_{72}c_7\hat{J}_3^7 - J_{82}c_8\hat{J}_3^8 - J_{10-2}c_{10}\hat{J}_1^{10})\mathrm{d}D_7 \\
+&(\hat{K}_{28} - J_{22}c_2\hat{J}_4^2 - J_{32}c_3\hat{J}_2^3 - J_{72}c_7\hat{J}_4^7 - J_{82}c_8\hat{J}_4^8 - J_{10-2}c_{10}\hat{J}_2^{10})\mathrm{d}D_8
\end{aligned} \tag{2.72}$$

The terms from $m = 3$ to $m = 8$ can be easily calculated. On the basis of these manipulations, formulation (2.70) turns into $\boldsymbol{H}_{8\times8}\boldsymbol{E}_{8\times1}$ and $\boldsymbol{E} = [\mathrm{d}D_1\ \mathrm{d}D_2\ \cdots\ \mathrm{d}D_8]^T$. The coefficient matrix $\boldsymbol{H}$ is determined by the following equations:

$$\begin{aligned}
H_{(2i-1)j} &= \hat{K}_{(2i-1)j} - \sum_{p=1}^{p^*} J_{gj}c_g\hat{J}_{2s-1}^g \\
H_{(2i)j} &= \hat{K}_{(2i)j} - \sum_{p=1}^{p^*} J_{gj}c_g\hat{J}_{2s}^g
\end{aligned} \tag{2.73}$$

The scripts are defined as follows:

- i: Sequence number of truss node. ($i = 1, 2, 3, 4$)
- j: Sequence number of degree of freedom in the global system. ($j = 1, 2, ..., 8$)
- p: Local number of truss member that having node i. (For example, global sequence numbers of truss members 2, 5 and 6 turn into $p = 1, 2, 3$ in the case of $i = 1$)
- g: Global number of truss member having node i. (For example, g can be denoted as $g = g(p)$. Therefore, in case of $i = 1$, $g(1) = 2$, $g(2) = 5$, $g(3) = 6$)
- p^*: Total number of truss members having node i.
- s: Local sequence number of node i of truss member g. (For example, node $i = 1$ and node $i = 4$ in the global system turn into $s = 1$ and $s = 2$ in the case of $g = 2$)

Chapter 3

Dynamic Simulations

3.1. Introduction

In this chapter, dynamic simulations are conducted for the hanging truss structural system having SMA wires and ordinary wires. Typical examples are shown for the purpose of explaining the properties of the hanging truss, the ordinary wires and the SMA wires. The advantages of the combinations of SMA wires and ordinary wires and the combinations of the truss units having SMA wires and the truss units without wires are demonstrated from the vibration isolation and attenuation points of view.

3.2. Assumed Truss and Vibration Condition

In Figure 3.1(a), the black lines stand for rigid members, the green lines stand for the possible placements of the bracing wire members. Numbers assigned to the green lines shown in the figure serve as the identifiers of the wire members. In the simulation examples, the environmental motion is given in the form of vibrational motion of the support ceiling, whose corresponding displacement trajectory is sinusoidal shown as the waveform in Figure 3.1(b). The dynamic behavior of the peripheral end apparatus shown in Figure 3.1(a) in horizontal direction is to be examined. Corresponding parameters for the simulations and the characteristics of SMA wire are listed in Tables 3.1 and 3.2. In Table 3.1, the diameter of the ordinary wire is determined on the basis of the diameter of the SMA wire that is set in advance from the viewpoint of the same ultimate strength of those two kinds of wires. The vibration frequency of the support ceiling is 4Hz and the amplitude is 0.03m. We assume an apparatus of 5kg supported by the hanging truss. The total mass of the truss without the apparatus is 9.26kg; it should be noted that the mass is practically due to the mass of rigid members. The time step for the numerical integration is 50μs. This small time step is for the purpose of dealing with the material nonlinearity

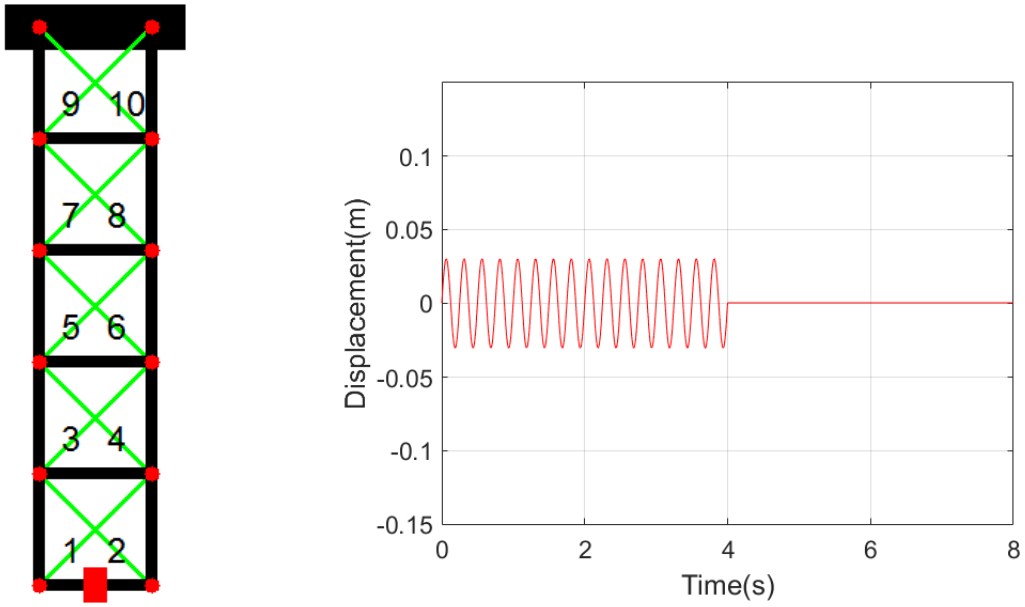

(a) Truss configuration (b) Horizontal dynamic motion

Figure 3.1: Configuration of the truss and vibrational motion of support ceiling

Table 3.1: Simulation conditions

Member diameter (mm)	rigid	a_R	10mm
	wire	a_w	1.6mm
	SMA	a_{sma}	1mm
Young's modulus (GPa)	rigid	E_R	210GPa
	wire	E_w	210GPa
Density (kg/m^3)	rigid	ρ_R	7860kg/m^3
	wire	ρ_w	7860kg/m^3
	SMA	ρ_{sma}	6500kg/m^3

and geometric nonlinearity of this kind of truss structural system.

3.3. Typical Behaviors of the Hanging Truss

The following simulations are conducted to illustrate the vibration isolation capability of the hanging truss with the pendulum effect. In Figure 3.2(a), there are no bracing wires placed at

Table 3.2: SMA characteristics

Maximum phase transformation strain	Λ	0.05
Young's modulus of austenite phase	E_A	70GPa
Young's modulus of martensite phase	E_M	30GPa

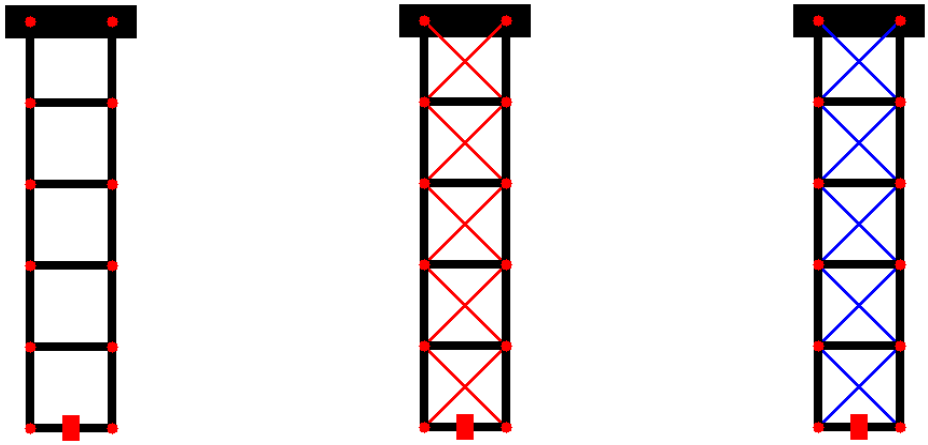

(a) No bracing wires (b) 10 SMA wires (c) 10 ordinary wires

Figure 3.2: Configurations of trusses for demonstration of influence of bracing member types

the hanging truss. Therefore, this structure becomes a mechanism that is unstable if it is not in hanging configuration. However, under the influence of the gravitational force, stability of a structure of this type can be guaranteed in many situations.

Figures 3.3-3.6 show the corresponding dynamic behaviors of acceleration of the peripheral end apparatus of the structure shown in Figure 3.2(a). In the four results of Figures 3.3-3.6, from the acceleration point of view, we confirmed the vibration isolation effect; the acceleration amplitude of the peripheral end is significantly smaller than the acceleration amplitude of the support ceiling. At the beginning of vibration, owing to no bracing wire members, the vibration transmission from the support ceiling to the peripheral end take some time. In addition, due to the influence of the inertia force of the apparatus, vibration isolation effect is obvious at the beginning of the vibration of the support ceiling. Displacement of the support ceiling is rightward, and acceleration is leftward at the very beginning of vibration of the support ceiling. After a period of time, vibration from the support ceiling transmitted to the peripheral end and we can consider that after vibration transmission, the acceleration of the peripheral end is also leftward because the accelerations are minus at the beginning of obvious vibration of the peripheral end as can be seen in Figures 3.3-3.6.

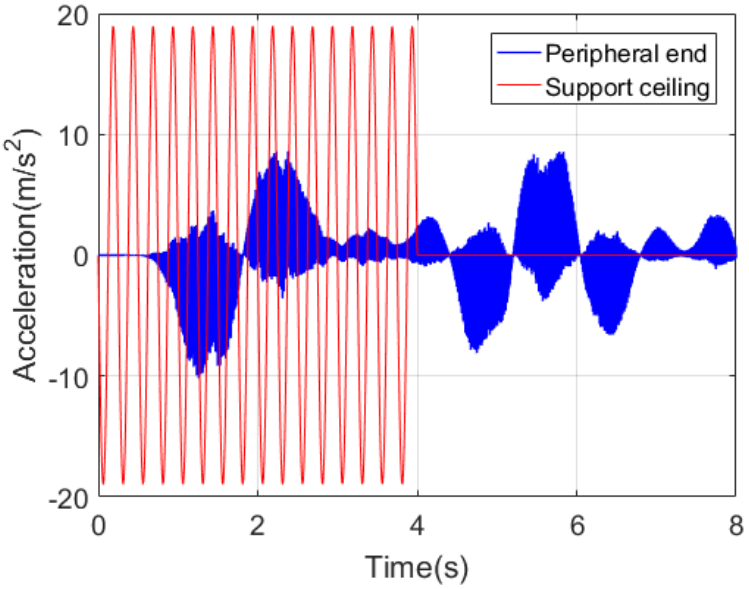

Figure 3.3: Dynamic behaviors of the truss in Figure 3.2(a) in case that the mass value of the peripheral end apparatus is 0kg

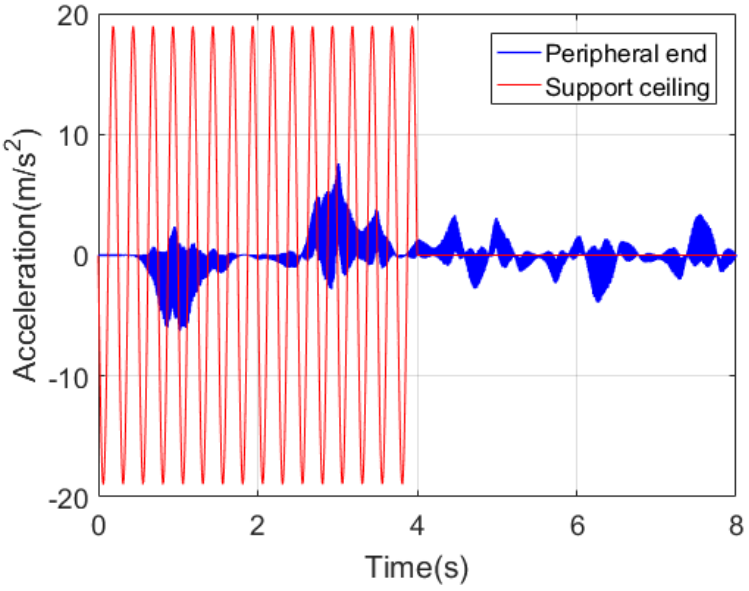

Figure 3.4: Dynamic behaviors of the truss in Figure 3.2(a) in case that the mass value of the peripheral end apparatus is 5kg

Figures 3.3-3.6 also show the influence of the mass of the apparatus assumed at the peripheral end on the dynamic behaviors. From the results in Figures 3.3-3.5, we conclude the vibration

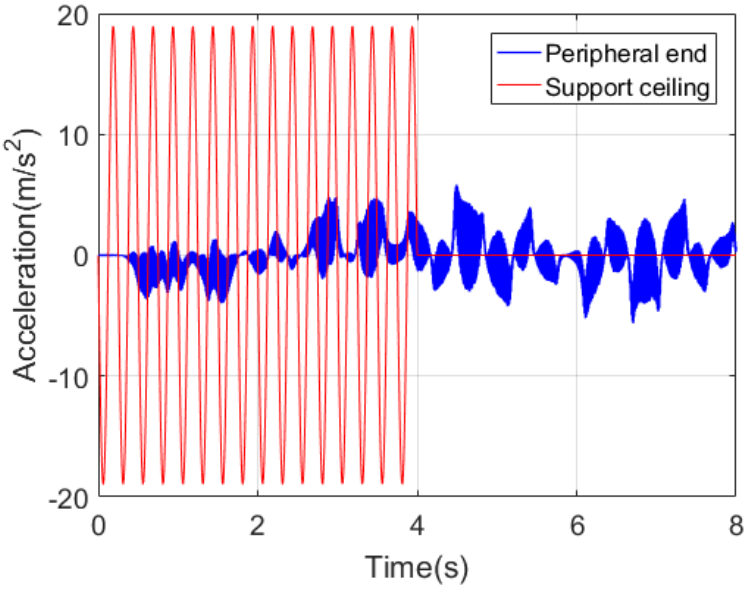

Figure 3.5: Dynamic behaviors of the truss in Figure 3.2(a) in case that the mass value of the peripheral end apparatus is 20kg

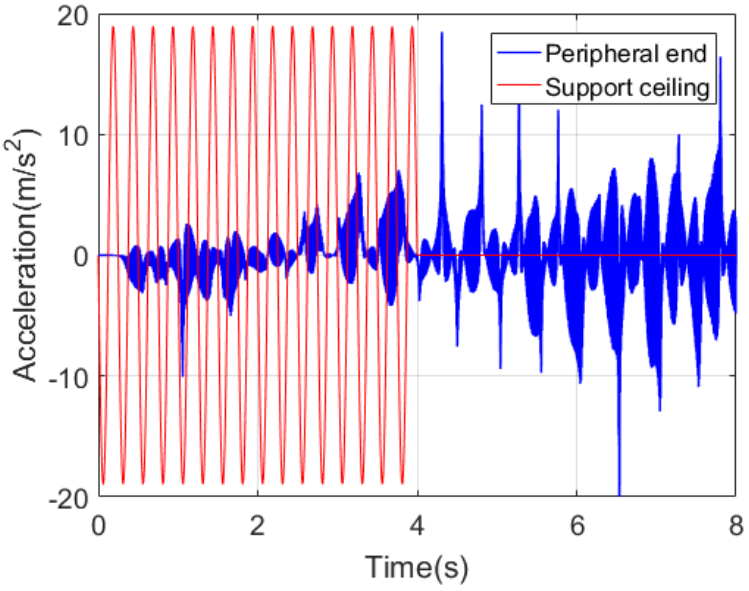

Figure 3.6: Dynamic behaviors of the truss in Figure 3.2(a) in case that the mass value of the peripheral end apparatus is 40kg

isolation effect are sufficient with those mass values of the peripheral end apparatus. The RMS value of the support ceiling vibrational motion is 9.47m/s^2 and the RMS values of the results

Table 3.3: RMS values of the acceleration results

	Condition		RMS(0s − 8s)
Type	Mass(kg)	Result	(m/s^2)
No bracing wires	0kg	3.3	2.35
No bracing wires	5kg	3.4	1.29
No bracing wires	20kg	3.5	1.53
No bracing wires	40kg	3.6	2.77
10 SMA wires	5kg	3.7(b)	9.31
10 ordinary wires	5kg	3.8(b)	19.12
4 SMA wires	5kg	3.11(b)	1.57

are listed in Table 3.3. The RMS values of acceleration of Figures 3.3, 3.4 and 3.5 are 2.35m/s^2, 1.29m/s^2 and 1.53m/s^2, respectively. These values illustrate the excellent vibration isolation capability of the truss structures evaluated in terms of acceleration compared with the RMS value of the vibrational motion of the support ceiling. However, in the case of 40kg of the mass value , the exerted vibration energy is significantly converted into the vibration of the peripheral end as shown in Figure 3.6. The RMS value of acceleration of Figure 3.6 is 2.77m/s^2, and is obviously larger than the RMS values of Figures 3.3, 3.4 and 3.5; although the value is still smaller than that of the support ceiling. Therefore, the isolation effect can not be simply guaranteed with relatively large mass at the peripheral end of the hanging truss. We think there are other factors that influence the value of acceleration of the peripheral end except for the mass value. For example, vibration transmission from the support ceiling to the peripheral end can be delayed by means of increasing the truss units.

Figures 3.7 and 3.8 show the dynamic results that are adopted to demonstrate the influence of the mechanical properties of SMA and ordinary wires on the structural dynamic characteristics of the truss. In Figure 3.2, the red lines are SMA wire members and the blue lines are ordinary wire members. Figures 3.7(a) and 3.7(b) are the displacement and acceleration behaviors of the truss in Figure 3.2(b). In Figure 3.7(a), vibration isolation and attenuation effects due to SMA wires are demonstrated. When the support ceiling vibrated, in the stage of transient response of 0s-2s, the deformation of the truss is significant; in the stage of steady state of 2s-4s, vibration isolation effect is demonstrated. At the time period of 4s-8s, vibration attenuation effect is shown due to the hysteretic loop of SMA wires. The RMS value of acceleration in Figure 3.7(b) is 9.31m/s^2, which demonstrates that the vibration isolation of the truss with units having

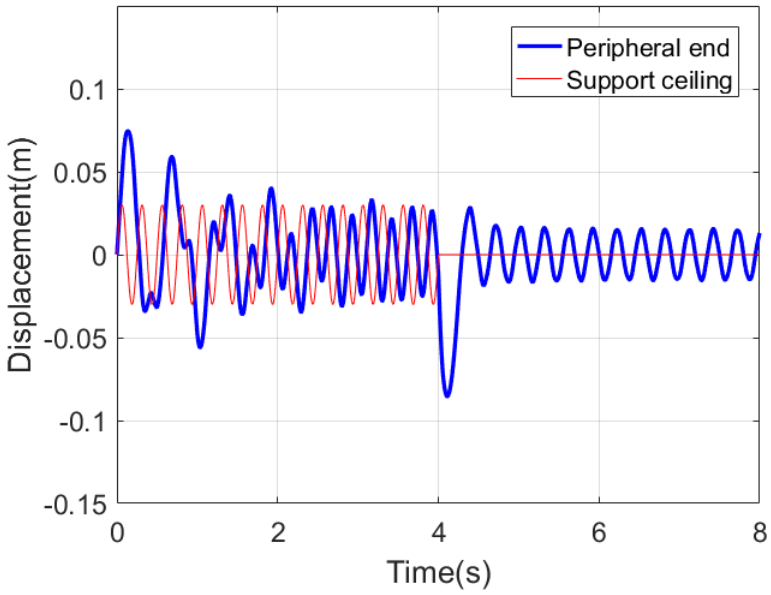

(a) Displacement behavior

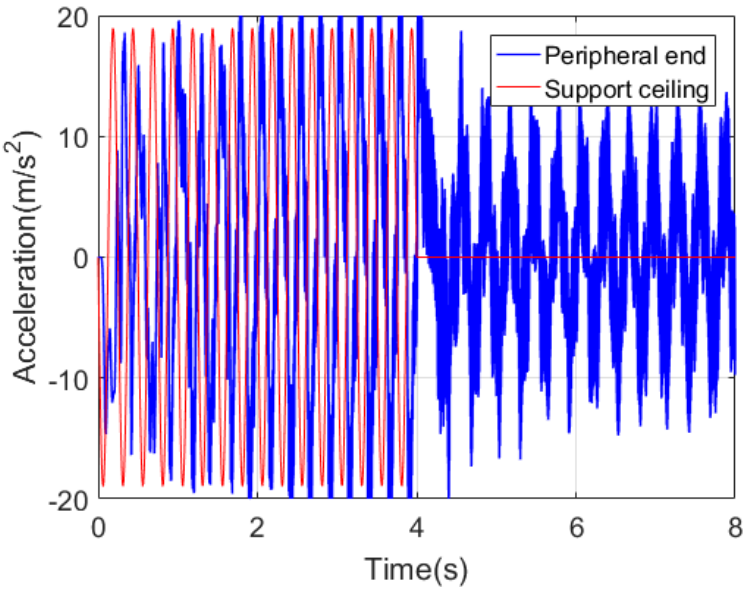

(b) Acceleration behavior

Figure 3.7: Dynamic behaviors of the truss in Figure 3.2(b)

bracing of SMA wires is worse than the truss with units having no bracing wires.

Figures 3.8(a) and 3.8(b) are the displacement and acceleration behaviors of the truss in

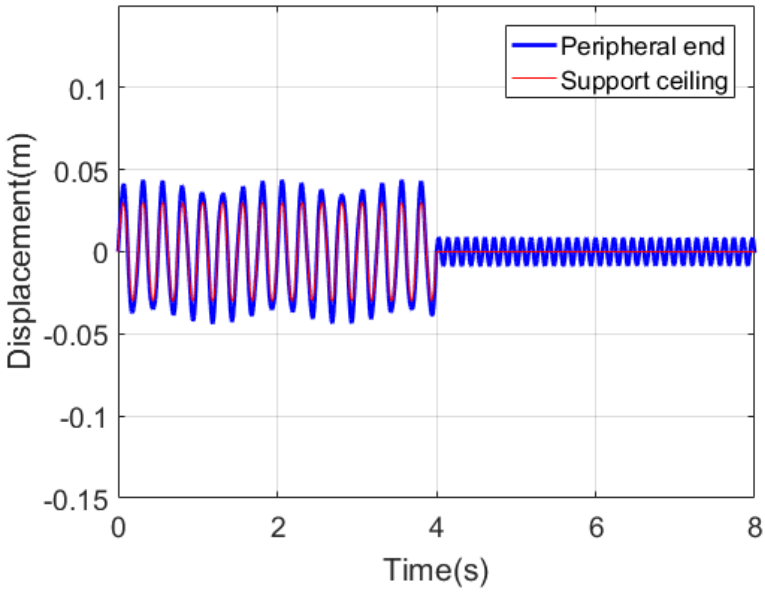

(a) Displacement behavior

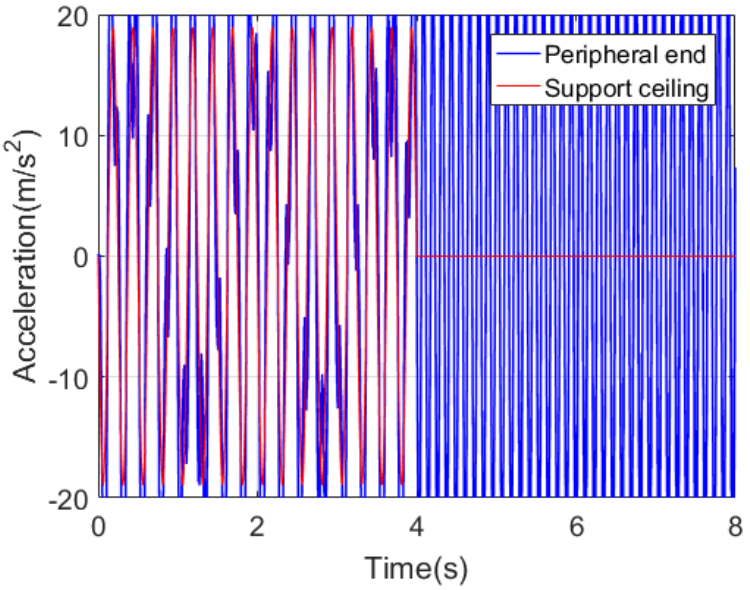

(b) Acceleration behavior

Figure 3.8: Dynamic behaviors of the truss in Figure 3.2(c)

Figure 3.2(c). Since the ordinary wires have a higher stiffness than the SMA wires, the obtained behavior at time period of 0s-4s is also vibratory but relatively stable as shown in Figure 3.8(a), compared with the result shown in Figure 3.7(a). The RMS value of acceleration in Figure

3.8(b) is 19.12m/s^2, which is significantly larger than the case in Figure 3.7(b). However, the residual vibration amplitude in Figure 3.8(a) is smaller than the residual vibration amplitude in Figure 3.7(a). This is because the deformation of the truss structure having ordinary wires is smaller than the truss structure having SMA wires due to the relatively high stiffness of the ordinary wires.

Comparison between the two results in Figures 3.7(a) and 3.8(a), shows the obvious differences of the mechanical properties between the two kinds of wires. Combination of these two types of wires with different mechanical properties is expected to enable the structure to improve vibration attenuation as well as vibration isolation capabilities simultaneously.

Figure 3.9(a) is a column-type hanging truss having 10 truss units but without any bracing wire members. From the corresponding dynamic behavior result of acceleration in Figure 3.9(b), we can see the vibration isolation effect in the time period of 0s − 4s. The RMS value in this time period is 1.25m/s^2. The vibration isolation is especially obvious at the time period of 0s − 1s. The RMS value at this time period is 0.04m/s^2. This is due to the delay effect of vibration transmission from the support ceiling to the peripheral end.

Figure 3.9(c) is a hanging truss structure having 10 truss units with 20 SMA wires. And the corresponding acceleration behavior is the result of Figure 3.9(d). The RMS value of acceleration of the apparatus assumed at the peripheral end in the time period of 0s − 4s is 7.95m/s^2. From the two acceleration behaviors of Figures 3.9(b) and 3.9(d) in the time period of 0s − 4s we can see that vibration isolation of truss as shown in Figure 3.9(a) is better. The RMS values of Figures 3.9(b) and 3.9(d) in the time period of 4s − 8s are 2.11m/s^2 and 5.16m/s^2 respectively. Therefore, after vibration motion of the support ceiling ceased, the residual vibration of Figure 3.9(b) is smaller than Figure 3.9(d). Vibration attenuation effect in Figure 3.9(d) can be seen; however, in the stage of free vibration after the process of energy dissipation, owing to the unattenuated energy, the residual vibration can not be suppressed due to the mechanical property of SMA wires in pure austenite phase. The bracing members of SMA wires can attenuate vibration energy and can transmit the vibration energy from support ceiling to peripheral end simultaneously. This is a trade-off relationship of the bracing SMA wire members from vibration suppression point of view.

The comparison between the results in Figures 3.4 and 3.9(b) demonstrates that the vibration isolation of the truss in Figure 3.9(a) is better than the truss in Figure 3.2(a). Therefore, the stage of the truss unit has an influence on the isolation effect as have been mentioned above. In case of no bracing wire members, the vibration transmission from the support ceiling to the peripheral end takes more time with more stages of truss unit. Larger numbers of truss bays show better isolation effect in such cases in the fixed time period.

The comparison between the results in Figures 3.7(b) and 3.9(d) demonstrates that the vibration isolation of the truss in Figure 3.9(c) is better than the truss in Figure 3.2(b). Therefore,

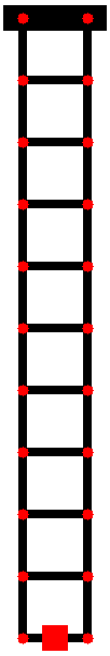

(a) Truss configuration $k = 0$

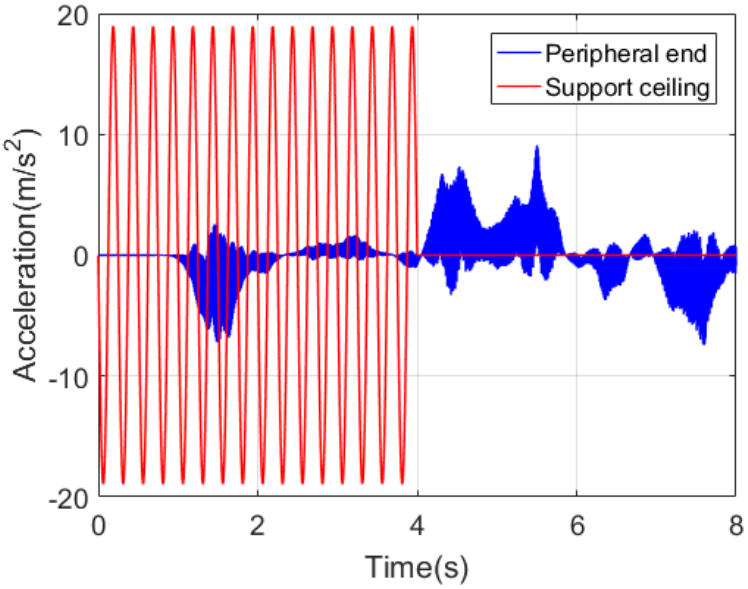

(b) Acceleration of support ceiling in case of $k = 0$

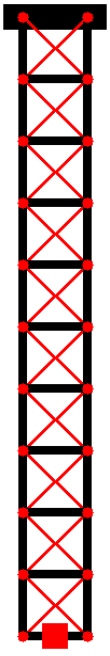

(c) Truss configuration $k = 20$

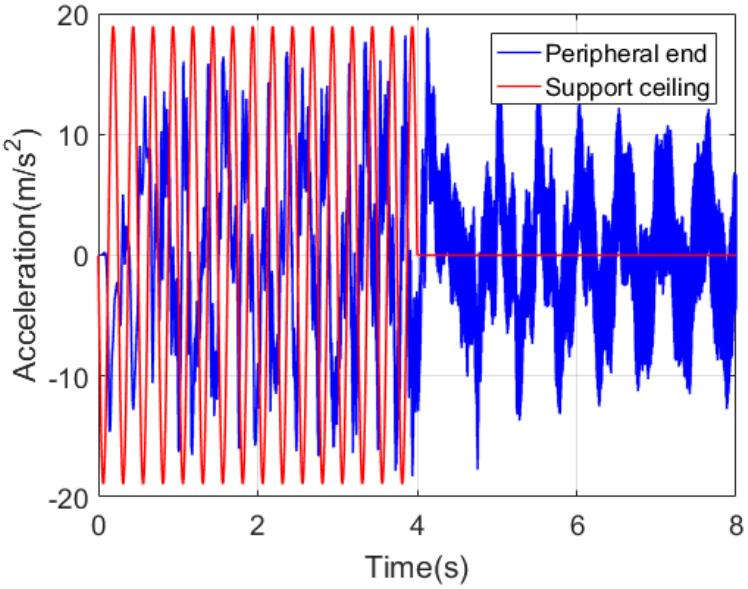

(d) Acceleration of support ceiling in case of $k = 20$

Figure 3.9: Dynamic behaviors of the hanging truss structures

the number of stages of the truss unit also has an influence on the isolation effect with bracing members. Although the vibration transmits from support ceiling to peripheral end, owing to the small stiffness and the hysteretic loop of the SMA wire members, the vibration transmission can be suppressed. This contributes to the vibration isolation effect of this kind of hanging truss structure. Larger numbers of truss bays show better isolation effect due to more energy consumption by the conspicuous characteristic of the pseudo-elasticity of SMA wire members in such cases.

3.4. Combination of SMA and Ordinary Wires

Hysteretic loop and variable stiffness characteristic of SMA wires enable the truss structure to have the capabilities of vibration attenuation and isolation from the deformation point of view. In the case of low strain range (without phase transformation) and slack state, such kind of SMA wires can be replaceable to ordinary wires; simultaneously, owing to the relatively high mechanical stiffness of the ordinary wires, stability of the peripheral end can be maintained to some extent.

For instance, Figure 3.10(a) is a truss structure having 8 SMA wires and 2 ordinary wires. Figure 3.10(b) is the corresponding displacement behavior of the peripheral end apparatus in horizontal direction. This result demonstrates vibration isolation effect in case that support ceiling vibrated, as well as vibration attenuation effect in case that support ceiling vibration ceased.

Figure 3.10(c) is the corresponding time history of the natural frequency of the truss structure in Figure 3.10(a). The blue line represents the time history of the natural frequency, and the red line indicates the environmental vibration frequency of the support ceiling. The initial natural frequency is 3.47Hz. In the transitional period of 0s-2s, the natural frequency changes drastically as the mechanical properties of the SMA wires; in the stage of steady state of 2s-4s, natural frequency changes periodically, which demonstrates the variable stiffness of truss structural system as a whole. It should be noted that in the calculation process, in the case that the two wires at the same truss unit are in slack state or in taut state simultaneously, the natural frequency of the truss becomes extremely small or large suddenly. The slack possibility of wire, the variable stiffness of SMA and relatively small stiffness property of wire members contribute to the vibration isolation effect of the truss structure. The RMS value of displacement in Figure 3.10(b) is 0.022m, which is smaller than the RMS value of displacement in Figure 3.7(a), which is 0.026m. These RMS values corresponding to the truss structures in Figures 3.2(b) and 3.10(a) indicate that an appropriate combination of SMA wires and ordinary wires plays an important role in the ability of truss structural system against environmental vibration from the vibration

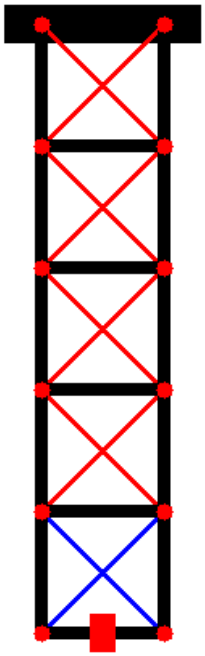

(a) Configuration

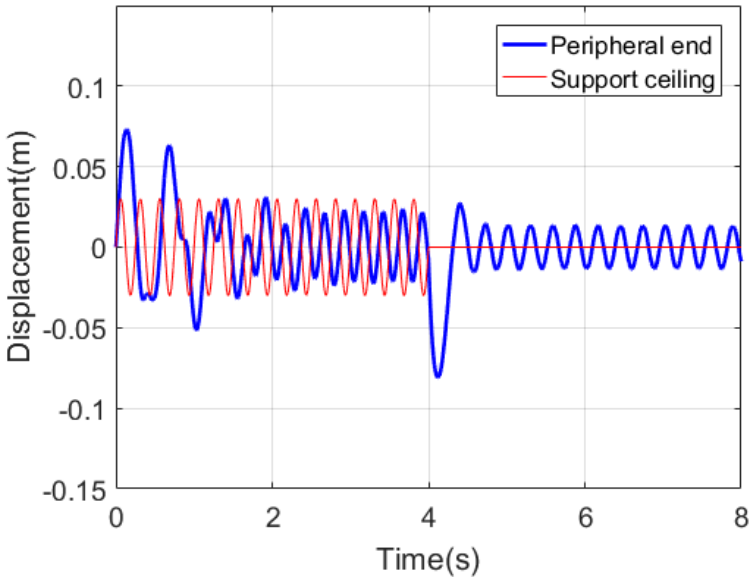

(b) Displacement behavior

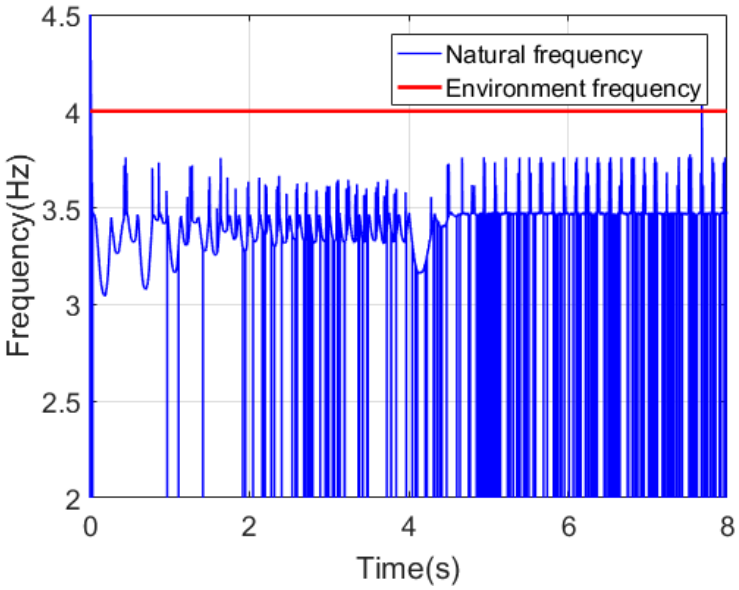

(c) Time history of natural frequency

Figure 3.10: Dynamic behavior of the truss having 8 SMA wires

isolation point of view in the case of being evaluated in terms of displacement criterion.

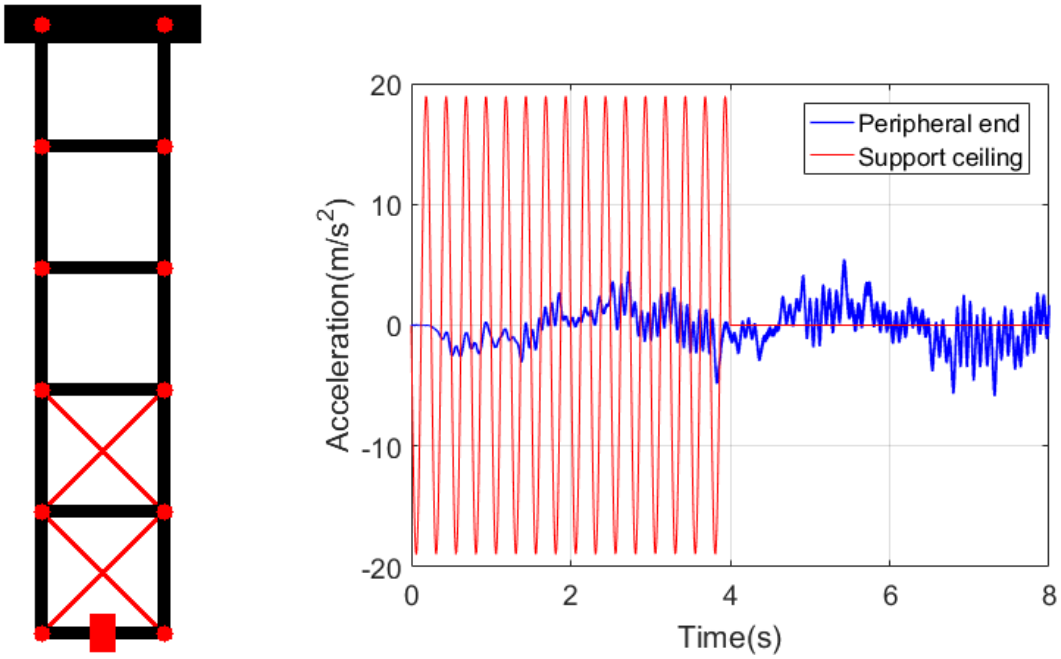

(a) Configuration (b) Dynamic behavior of the truss

Figure 3.11: Dynamic behavior of the truss having 4 SMA wires

3.5. Truss Units with and without SMA Wires

Hanging configuration of unstable mechanism has the effect that it can isolate its peripheral end from the support ceiling vibration under the vibration condition of small amplitude and relatively high frequency. However, the passive vibration control effect is often not very efficient by using pure passive isolation techniques [56]. It is necessary to apply material with the capability of consuming energy, such as SMA material. There are two main purposes for using SMA in isolation devices. Firstly, it helps the isolation device to withstand large deformations by increasing the lateral stiffness of the device. Secondly, it brings back the isolation device to its original position [25]. Combination of unstable mechanism in hanging configuration and the mechanical characteristics of SMA wire is expected to improve this vibration isolation capability. The following example is adopted to demonstrate this phenomenon.

The result in Figure 3.11(b) is the acceleration behavior of the truss in Figure 3.11(a). In order to make a comparison in the time period of 0s-4s between the truss in Figure 3.2(a) and the truss in Figure 3.11(a), the same vibration condition is adopted. In addition, the configuration is the same as well except for the 4 SMA wires in Figure 3.11(a). We discuss the vibration isolation effect of 0s-4s in the results shown in Figures 3.4 and 3.11(b). The RMS values of the

time period of 0s-4s in Figures 3.4 and 3.11(b) are 1.57m/s^2 and 1.45m/s^2, respectively. These two values illustrate that with appropriate arrangement of SMA wires, the vibration isolation effect can be improved.

3.6. Summary

In this chapter, we discussed the dynamic behaviors of the hanging truss structural system having SMA wires and ordinary wires. The typical characteristics of the truss structures have been shown by displaying the hanging truss having no bracing members, having SMA bracing wire members and having ordinary wire members. The hanging truss structure without bracing wire members is able to suppress the vibration transmission from support ceiling to the peripheral end resembles the characteristics of pendulum structure. Hanging truss structure is able to attenuate the vibration energy due to the conspicuous characteristic of pseudo-elasticity of SMA wire members. The ordinary wire members contribute to relative stability of the truss structure from the deformation point of view.

Combination of SMA wire as well as ordinary wire demonstrates vibration attenuation and relative stability from the deformation point of view. Combination of truss units with and without SMA wires shows vibration isolation and attenuation capabilities from the acceleration viewpoint due to the vibration transmission suppression by the truss units without bracing wire members and vibration absorption by the truss units having SMA wire members.

Chapter 4

Optimization Problems

4.1. Introduction

In this chapter, several optimization problems are taken into account. We have demonstrated in chapter 3 that the hanging truss structure having a number of SMA wires demonstrates vibration isolation and attenuation capabilities. From this viewpoint, optimization is conducted for the purpose of obtaining the best configurations of the SMA wires. Reducing unnecessarily large numbers of bracings is of great interest to make a design cost-effective [57]. In the current problem, vibration attenuation effect is sufficient in case of large number of SMA wire members; however, the amount of vibration transmission energy increases in such cases. Therefore, appropriate number of SMA wire members plays a significant role in vibration attenuation because of those hysteretic loops and vibration isolation because of suppression of vibration transmission.

Truss structural system having SMA wire members as well as ordinary wire members shows both of the capabilities of vibration isolation and attenuation from the deformation point of view. Hysteretic loops of pseudo-elastic SMA wires attenuate the vibration energy and relative large stiffness of the bracing ordinary wire members contribute to stability of the truss structure. In the case of small strain state and slack state, the SMA wire members are replaceable to the ordinary wire members. From these considerations, the optimization problem is conducted in order to calculate the optimal configurations of the SMA wires and the ordinary wires under the constraint condition of the number of the SMA wires.

In the case that the sectional area of the bracing wire members are small, it is close to the situation that there are no braces. In the case that the sectional area of the bracing wire members are large, relative stability of the hanging truss can be shown from the deformation point of view. In addition, more exerted energy by the support ceiling can be attenuated by SMA wires with larger sectional area in the form of phase transformation strain energy due to

the hysteretic loop. Small sectional area of the bracing wire members near the support ceiling or peripheral end are benefit for vibration isolation just as the normal structures which have flexible connection between the basement and the objective structure. Therefore, both of the values and the distributions of the sectional area of the bracing wire members are significant for the dynamic characteristics of the hanging truss structure. The optimal sectional area of the SMA wire bracing members are obtained for the objectives of vibration isolation and attenuation.

4.2. Optimization Problem Description

In this section, a combinatorial optimization on the configuration of SMA wire members is dealt with using a GA-based method from the viewpoints of vibration isolation and attenuation under the constraint condition of the number of the SMA wires. Traditional gradient-based optimization approach can not cope with the optimization problem with discontinuous design variables. GA-based optimization method with stochastic search approach is able deal with this kind of problem appropriately. The evolutionary process of NSGA-based method which contains the elite preservation strategy is demonstrated. In order to reduce the calculation time, a method coupled with the evolutionary optimal algorithm is proposed. The crossover operator and the mutation operator coping with the constraint condition of the number of the SMA wires are proposed. The relationships between the placement of the SMA wire members and the objective functions are discussed. The appropriateness of the proposed optimal calculation algorithm has been confirmed by the simulated examples.

4.2.1 Formulation of Objective Functions

The objective functions are formulated as the RMS values of the horizontal acceleration of the apparatus assumed at the peripheral end. The vibration isolation and attenuation capabilities are respectively evaluated in terms of the acceleration during and after the vibratory motion of the support ceiling and are expressed as follows:

$$\begin{aligned} W_k &= \left(\frac{1}{T_E} \int_{t=0}^{t=T_E} a_p^2 \mathrm{d}t \right)^{(1/2)} \\ V_k &= \left(\frac{1}{T_C} \int_{t=T_E}^{t=T_E+T_C} a_p^2 \mathrm{d}t \right)^{(1/2)} \end{aligned} \tag{4.1}$$

where T_E is the time period of the vibratory motion of the support ceiling and T_C is the evaluation time period after the vibration ceased. Subscript k reflects the number of SMA wires installed in the truss. Parameter a_p is the acceleration of the apparatus in horizontal direction.

4.2.2 Optimization of Configuration of SMA Wires

In case of the fixed number of SMA wire members, the vibration isolation and attenuation effects of the hanging truss structural system are significantly influenced by the distribution of the SMA wire members. In order to take account of this multi-objective optimization problem, we deal with the following minimization problem based on the multi-objective function:

$$\begin{aligned} &\text{Minimize } F = F(W_k, V_k) \\ &\quad \text{with respect to } P_{k(1)}, P_{k(2)}, ..., P_{k(v)}, ..., P_{k(N_k)} \end{aligned} \tag{4.2}$$

where F is the Pareto ranking value of the two objective functions. Pareto ranking describes the relationship of predominance among all of the values in the Pareto solutions and the process for determining the Pareto ranking values is as follows:

step 1: Set $r = 1$.

step 2: Find all the non-dominated designs. They are referred to as the rth Pareto front.

step 3: Eliminate the rth Pareto front.

step 4: Repeat from step 2 until all the designs are eliminated, with $r \leftarrow r + 1$.

The non-dominant design is explained as follows: a point $\boldsymbol{y}^* \in \boldsymbol{Y}$ is called the non-dominated design if and only if there does not exist another point $\boldsymbol{y} \in \boldsymbol{Y}$ such that $\boldsymbol{Z}(\boldsymbol{y}) \leq \boldsymbol{Z}^*(\boldsymbol{y})$, with at least one $Z_q(\boldsymbol{y}) < Z_q(\boldsymbol{y}^*)$ for minimization problem [58]. The process for the determination of the non-dominated designs can refer to Appendix 4.A. Parameter $P_{k(v)}$ is the vth combinatorial pattern of k-SMA-wire case. Parameter N_k is the total number of the installation patterns of k SMA wires. Design variable $P_{k(v)}$ is expressed in the following binary form as:

$$P_{k(v)} = [b_1\ b_2\ \cdots\ b_{2B}],\ b_i = \begin{cases} 0 \text{ (no wire)} \\ 1 \text{ (SMA wire)} \end{cases}$$

Note that the number of $'1'$ bits in $P_{k(v)}$ is constrained to k. The bit length K corresponds to the maximum possible number of SMA wires, where $K = 2B$ and B is the number of bays of the truss in the current study.

4.2.3 Optimization Approach

In this subsection, a NSGA-based multi-objective optimization approach is used [42]. This approach uses the elite preservation strategy. The constraint condition is the number of the SMA wires. The algorithm is shown as follows:

step 1: Prepare N_{pop} individuals as parent population. Generation $G = 1$.

step 2: Evaluate W_k and V_k.

step 3:

(1) $G = 1$: Determine the rank values.

(2) $G > 1$: Select N_{pop} individuals as parent population in G from the offspring and parent population in $G - 1$ based on the order of rank values.

step 4: Perform crossover and mutation operators to generate the offspring population in G.

step 5: Repeat from step 2 to step 4.

The probability of selection of the wth individual [59] in the process of roulette is expressed as:

$$P_w = \frac{F_w - (F_{max} + 1)}{\Sigma_{w=1}^{N_{pop}} \{F_w - (F_{max} + 1)\}} \tag{4.3}$$

where parameter F_w is the Pareto ranking value of the wth individual, parameter F_{max} is the total number of layers of the Pareto fronts which can be attained on the basis of the determination process of the Pareto front ranking as in section 4.2.2. In order that the rearmost layer of the Pareto front can be selected, we plus 1 to F_{max} as in Equation 4.3.

Since we take into account the fixed number of SMA wires of the truss as the constraint condition, the numbers of $'1'$ and $'0'$ bits of the resultant offspring have to be maintained. We

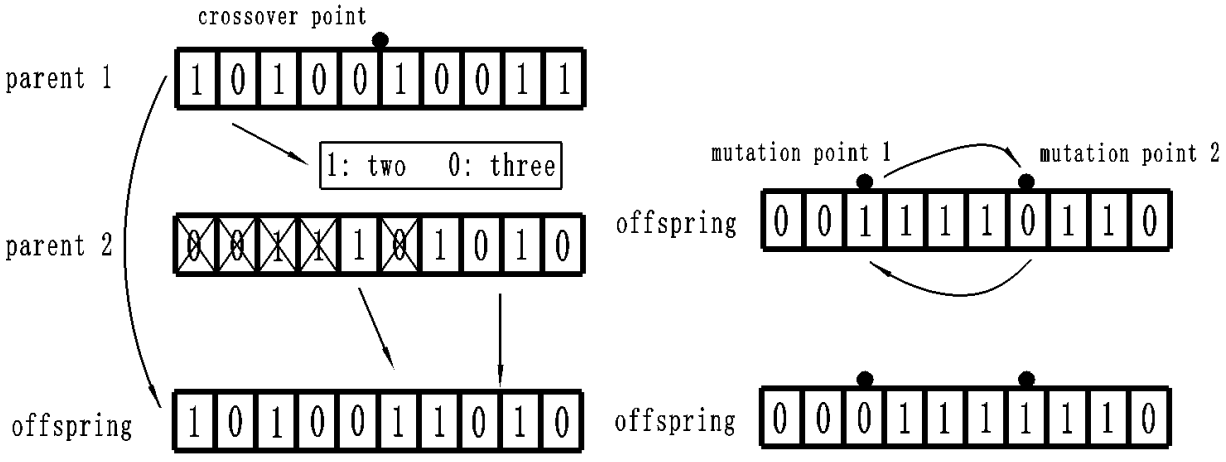

(a) Crossover (b) Mutation

Figure 4.1: Proposed operators

introduce the following crossover and mutation operators to cope with the situation. Figure 4.1 illustrates these operations. The crossover operation shown in Figure 4.1(a) is as follows:

step 1: Determine the crossover point randomly in parent 1.

step 2: Replicate the left part of the crossover point of parent 1 to the left part of the offspring.

step 3: Cancel the same numbers of 1 and 0 bits of the replicated part from the left part of parent 2.

step 4: Transfer the rest bits of parent 2 to the right part of the offspring in accordance with the order.

The mutation operation is performed as shown in Figure 4.1(b) and expressed as:

step 1: Determine the positions of 1 and 0 of the offspring.

step 2: Choose a position of 1 and a position of 0 randomly.

step 3: Change the positions of the selected 1 and 0.

For the purpose of reducing the calculation time of the optimization process, we propose a method for dealing with this situation. All of the individual bit patterns appeared in the course of calculation are recorded along with the corresponding values of the objective functions. Evaluation of the objective functions are performed based on the record in the case that the pattern to be evaluated is already in the record.

4.3. Truss with or without SMA Wires

With the constraint condition of the fixed number of bracing SMA wires, the optimal design is conducted by means of the NSGA from the viewpoints of vibration isolation and attenuation. Vibration isolation and attenuation effects are evaluated by the RMS values of acceleration in the time periods of 0s − 4s and 4s − 8s, respectively. The optimal designs for the cases of constraint condition of SMA wires, $k = 2, 4, 6, 8, 10$ are conducted. Parameters of the materials of rigid body and SMA in this chapter are the same as in Chapter 3. Vibration frequency of the support ceiling is 5Hz and the amplitude is 0.03m. Mass of the apparatus in the peripheral end is 5kg. In the calculation process, the parameters are as follows for the multi-objective genetic algorithm.

- Population size: $N_{pop} = 50$.
- Crossover probability: $P_{cr} = 0.8$.

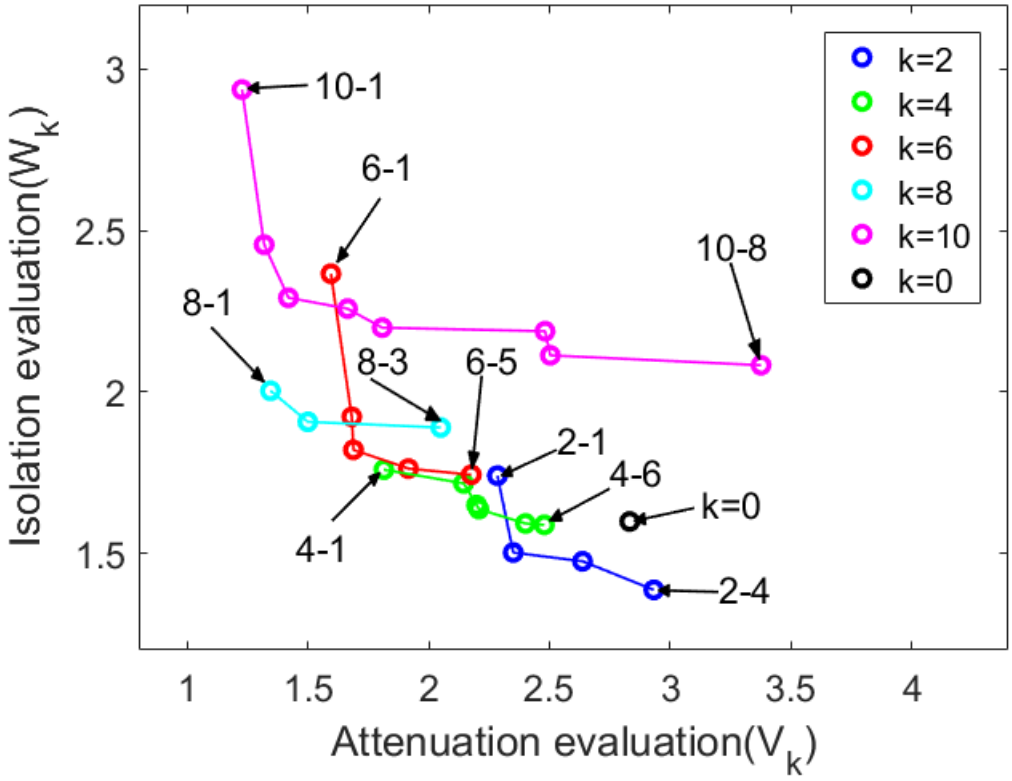

Figure 4.2: Pareto solutions with the conditions of $k = 0, 2, 4, 6, 8, 10$

- Mutation probability: $P_{mu} = 0.01$.
- Evolution generation: $N_{gen} = 100$.

4.3.1 Pareto Fronts and Numbers of SMA Wires

Pareto front solutions with the constraint conditions of $k = 2, 4, 6, 8, 10$ are shown in Figure 4.2. The abscissa axis is the RMS value in the time period of 4s − 8s, which describes the objective function of vibration attenuation; the ordinate axis is the RMS value in the time period of 0s−4s, which describes the objective function of vibration isolation. The attached label $k - c$ denotes the optimized configurations in Figure 4.3. Label c means the number of the configuration in the case of k SMA wires. For example, $10 - 1$ is the coordinate of the objective functions of the first optimized configuration with 10 SMA wires that is shown as in Figure 4.2 and the corresponding truss is shown in Figure 4.3(s) with the label. For the sake of avoiding untidiness, only the first and the last labels are indicated for each of the Pareto fronts in Figure 4.2. The solutions listed from the left to the right in the Pareto fronts in Figure 4.2 with $k - *$ correspond

to the truss configurations from the left to the right in Figure 4.3 with $k - *$, respectively.

We can see that the moving tendency of Pareto front with different values of k is that the Pareto front moves from the lower right to the upper left in accordance with the increase of the number of SMA bracing wires. Truss structures in case of small number of SMA wire members show more advantage in vibration isolation and less advantage in vibration attenuation and in case of relatively large number of SMA wire members demonstrate opposite effects.

4.3.2 Influence of Configurations of SMA Wires

In Figure 4.2, we can see that the vibration isolation effect when $k = 0$ is excellent but its vibration attenuation effect is worse than most of other solutions. This demonstrates the capability of vibration attenuation of the bracing SMA wires. However, the solution $k = 0$ dominates the solution $10 - 8$. It means that both of the vibration isolation and vibration attenuation effects for the case of $k = 0$ is better than the solution $10 - 8$. This indicates that an unsuitable placement of SMA wires does not contribute to the vibration attenuation capability even in the case of large number of SMA wires. This is due to the unattenuated vibration energy transmitted from the support ceiling to the peripheral end. In addition, the vibration isolation capability due to the pendulum effect of the hanging truss is hindered by the SMA wires in such a case. These conclude that appropriate placement of bracing SMA wires is quite significant for the performance of this truss structure from the viewpoints of vibration isolation and attenuation.

4.3.3 Influence of Number of SMA Wires

On the basis of the values of criteria given in Figure 4.2, the optimal designs have better vibration attenuation capability in the case of more SMA wires. In contrast to that, the vibration isolation capability becomes more ineffective in accordance with the number of SMA wires in general. It should be noted, however, that the result of trusses in Figures 4.3(b) and 4.3(c) corresponding to the solutions $2 - 2$ and $2 - 3$ show better performance in both attenuation and isolation capabilities than the truss having no SMA wires.

Even in the case of small number of SMA wires, the residual vibration is destined to be attenuated due to energy absorption by the hysteretic loop of pseudo-elastic SMA wires. Thus, the RMS value of the trusses in Figures 4.3(b) and 4.3(c) after the vibration of the support ceiling ceased are smaller than the truss having no SMA wires. The hysteretic loop of the SMA wire also contributes to vibration isolation due to phase transformation strain energy consumption. The vibration transmission due to the bracing SMA wire members is attenuated by the hysteretic loops in the time period of vibration of the support ceiling. The RMS values of these

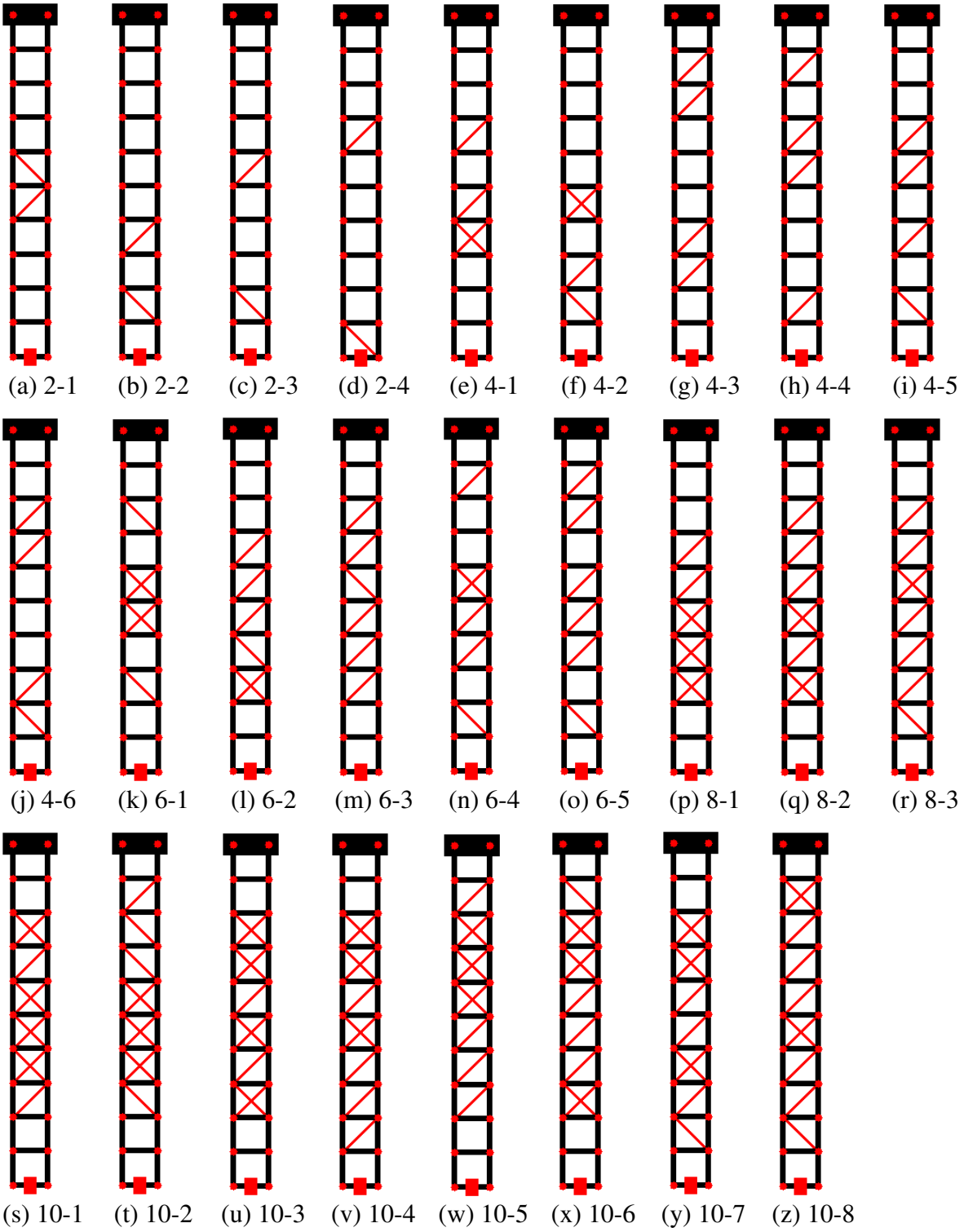

Figure 4.3: Optimal configurations of the truss

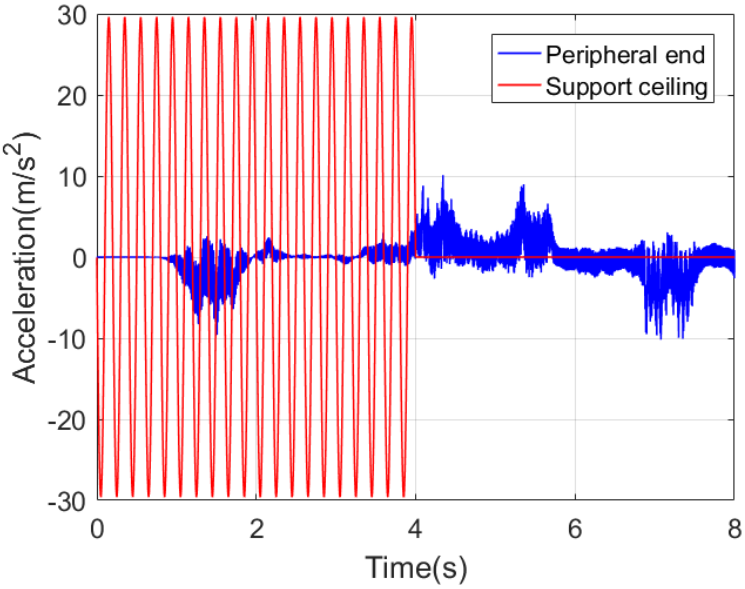

Figure 4.4: Acceleration behaviors of the truss structure in Figure 4.3(b)

two configurations are smaller than the truss having no SMA wires. The trade-off relationship between the vibration transmission by the bracing members and the energy consumption by the hysteretic loop of the SMA wires can be understood. Suitable number of SMA wires is significant for the performance of the hanging truss against the environmental vibration.

4.3.4 Overall Tendency of Optimal Configurations

All of these optimal configurations in Figure 4.3 have two common features. One is that there are no SMA wire members in the truss units which are near the support ceiling or near the apparatus except for the configuration in Figure 4.3(d). This is a typical feature of structural system for the suppression of vibration transmission from basement to the objective structure by flexible connections at the basement as well as at its peripheral end. The vibration transmission from the ceiling to the truss and from the truss to the peripheral end are suppressed in the case that there are no bracing wire members in the truss unit near the peripheral end as well as the support ceiling. On the basis of this kind of arrangement, the vibration transmission from the support ceiling to the peripheral end can be suppressed due to the effect of pendulum and the energy exerted by the ceiling can be absorbed due to the SMA wire members in the middle truss units simultaneously.

The other common feature is that with an emphasis on vibration isolation, the placement of the SMA wire members becomes approximately more and more decentralized as shown in

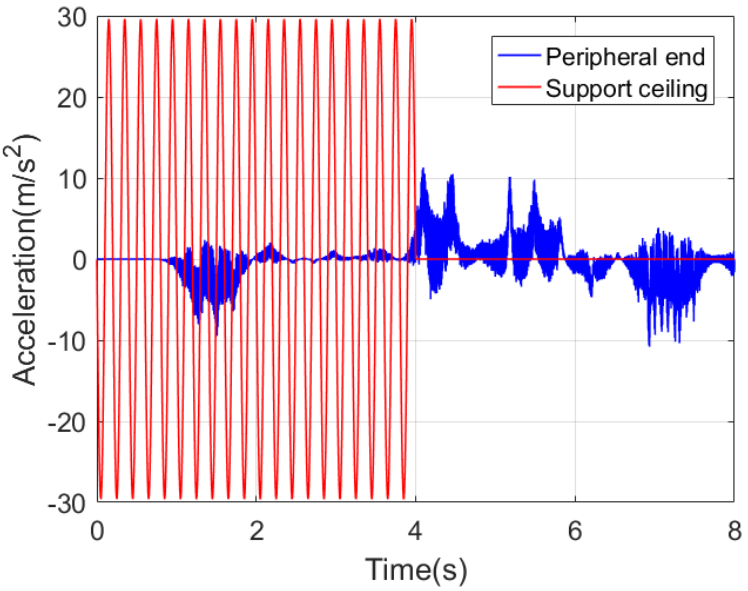

Figure 4.5: Acceleration behaviors of the truss structure in Figure 4.3(c)

Figure 4.3. Owing to the hanging truss structures with ubiquitously distributed placement of the SMA wires, more truss nodes are influenced by the force of the SMA wire members. The residual vibration becomes more significant in such distributions due to more nodes are influenced by the stiff SMA wires in the pure austenite phase. The energy absorption for the attenuation is not sufficient in such cases. On the contrary, in the case of intensively distributed placement of the SMA wires, vibration transmission becomes non-significantly due to less truss nodes are affected by the force of the bracing members and less vibration energy can be transmitted to the peripheral end. Thus, the RMS values of these trusses become smaller relative to the trusses with ubiquitously distributed SMA wires after the vibration of the support ceiling ceased.

In all of these optimal configurations, the number of right-up diagonal SMA wires is significantly larger than the number of right-down diagonal SMA wires. On the basis of the calculations, we noticed that in the time period of 0s-4s, in the cases that the number of the bracing wire members are small, the deformation of the right-up SMA wire is significantly larger than the deformation of the right-down SMA wires. More hysteretic loop can be utilized to consume the vibration energy in such configurations that the number of right-up diagonals is larger than the right-down diagonals.

Most of these optimal configurations demonstrate better vibration attenuation effects than the hanging truss having no bracing members since no energy consumption members are in the hanging truss without SMA wire members. A few number of the optimal configurations with larger RMS values than the hanging truss having no SMA wires after the vibration of the ceiling

ceased. The reason is that the vibration is transmitted by those bracing SMA wire members to the peripheral end; however, those transmitted vibration energy can not be totally attenuated due to the pure austenite phase of those SMA wire members after the vibration of the support ceiling ceased.

4.4. SMA and Ordinary Wire Combination

Optimization of dynamic behaviors of hanging truss structure having SMA wires as well as ordinary wires are dealt with in this section. In the case of statical indeterminacy of the hanging truss topology, the effect of the hanging configuration is not remarkable. The optimization formulation and the optimization algorithm are the same as the section 4.2. The crossover operation and mutation operation can be considered the same as the operators in section 4.2. Vibration attenuation is achieved by utilizing the pseudo-elastic SMA wires. In case of slack state or small strain (pure austenite) state, the SMA wires can be replaceable to the ordinary wires from material saving viewpoint. Moreover, relative large stiffness of the ordinary wire members contributes to vibration isolation from the deformation point of view.

4.4.1 Formulations of Objective Functions

Effect of vibration isolation is evaluated in terms of the difference of the maximum displacement on the right and on the left of the peripheral end node of the truss, throughout the vibration period of the support ceiling. The maximum amplitude of the peripheral end nodal point in horizontal direction on the right side and left side in that time period are denoted as A_{IR} and A_{IL} respectively, the objective function for vibration isolation can be determined by:

$$W = \frac{A_{IR} - A_{IL}}{2A_C} \tag{4.4}$$

where parameter A_C is the amplitude of the vibration motion of the ceiling.

The objective function for vibration attenuation is evaluated during a period of time after support ceiling ceased. The maximum displacement of the peripheral end nodal point in horizontal direction on the right side and the maximum displacement on the left side are denoted as A_{AR} and A_{AL} respectively. The objective function for vibration attenuation can be calculated as:

$$V = \frac{A_{AR} - A_{AL}}{A_C} \tag{4.5}$$

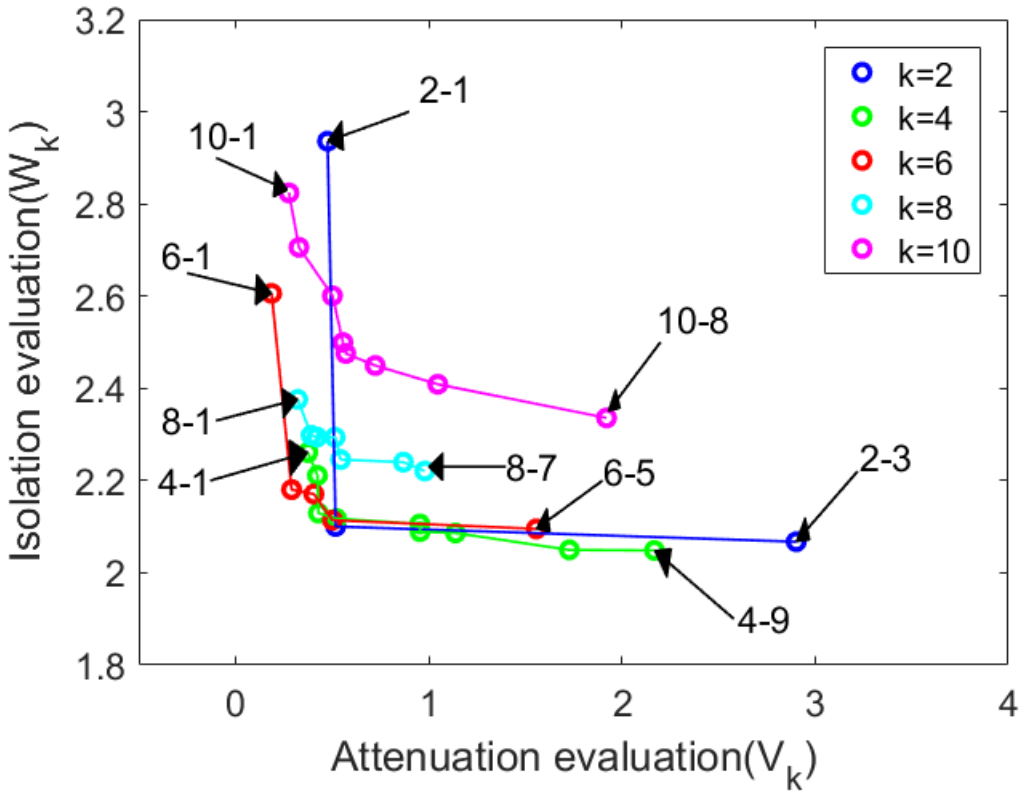

Figure 4.6: Pareto solutions with the conditions of $k = 2, 4, 6, 8, 10$

4.4.2 Influence of Numbers of SMA Wires

The Pareto front solutions with constraint condition of $k = 2, 4, 6, 8, 10$ are shown in Figure 4.6. The abscissa axis is the attenuation evaluation function and the ordinate axis is the isolation evaluation function by the criterion of deformation. The same as in section 4.2, we use the label $k - c$ to represent the optimized configurations that shown as in Figure 4.6.

The attenuation capability of the trusses in case of $k = 6$ are more effective than the trusses in case of $k = 4$, and the isolation capability of the trusses in case of $k = 4$ are more effective than the trusses in case of $k = 6$ in generally. This is due to the relative large stiffness of the ordinary wire members. The deformations of the truss in case of small number of SMA wire members are small in the time period of vibration of the support ceiling. Therefore, vibration isolation in case of small number of SMA wire members is more efficient generally. However, vibration attenuation capability in case of large number of SMA wire members is more effective due to more energy can be attenuated by the hysteretic loop of the bracing SMA wire members.

4.4.3 Influence of Configurations of SMA Wires

The behaviors of the solutions $2-1$ and $2-2$ are tremendously different. Their displacement behaviors are shown in Figure 4.8. The vibration attenuation performances of these two trusses are approximately same; however, the vibration isolation performances are significantly different. The vibration amplitude of the truss $2-1$ in the period of 0s-4s is larger than the vibration amplitude of the truss $2-2$. Although these two truss structures have the same number of SMA wire and ordinary wire members, in case of different configurations, the dynamic behaviors are tremendously different.

The exerted forces of the members near the support ceiling are larger than the members near the peripheral end. The positions of the two SMA wire members in the truss $2-1$ are closer to the support ceiling compared with the two SMA wire members in the truss $2-2$. In the time period of 0s-4s, as can be seen in Figure 4.9, the deformations of the two SMA wire members in the truss $2-1$ are larger than that of the two SMA wire members in the truss $2-2$ on account of the small distances between the SMA wires and the support ceiling.

4.5. SMA Wire Section Optimization

Sectional area of the bracing SMA wire members of the hanging truss structure play a significant role in vibration isolation and attenuation. Vibration transmission does not occur significantly in case of thin bracing SMA wire members. Hence the vibration isolation effect is meliorated. Vibration transmission from the support ceiling to the peripheral end occur significantly in case of thick bracing SMA wire members; however, vibration attenuation capability due to energy absorption is sufficient. There is a trade-off relationship between vibration transmission and energy absorption taking account of the sectional area of the bracing SMA wire members. In this section, the optimal sectional area of the SMA wire bracing members are obtained for the objectives of vibration isolation and attenuation.

4.5.1 Formulation for the Sectional Area Optimization

The multi-objective optimization problem is as follows:

$$\begin{aligned} &\text{Minimize} \quad F = F(W, V) \\ &\quad \text{with respect to} \quad D_1, D_2, ..., D_i, ..., D_N \\ &\quad \text{Subject to} \quad D_{min} \leq D_i \leq D_{max} \end{aligned} \tag{4.6}$$

where the parameter D_i is the diameter of the ith SMA wire member. The maximum and minimum of the diameters of the bracing SMA wire members are denoted as D_{max} and D_{min} respectively. The continuous design variable is discretized by utilizing 16 bits binary code. For instance, D_{max} is expressed as 1111 1111 1111 1111 and D_{min} is expressed as 0000 0000 0000 0000. The diameter value of the ith member D_i is the interpolation of D_{max} and D_{min}.

4.5.2 Results of the Optimization Problem

Configuration of the hanging truss shown in Figure 4.10(a). The maximum diameter D_{max} and the minimum diameter D_{min} are assumed to be 2mm and 0mm, respectively. Result of the Pareto front is shown in Figure 4.10(b). We can see in the figure that the number of the optimal designs are 21. The corresponding optimal configurations from left to right in Figure 4.10(b) are denoted as C_1 to C_{21}, respectively. Figure 4.11 demonstrates the relative relationship of the sectional area values of the optimal solutions.

In all of the optimal solutions, the values of D_5, D_6, D_{11}, D_{18} and D_{20} are significantly smaller than the others. D_5 and D_{20} are approximate to zero. The sectional area in the truss units near the support ceiling as well as the peripheral end are small. This tendency is the same as the optimal configurations in section 4.2, where there are few bracing wires in the truss units near the support ceiling as well as the peripheral end. Under this kind of configurations, the vibration transmission from the support ceiling to the truss structure and from the truss structure to the peripheral end do not occur significantly. The residual vibration after the vibration of the support ceiling ceased is not sufficient.

The values of D_4, D_7, D_8 and D_{17} are significantly larger than the others. These large sectional area of the bracing SMA wire members are distributed in the middle part of the trusses. In addition, vibration energy exerted by the support ceiling can be attenuated in the form of phase transformation strain energy mainly by these SMA wire members.

The acceleration behaviors of the solutions of C_1, C_2, C_{15} and C_{21} are shown in Figure 4.12. These behaviors manifest that the differences of the behaviors among these optimal solutions are not significant. In the time periods of 0s-4s and 4s-8s, vibrations of the peripheral end are alleviated by such kind of optimal solutions. The values of the evaluation functions are as follows: $V_{C_1} = 0.41\text{m/s}^2$, $V_{C_2} = 0.43\text{m/s}^2$, $V_{C_{15}} = 0.62\text{m/s}^2$, $V_{C_{21}} = 0.76\text{m/s}^2$, $W_{C_1} = 1.43\text{m/s}^2$, $W_{C_2} = 1.42\text{m/s}^2$, $W_{C_{15}} = 1.33\text{m/s}^2$, $W_{C_{21}} = 1.25\text{m/s}^2$.

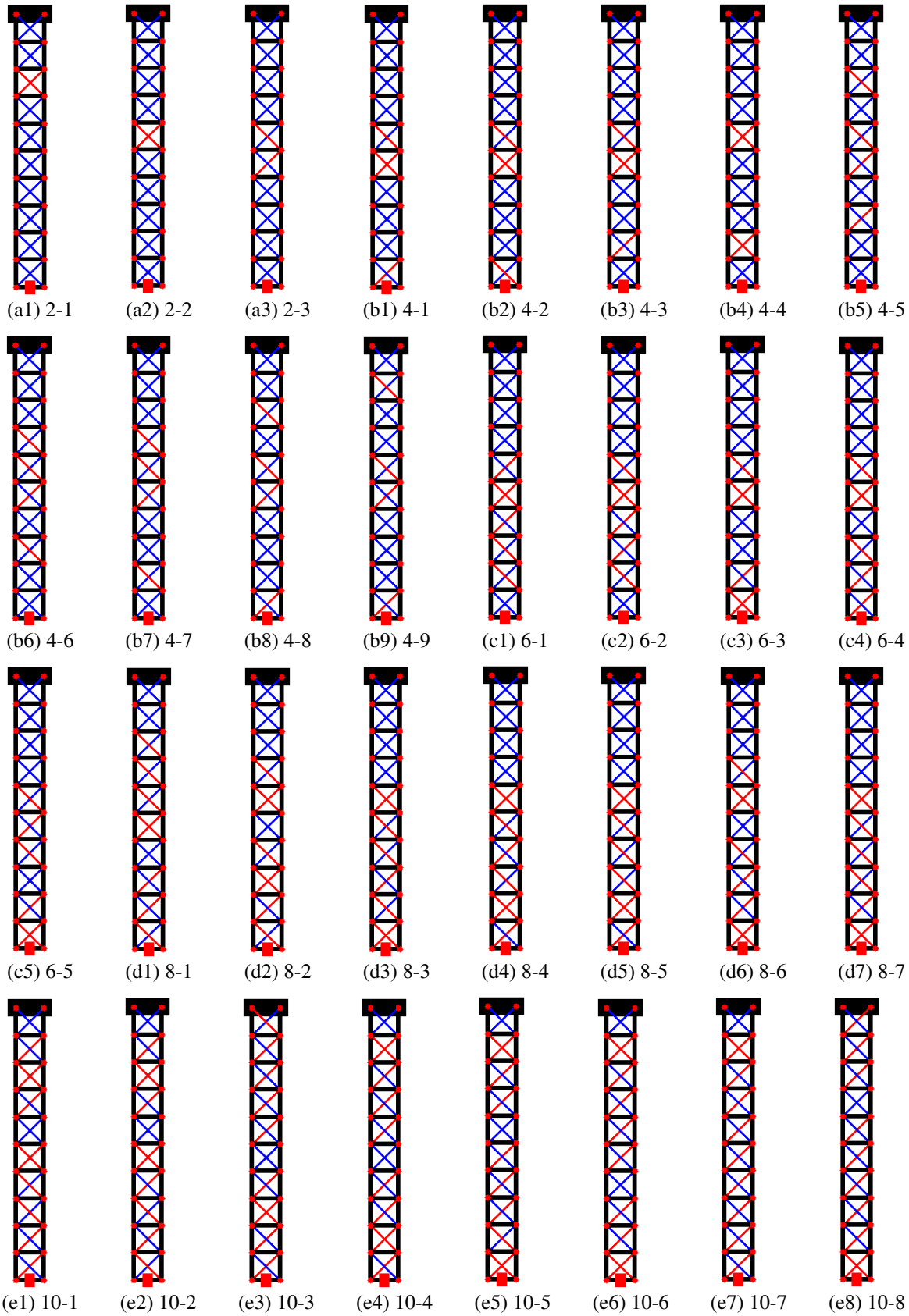

Figure 4.7: Optimal configurations of the truss

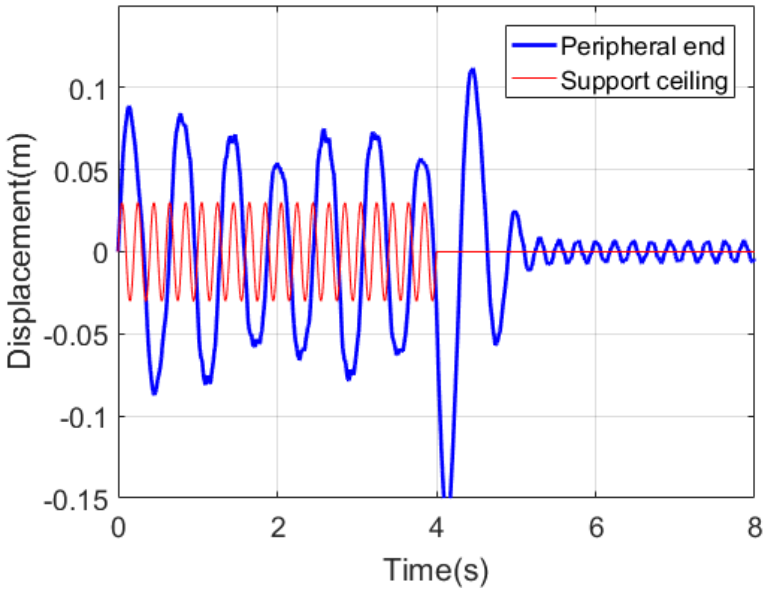

(a) Truss 2-1

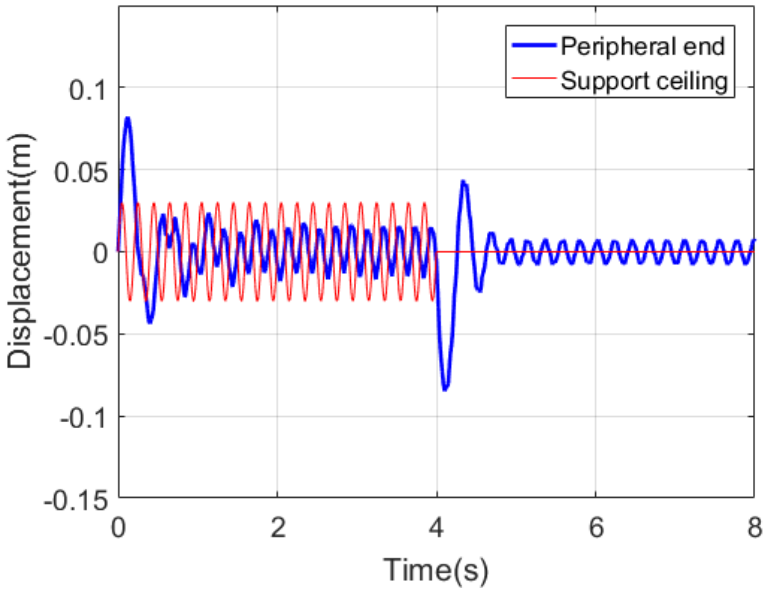

(b) Truss 2-2

Figure 4.8: Displacement behaviors of the truss structures

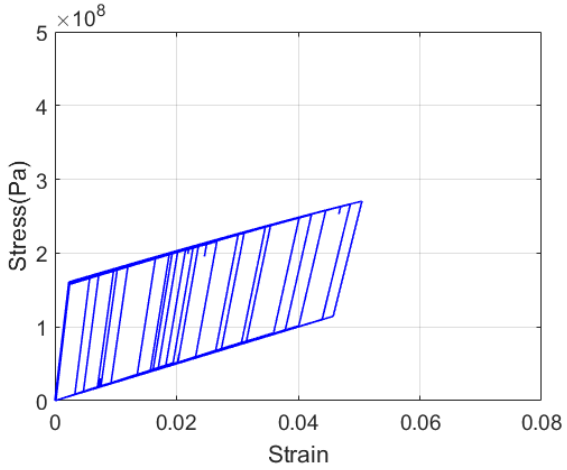

(a) Member 15 of truss 2-1

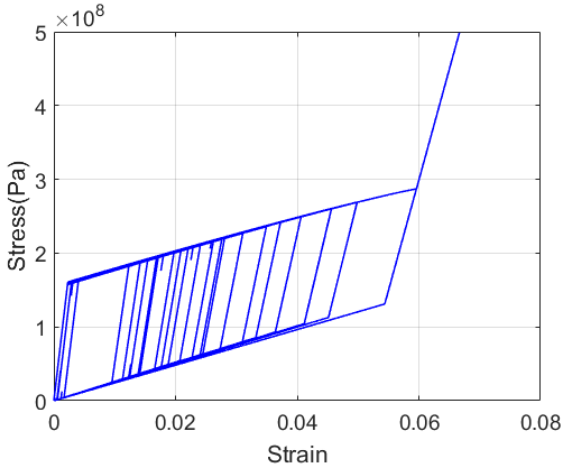

(b) Member 16 of truss 2-1

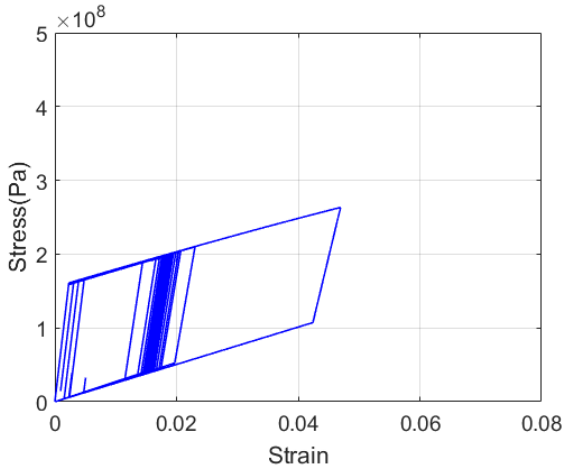

(c) Member 11 of truss 2-2

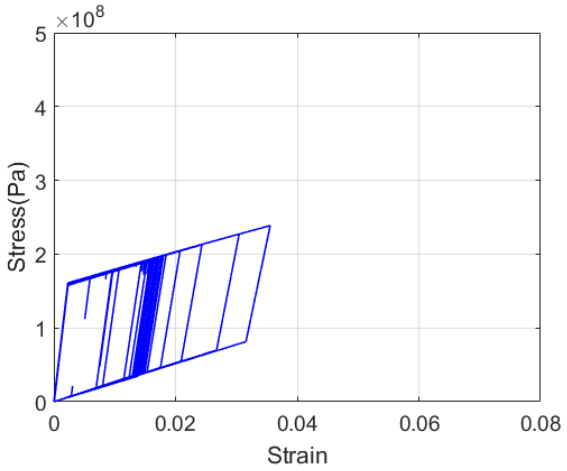

(d) Member 12 of truss 2-2

Figure 4.9: Stress-strain relations of the SMA wire members

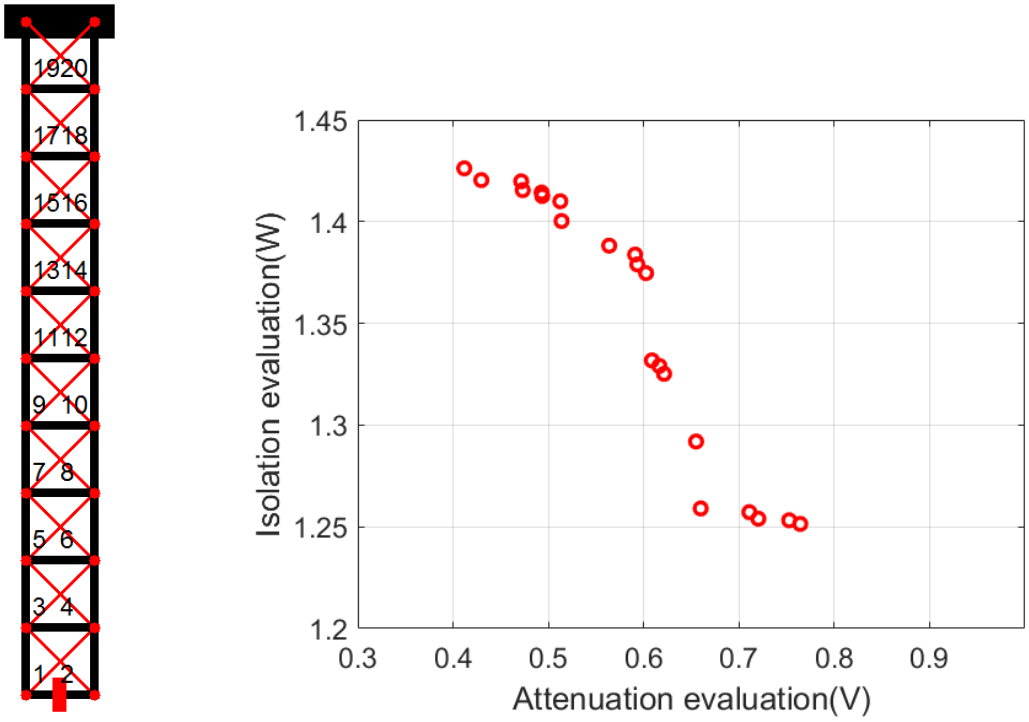

(a) Truss with number (b) Pareto front

Figure 4.10: Truss configuration and the Pareto front

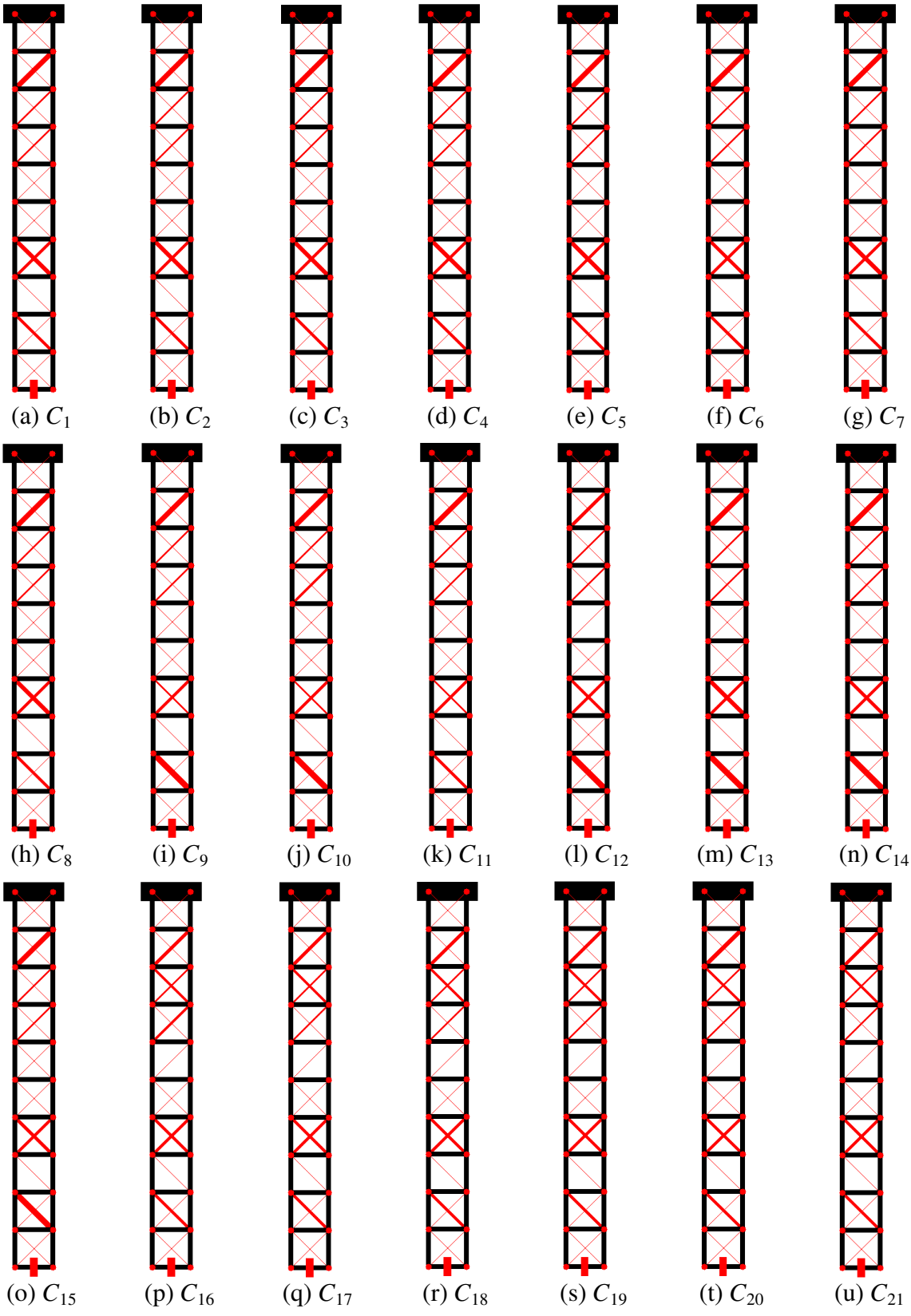

(a) C_1 (b) C_2 (c) C_3 (d) C_4 (e) C_5 (f) C_6 (g) C_7

(h) C_8 (i) C_9 (j) C_{10} (k) C_{11} (l) C_{12} (m) C_{13} (n) C_{14}

(o) C_{15} (p) C_{16} (q) C_{17} (r) C_{18} (s) C_{19} (t) C_{20} (u) C_{21}

Figure 4.11: Optimized configurations of the truss structures

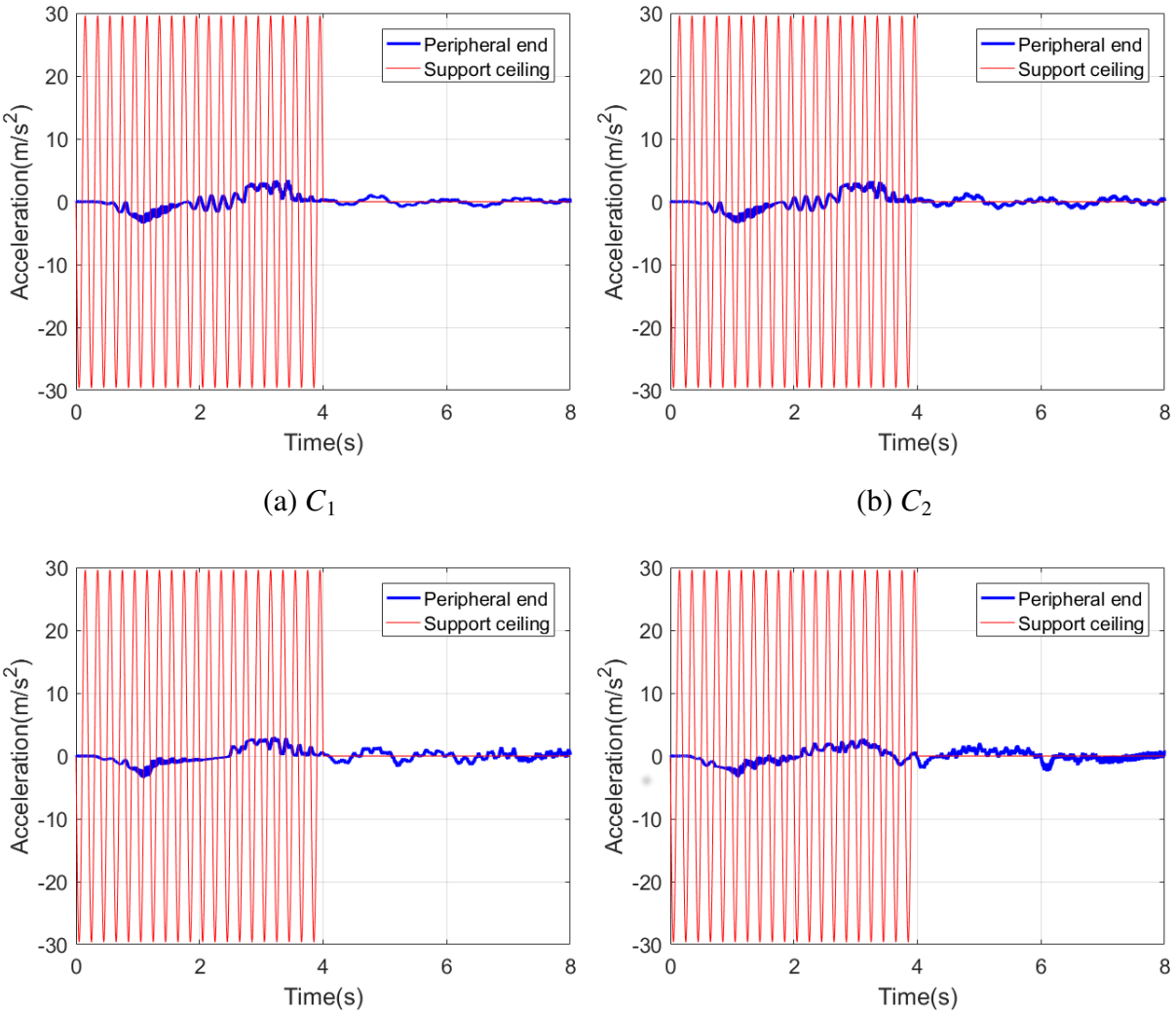

(a) C_1 (b) C_2

(c) C_{15} (d) C_{21}

Figure 4.12: Dynamic behaviors of the optimized truss stuctures

4.6. Summary

In this chapter, optimization problems have been dealt with from the vibration isolation and attenuation points of view. Combination of truss unit having SMA wire members and truss unit without SMA wire members are calculated. On the basis of the calculations, we obtained that most of the optimal configurations have one common feature that the SMA wires are placed significantly in the middle of the optimally designed trusses. The placements of SMA wires in optimal solutions show a tendency of decentralization in the case of emphasis on vibration isolation.

Combinatorial optimization problem is dealt with by combining the SMA wire members and the ordinary wire members. The objective functions are the deformations of the peripheral end apparatus. The number and the configuration of the SMA wire members are key factors that influence of the performance of the dynamic behaviors of the truss structure. Truss structure with small number of SMA wire members show more efficient vibration isolation effect due to the relative large stiffness of the ordinary members; truss structure with large number of SMA wire members show more efficient attenuation effect due to vibration absorption by the hysteretic loop of the SMA wires.

Optimization problem of hanging truss structural system having SMA wires is dealt with on the sectional area of the bracing SMA wire members. The obtained optimal solutions demonstrate the same tendency as the configuration optimization problem. The sectional area of the SMA wire members near the support ceiling as well as the peripheral end are small. This kind of distribution of the sectional area values is benefit for suppression of vibration transmission. Moreover, the transmitted vibration energy is absorbed by the SMA wires in the middle part of the truss structures due to the hysteretic loops.

Appendix 4.A Search of Non-Dominant Designs

The process for determining the non-dominated designs is as follows:

step 0: Determine the rank values in terms of V_k and W_k, respectively.

step 1: Denote the first individual as $n_I = 1$.

step 2: Find the individuals with higher ranks than n_I in terms of V_k and W_k, respectively.

step 3: If the individuals with higher rank in terms of $V_k(W_k)$ are also with higher rank in terms of $W_k(V_k)$ than n_I, then n_I is dominant. Otherwise, n_I is non-dominant.

step 4: Repeat from step 2 until all the designs are examined, with $n_I \leftarrow n_I + 1$.

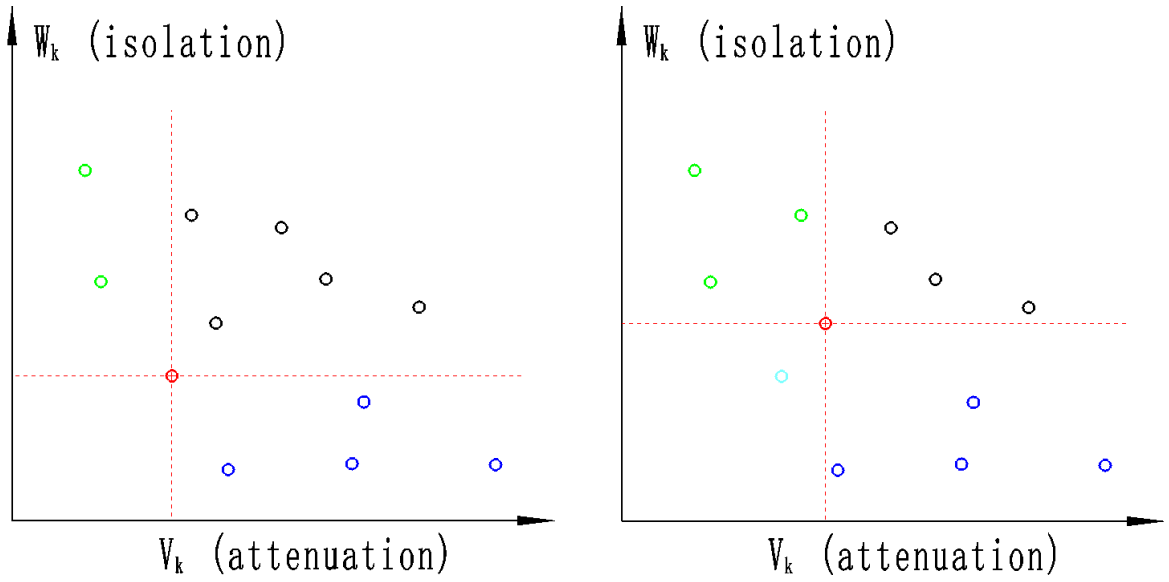

(a) Non-dominant design (b) Dominant design

Figure 4.13: Explanation for search of non-dominant designs

In Figure 4.13(a), the red circle is a non-dominant design. The black circles are represent the individuals that have lower rank values than the red circle. The blue circles represent the individuals with higher rank values in terms of W_k and lower rank values in terms of V_k than the red circle. The green circles represent the individuals with higher rank values in terms of V_k and lower rank values in terms of W_k than the red circle. In Figure 4.13(b), the red circle is a dominant design. The black, blue and green circles have the same meaning with Figure 4.13(a). The cyan circle represents the design with higher rank values than the red circle in terms of both of W_k and V_k.

Chapter 5

Several Other Dynamic Examples

5.1. Introduction

In the aforementioned contents, we have discussed the fundamental theories and models of the truss structural system having SMA wire members. In this chapter, several other examples on dynamics are demonstrated on this kind of truss structural system. The dynamic behaviors of three-dimensional truss are discussed. The influences of the sub-loop behavior of the SMA material on the dynamic characteristics of the truss structure are demonstrated. Dynamic behavior of a truss having SMA wires with cosine model is shown. Dynamic behaviors of truss structures with other topologies are discussed.

5.2. Three-Dimensional Truss

Figure 5.1(a) is a hanging truss structural system having no bracing wire members in three-dimension space. Figure 5.1(b) is the corresponding acceleration behavior in the vibration direction of the support ceiling. Vibration amplitude and frequency of the support ceiling are 5Hz and 0.05m, respectively. The mass of the apparatus in the peripheral end is 7.4kg. In Figure 5.1(b), we can see that vibration transmission from the support ceiling to the peripheral end is non-significant due to no bracing wire members or due to pendulum effect.

Figure 5.2(a) is a hanging truss structural system having SMA wire members in three-dimension space. Figure 5.2(b) is the corresponding acceleration behavior in the vibration direction of the support ceiling. Vibration conditions and the mass value of the apparatus are the same as in Figure 5.1.

In Figure 5.2(b), the vibration isolation effect is demonstrated; however, due to the influence of vibration transmission by the bracing SMA wire members, the isolation effect in Figure 5.2(b) is not significant compared with that of Figure 5.1(b). Vibration attenuation effect in

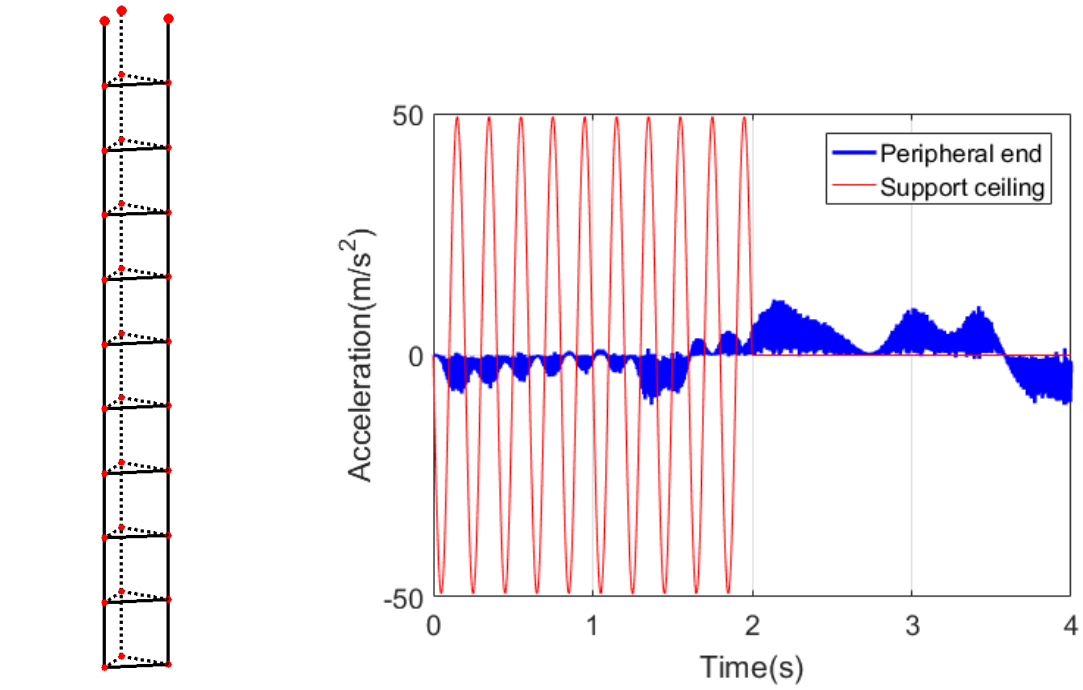

(a) Truss configuration (b) Acceleration behavior

Figure 5.1: Dynamic behavior of a hanging truss without bracing members

Figure 5.2(b) can be seen. The residual vibration can not be attenuated due to the unattenuated vibration transmitted from support ceiling to the peripheral end by the bracing SMA wire members.

5.3. Influence of the Sub-Loop Behavior

In order to make comparisons between the constitutive model with and without the sub-loop behavior, dynamic calculations are conducted. Figure 5.3(a) is the configuration of a hanging truss structure, the small red circles are the nodes of the truss, and the larger ones are assumed to be placed at the support ceiling. All of the diagonal members are SMA wire members and the others are rigid members. It is assumed that there is an apparatus supported at the tip end of the hanging truss and the mass value of the apparatus is 35.19kg. The mass value of the truss structural system without the apparatus is 14.99kg. Figure 5.3(b) is the dynamic motion of the support ceiling. The vibration amplitude and the vibration frequency of the support ceiling are 0.05m and 5Hz, respectively. Motion of the support ceiling is a sinusoidal wave which endures 2 seconds, and in the time period of $2 - 100$s, motion of the support ceiling ceased. Dynamic behaviors of the peripheral end in the direction of motion of the support ceiling is to

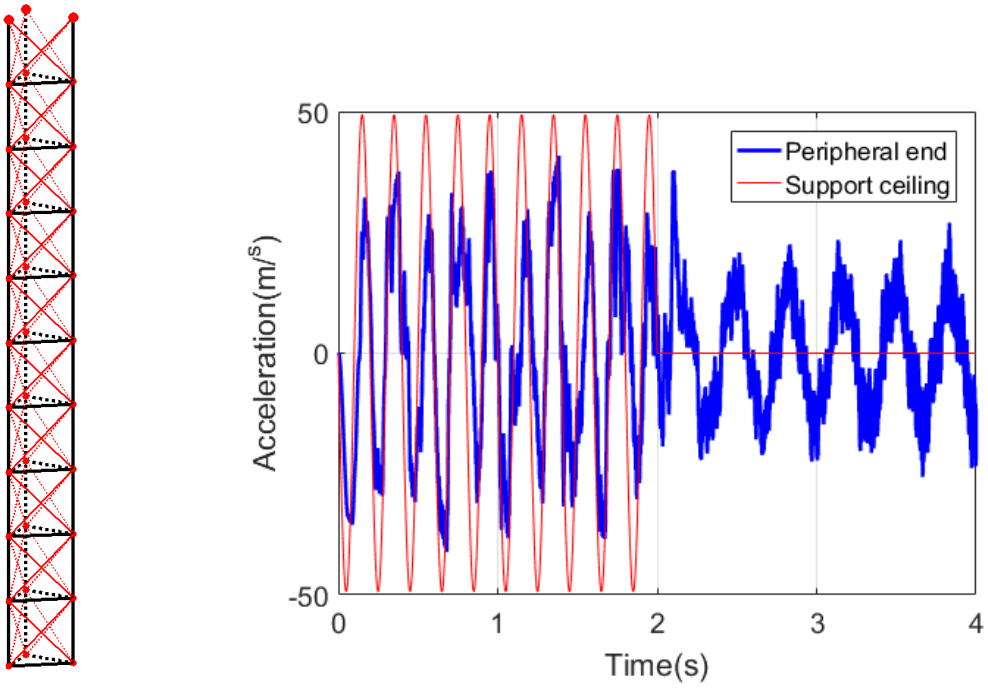

(a) Truss configuration (b) Acceleration behavior

Figure 5.2: Dynamic behavior of a hanging truss with SMA bracing members

Table 5.1: SMA characteristics

Maximum phase transformation strain	Λ	0.05
Young's modulus of austenite phase	E_A	70GPa
Young's modulus of martensite phase	E_M	30GPa
Martensite phase transformation start strain	ϵ_s^{MA}	0.0023
Martensite phase transformation finish strain	ϵ_f^{MA}	0.0596
Austenite phase transformation start strain	ϵ_s^{AM}	0.0544
Austenite phase transformation finish strain	ϵ_f^{AM}	0
Martensite phase transformation start stress	σ_s^{MA}	161MPa
Martensite phase transformation finish stress	σ_f^{MA}	287MPa
Austenite phase transformation start stress	σ_s^{AM}	131MPa
Austenite phase transformation finish stress	σ_f^{AM}	0MPa

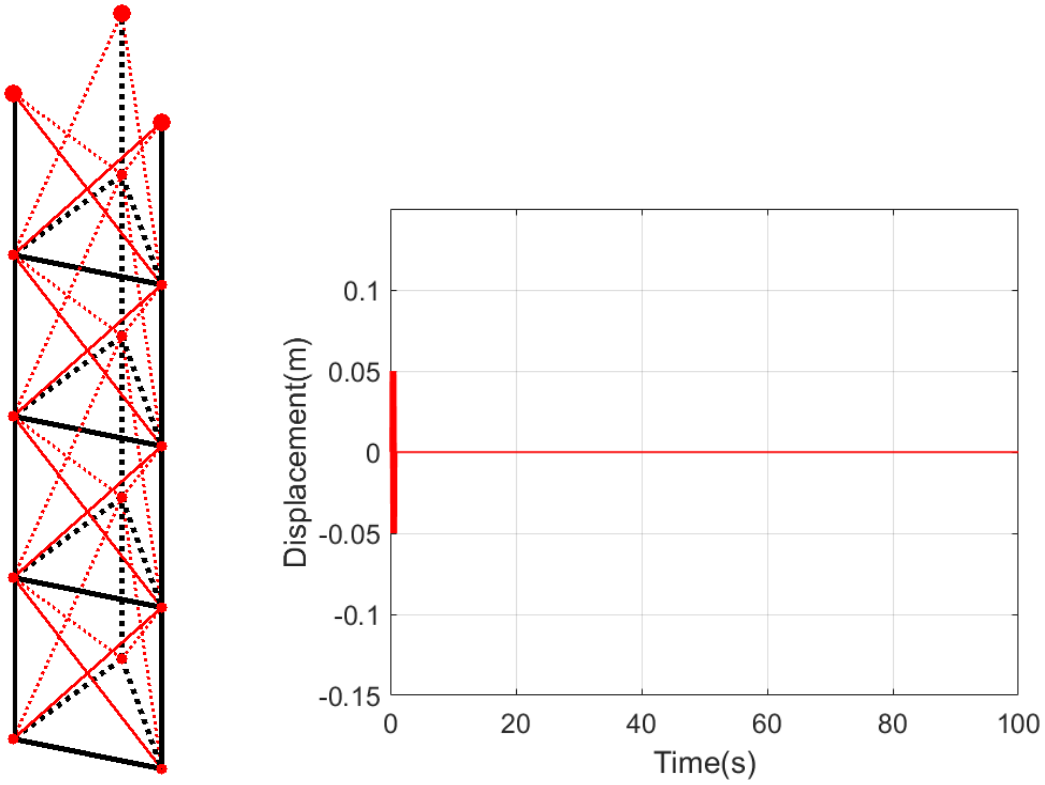

(a) Truss configuration (b) Horizontal dynamic motion

Figure 5.3: Configuration of the truss and the vibrational motion of support ceiling

be examined. Corresponding parameters for the simulations can be referred to [54]. Parameters for the SMA material are listed in Table 5.1 for both of the two constitutive models.

An SMA member must be under a state of stress in order to achieve high internal friction. Therefore, SMA members must be preloaded to a certain level if they are to be used as dampers [60]. The initial strains of the SMA wire members are set to be 0.03. Dynamic characteristics of the truss structure having SMA wires without and with sub-loop behaviors are shown in Figures 5.4(a) and 5.4(b). In the time period of $0 - 2$s, the characteristics of these two results are similar; however, when the motion of the support ceiling ceased, the energy exerted by the support ceiling are not absorbed in the result of Figure 5.4(a) completely; on the contrary, all the exerted energy has been absorbed in the result of Figure 5.4(b).

The result in Figure 5.4(b) reflects the pseudo-elasticity of the SMA material more sufficient due to the total attenuation of the energy. This is the contribution of the sub-loop behavior of the constitutive model of the SMA material as shown in Figure 5.5(b). Figures 5.5(a) and 5.5(b) are the stress-strain relationships of one of the SMA wire members in the truss structure of Figure 5.3(a) in the truss unit near the support ceiling. In Figure 5.5(a), the phase transformation occurs

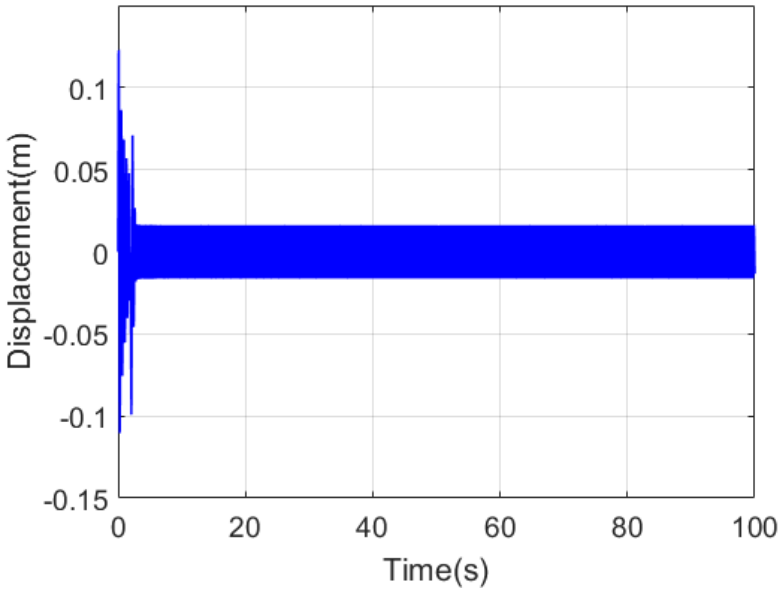

(a) Without sub-loop

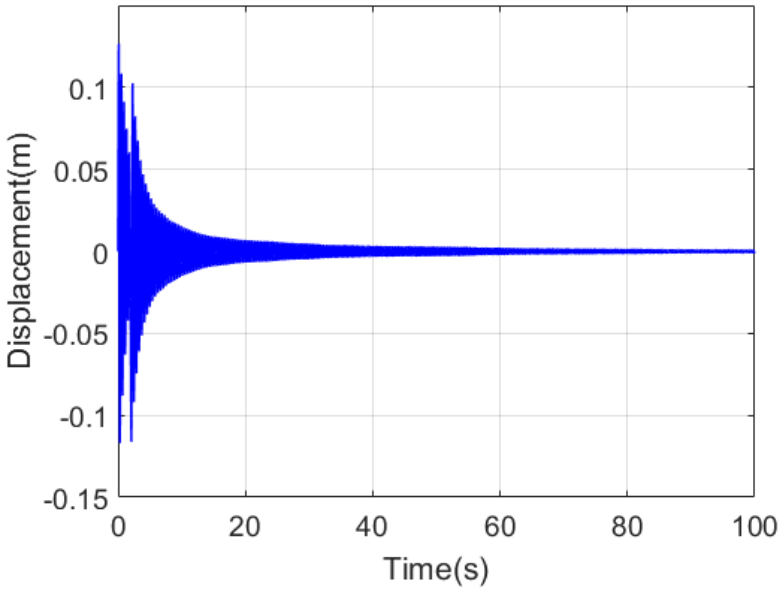

(b) With sub-loop

Figure 5.4: Displacement behaviors

only on the major loop of the forward and reverse phase transformations. Therefore, the energy can only be attenuated along the two lines in the major loop and can not be attenuated along the other lines, such as the pure austenite, pure martensite lines and the elastic area inside the

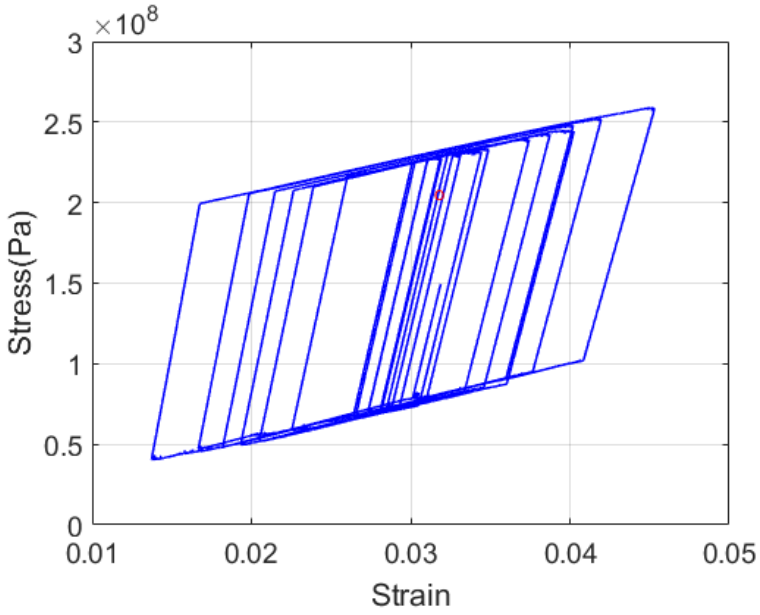

(a) Without sub-loop

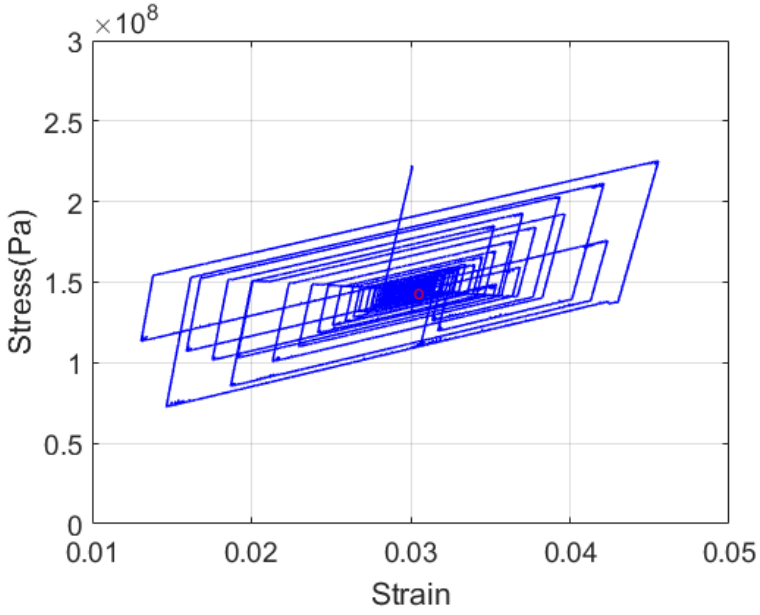

(b) With sub-loop

Figure 5.5: Time histories of constitutive relations of SMA wire member

major loop as shown in Figure 5.5(a). At the end of calculation, the behavior of the constitutive model arrives at the elastic area near the initial strain 0.03, which is denoted as a red circle in Figure 5.5(a). These elastic relations inside the major loop lead to the residual vibration of the

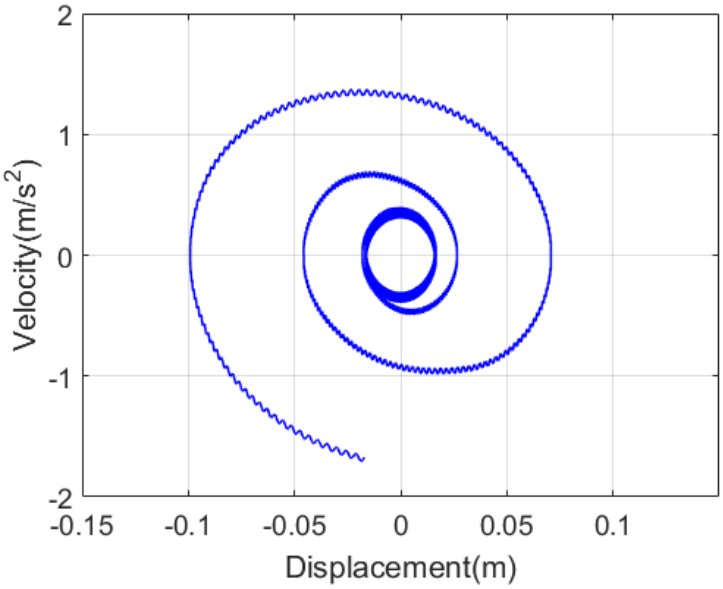

(a) Without sub-loop

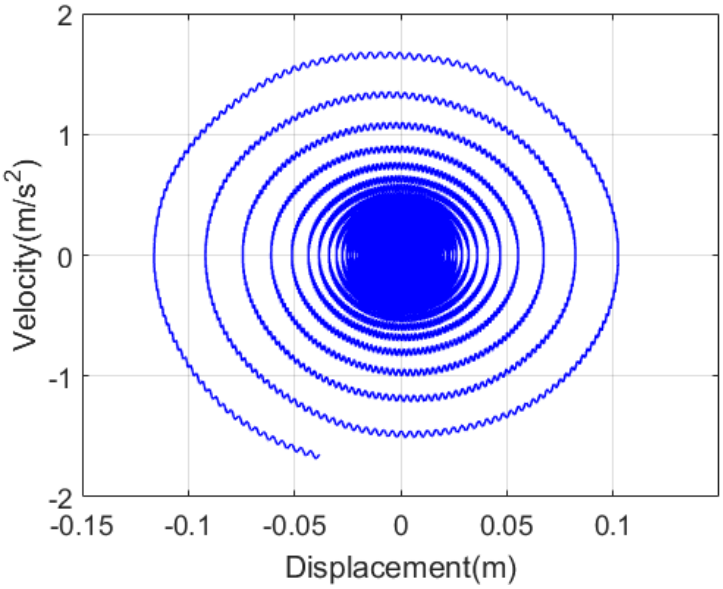

(b) With sub-loop

Figure 5.6: Phase plots of the dynamic behaviors

dynamic behavior of the truss structure as demonstrated in Figure 5.4(a). In Figure 5.5(b), phase transformations occur on various minor loops. The energy can be attenuated gradually as the behavior in Figure 5.5(b) moves toward the center of the constitutive model. This phenomenon

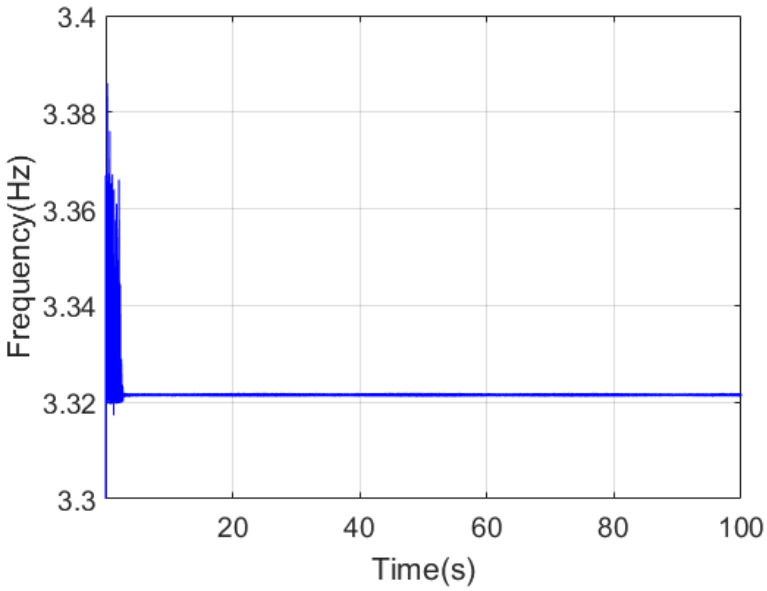

(a) Without sub-loop

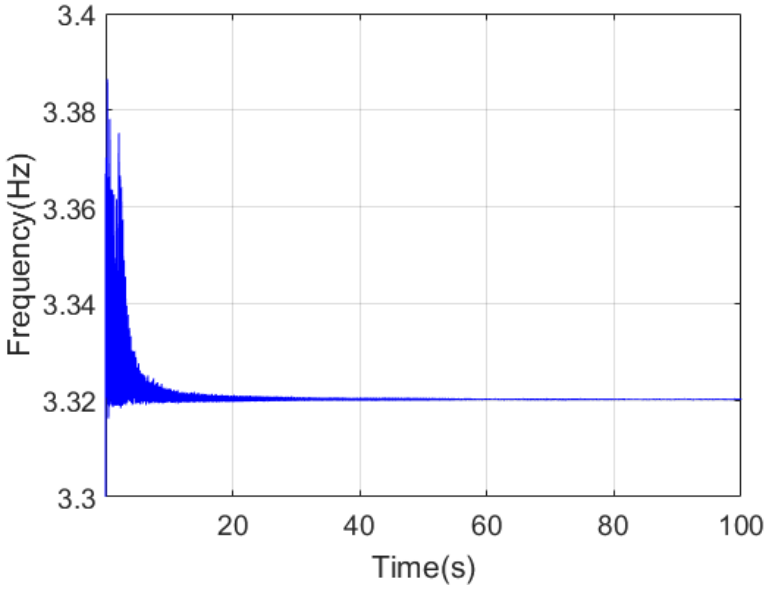

(b) With sub-loop

Figure 5.7: Time histories of the first natural frequency

contributes to the result in Figure 5.4(b), in which the energy has been absorbed thoroughly.

Figures 5.6(a) and 5.6(b) are phase plots of one of the tip end apparatus in the direction of support ceiling vibration after the motion of the support ceiling ceased. These two results

demonstrate the re-centering capability of the truss structural system having SMA wire members. The start points at the moment when the motion of support ceiling ceased are at the outside of the contours in these two figures. In Figure 5.6(a), behavior converges to a inner closed circle, which means the apparatus vibrates near the equilibrium position. At this time, behaviors of the SMA wire members are at the elastic range inside the major loop as the position of the small red circle in Figure 5.5(a). In Figure 5.6(b), behavior converges approximately to a point in the center of the figure, which means that all the energy is absorbed and the motion of the apparatus approximately ceased and the truss structure gets back to its original configuration. At this moment, behaviors of the SMA wire members approximately arrived at the centers of the constitutive models as one of the examples in Figure 5.5(b).

In Figure 5.5(a), owing to the phase transformations occur only on major loop, the efficiency of energy attenuation is larger at the beginning of the period after the motion of the support ceiling ceased and the speed of convergence becomes higher; therefore, the outside contour area of Figure 5.6(a) is smaller than Figure 5.6(b). The Curvature of the outside contour of Figure 5.6(a) is also larger than the curvature of the outside contour of Figure 5.6(b). This phenomenon can also be understood in Figures 5.7(a) and 5.7(b). These two figures are the time histories of the first natural frequencies of the truss structures without and with the sub-loop behavior of SMA wires. Owing to no SMA wires are compressed in the dynamic calculation, the variation range of the first natural frequency is narrow (3.31Hz – 3.39Hz). Figure 5.7(a) manifests that the convergent speed is high due to the constitutive model of SMA without the sub-loop. Figure 5.7(b) manifests that the convergent speed is low due to the constitutive model of SMA with the sub-loop behavior. The reason is that the same variation of strain value of SMA wire can obtain different area values in the constitutive model as in Figures 5.5(a) and 5.5(b).

5.4. SMA with Cosine Model

The truss structure in Figure 5.3(a) is dealt with using the SMA wires with cosine model. In the cosine model of the SMA material, the stages of phase transformation are nonlinear curves. This model suits the experimental observation well. The displacement behavior and the relationship of stress-strain of a SMA wire member are shown in Figure 5.8. Vibration amplitude and frequency of the support ceiling are 0.1m and 5Hz. Mass value of the apparatus is 5.56kg. Vibration of the support ceiling endures 1s. After vibration of the support ceiling ceased, exerted energy is attenuated by the pseudo-elastic SMA wire members as demonstrated in Figure 5.8(b).

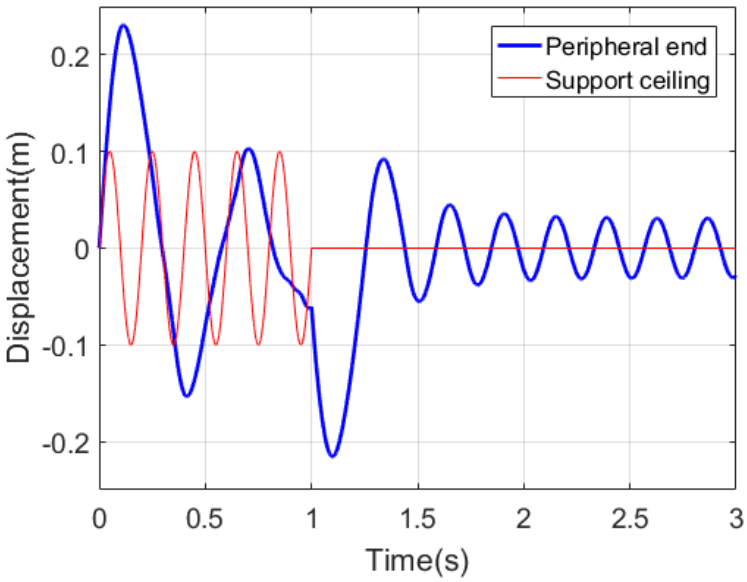

(a) Displacement behavior

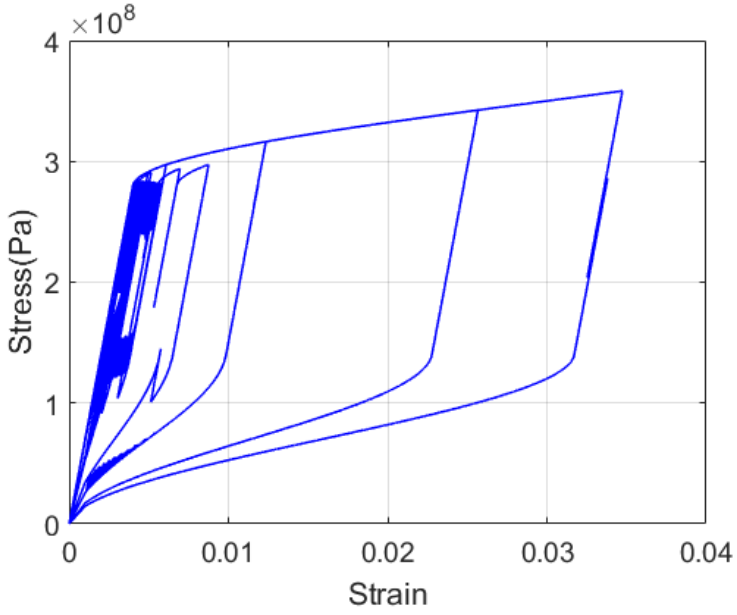

(b) Stress-strain relationship

Figure 5.8: Dynamic behavior of a truss with cosine model of SMA

5.5. Behaviors of Truss with Other Topologies

The displacement behaviors of the truss structural system with other topologies are shown in Figures 5.9 and 5.10. The amplitude and frequency of the support ceiling are 0.03m and 4Hz,

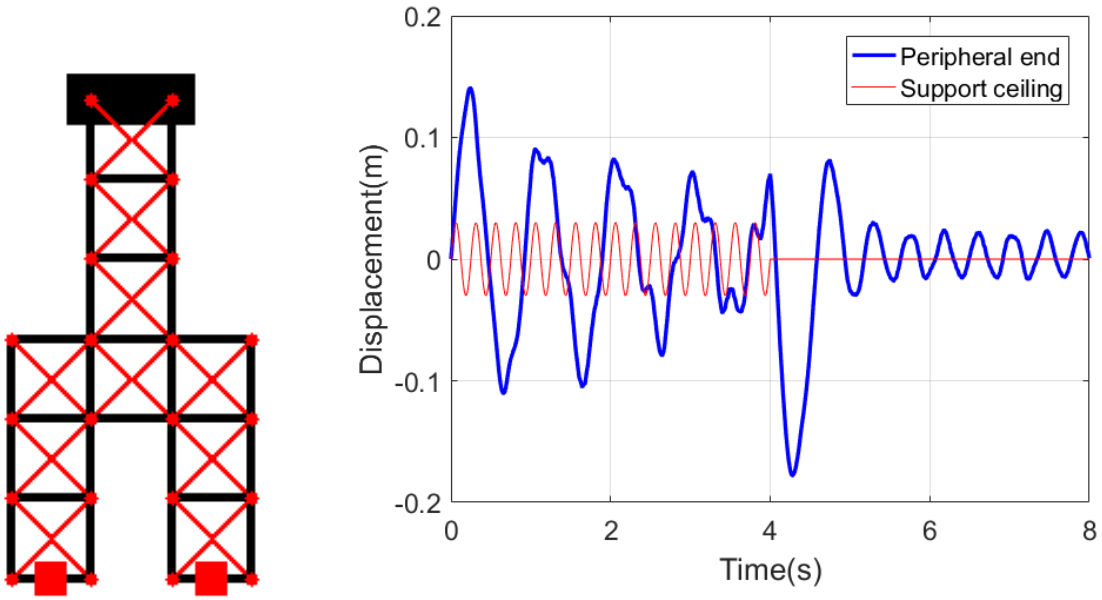

(a) Truss configuration (b) Displacement behavior

Figure 5.9: Time history of displacement of a truss

respectively. In Figures 5.9(b) and 5.10(b), vibration attenuation capability of the two truss structures with different topologies are shown.

5.6. Influence of Damping

In the contents discussed in the former chapters, all the attenuation effects are due to the pseudo-elasticity of SMA wires. In this section, for the purpose of realization, the damping matrix is taken into account in the dynamic equation. The damping matrix is assumed in the following form:

$$\boldsymbol{C}_{UU} = \hat{\alpha}\boldsymbol{M}_{UU} + \hat{\beta}\boldsymbol{K}_{UU} \tag{5.1}$$

The coefficients of $\hat{\alpha}$ and $\hat{\beta}$ are determined in the following equations:

$$\hat{\alpha} = \frac{2\hat{h}\omega_1\omega_2}{\omega_1 + \omega_2}, \quad \hat{\beta} = \frac{2\hat{h}}{\omega_1 + \omega_2} \tag{5.2}$$

where $\hat{h}$ is the attenuation constant. In case of steel frame, $\hat{h} = 1\% - 3\%$. Taking the SMA wire members into consideration, we choose $\hat{h} = 1\%$. ω_1 and ω_2 are two angular natural frequencies of the truss structures in a fixed time point. Therefore, the coefficients of $\hat{\alpha}$ and $\hat{\beta}$ should be updated in accordance with the variation of angular natural frequencies. In the numerical inte-

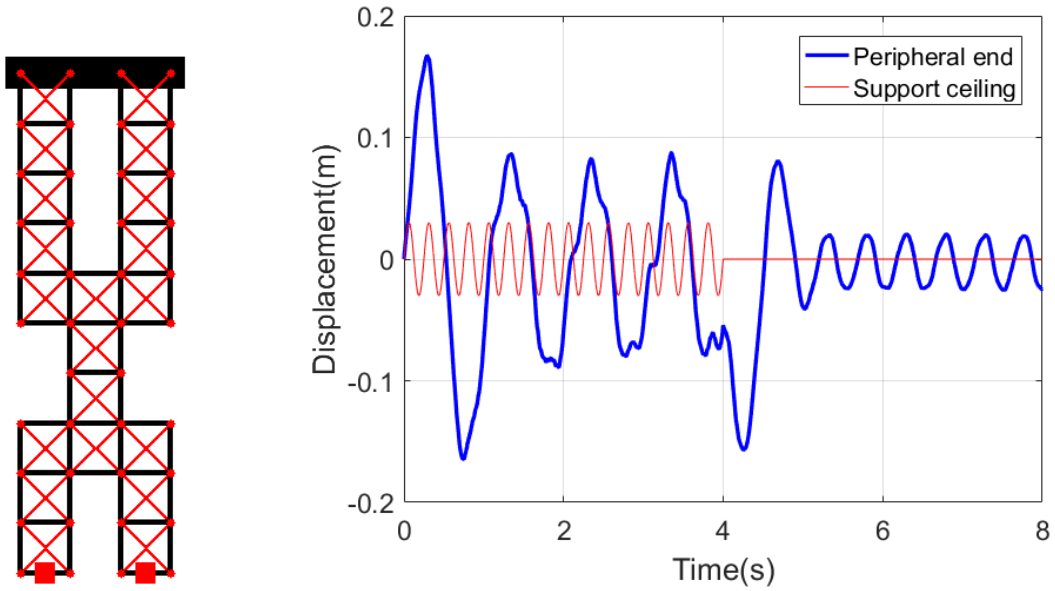

(a) Truss configuration (b) Displacement behavior

Figure 5.10: Time history of displacement of a truss

gration of the dynamic equation having damping matrix, the damping force should be linearized due to the nonlinear characteristics of stiffness matrix as well as the coefficients of $\hat{\alpha}$ and $\hat{\beta}$.

The truss structure in Figure 4.10(a) is dealt with. Vibration amplitude and frequency of the support ceiling are 0.1m and 5Hz. Mass value of the apparatus at the peripheral end is 5kg. The displacement behaviors without and with damping are shown in Figure 5.11. The acceleration behaviors without and with damping are shown in Figure 5.12.

As shown in Figure 5.11, the vibration amplitude of the peripheral end apparatus in Figure 5.11(a) is larger than Figure 5.11(b) in the time period of vibration of the support ceiling. This is due to the energy consuming by structural damping. After vibration motion of the support ceiling, the residual vibration is not attenuated in Figure 5.11(a) due to the pure austenite phase of the SMA wire members; however, the residual vibration in Figure 5.11(b) is attenuated gradually due to the structural damping. The behaviors of acceleration shown in Figure 5.12 demonstrate the same tendency.

5.7. Summary

In this chapter, several other examples on dynamic equations have been discussed. Dynamic behaviors of three-dimension truss have been shown. Influence of the sub-loop behavior of the

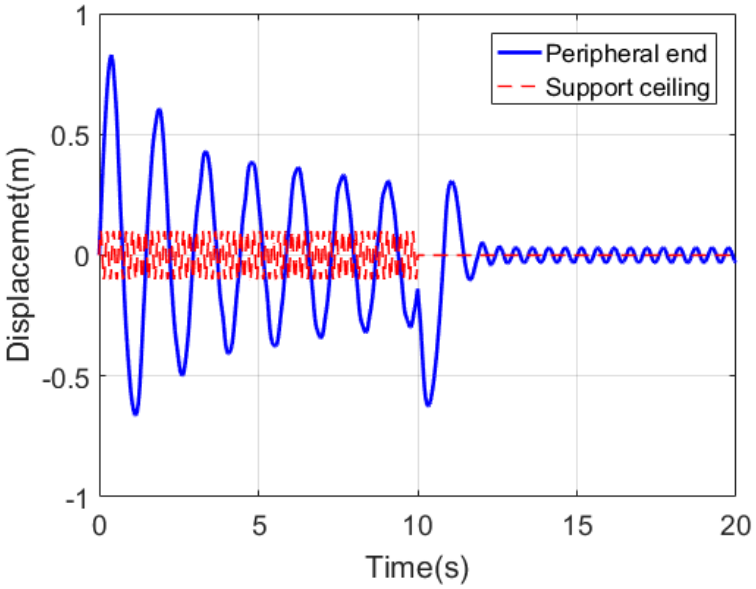

(a) Without damping

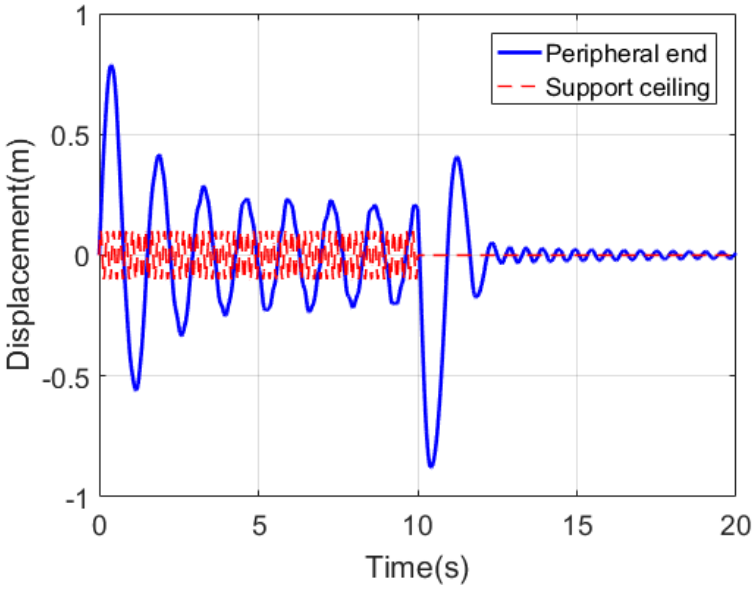

(b) With damping

Figure 5.11: Displacement behaviors with and without damping

SMA wire on the dynamic behaviors of has been confirmed. Dynamic behavior of truss having SMA wire members with cosine model has been demonstrated. Dynamic behaviors of the truss with the topologies other than hanging-type have been discussed. Comparison of the dynamic

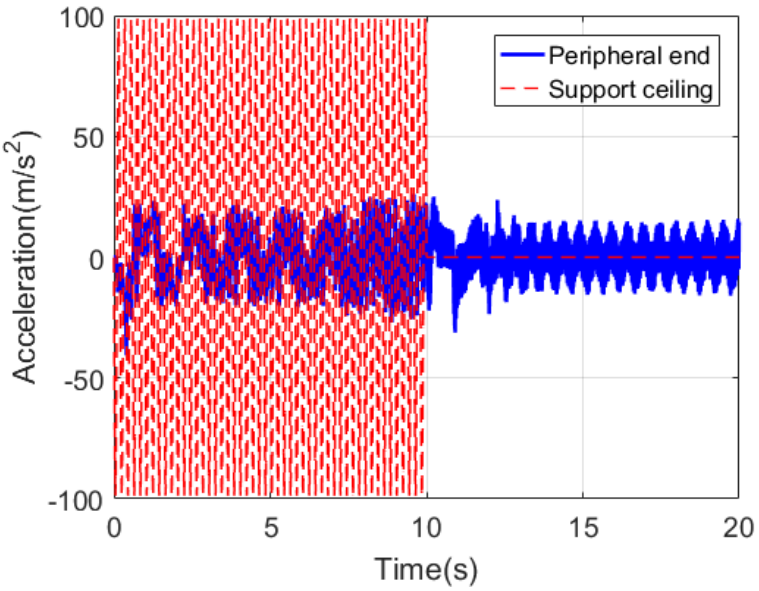

(a) Without damping

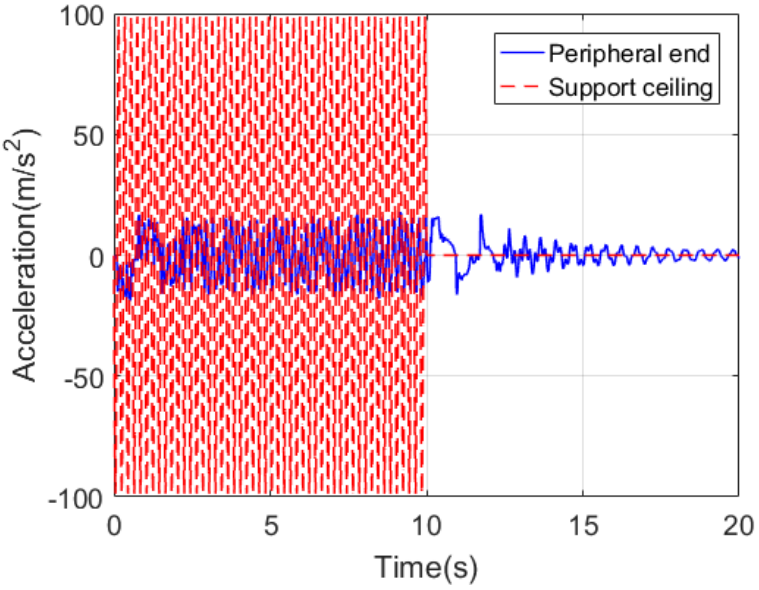

(b) With damping

Figure 5.12: Acceleration behaviors with and without damping

behaviors between the cases with and without damping has been made.

Chapter 6

Conclusion

This dissertation dealt with a kind of truss structural system in hanging configuration having SMA wire members. Dynamic characteristics of this kind of truss structural system have been discussed from vibration isolation and attenuation points of view. The influences of the number and the configuration of the SMA wire members have been discussed. Optimization approaches on the configurations and the sectional area have been constructed.

In Chapter 2, mathematical model of this kind of dynamic problem has been derived. For the purpose of dynamic calculation, a piecewise SMA model without considering the sub-loop behavior has been introduced. A pseudo-elastic constitutive model considering the sub-loop behavior has been developed. The dynamic equation of motion of the truss structural system having SMA wire members has been derived. In order to tackle the nonlinear characteristic of the dynamic problem, a numerical calculation process has been constructed. Adequacy for this dynamic model is confirmed from the viewpoint of energy confirmation.

In Chapter 3, dynamic behaviors of the truss structural system have been discussed. Vibration isolation effect of the hanging truss structure has been confirmed. Vibration attenuation of the hanging truss structure having SMA wire members has been shown. Influences of the behaviors of the vibration isolation by the mass value of the peripheral end apparatus and the stages of the truss unit have been demonstrated. Larger mass value of the apparatus, more inertia effect the truss has. In addition, more truss units, the vibration transmission takes more time from support ceiling to the peripheral end. In case of small strain state or slack state of the SMA wire members, the SMA wires can be replaceable to the ordinary wires. The relative large stiffness of the ordinary wires contributes to relative stability of the dynamic behaviors of the truss structure from the deformation point of view. Hanging truss structure with the combination of truss units having SMA wire members as well as truss units having no bracing SMA wire members demonstrates more sufficient vibration isolation effect.

In Chapter 4, optimization problems have been dealt with from three aspects: combination of truss units having SMA wire members and truss units having no SMA wire members,

combination of SMA wire members and ordinary wire members, sectional area of the SMA wire members. A multi-objective algorithm has been constructed using a GA-based method. The operators for the purpose of coping with the constraint condition have been proposed. In the optimal configurations of the first aspect, we confirmed that there are few SMA bracing wire members near the support ceiling or peripheral end. The hanging truss with this kind of placements of SMA wire members show more sufficient vibration isolation effect due to the pendulum effect and more sufficient vibration attenuation effect due to the bracing SMA wire members. In addition, on the basis of calculations of the third aspect, we discovered that the sectional area values of the SMA wire members near the support ceiling as well as the peripheral end are tremendously smaller than the other truss units. This tendency is coincide with the optimal configurations in the first aspect. The sectional area in the middle part of the truss are relatively large. The hanging truss with this kind of distribution of the sectional area values demonstrates more sufficient vibration isolation and attenuation effects. The results of the second aspect show that both of the number and the placement of the SMA wire and ordinary wire members are significant on the dynamic performances of the hanging truss structural system.

In Chapter 5, several other dynamic cases of the hanging truss structural system have been discussed. Dynamic behaviors of truss structures in three dimension have been discussed. In order to deal with the residual vibration of the behavior of the hanging truss having SMA wire members, a pseudo-elastic constitutive model was utilized in the dynamic calculation of the truss structure. The result manifests that the developed model is suitable for dealing with the residual vibration. Dynamic behavior of a truss having SMA wires with cosine model was shown. Besides the topology of hanging-type, the behaviors of the hanging truss with other topologies have been demonstrated. The effect of damping force has also been taken into account.

Bibliography

[1] Patil, S. S., and Awasare, P. J. Vibration Isolation of Lumped Masses Supported on Beam by Imposing Nodes Using Multiple Vibration Absorbers. *Mechanical Engineering Research*, 6(1), 88, 2016.

[2] Akhverdiev, K. S., and Mukutadze, A. M. Damper with Porous Anisotropic Ring. *Mechanical Engineering Research*, 6(2), 1, 2016.

[3] Tatemichi, I., Kawaguchi, M., and Abe, M. A Study on Pendulum Seismic Isolators for High-Rise Buildings. *The 2004 Council on Tall Buildings and Urban Habitat (CTBUH) Conference*, 2004.

[4] Sanap, S. B., Jadhal, P. D., and Dumne, S. M. Earthquake Response Mitigation of RC Building Using Friction Pendulum System. *American Journal of Engineering Research*, 3(11), 30-37, 2014.

[5] Narita, R., Kojima, T., Kuramochi, H., Toriya, T., Kitayama, N., Kuramochi, M., and Ohtsuka, T. Evaluation of Performance of Multi-Suspended Pendulum Isolation (MPI) Systme with Spatial Truss Structure. *12th World Conference on Earthquake Engineering*, 2000.

[6] Fallah, N., and Zamiri, G. Multi-Objective Optimal Design of Sliding Base Isolation Using Genetic Algorithm. *Scientia Iranica*, 20(1), 87-96, 2013.

[7] Murnal, P., and Sinha, R. A Seismic Design of Structure-Equipment Systems Using Variable Frequency Pendulum Isolator. *Nuclear Engineering and Design*, 231(2), 129-139, 2004.

[8] Jamalzadeh, A., and Barghian, M. Dynamic Response of a Pendulum Isolator System under Vertical and Horizontal Earthquake Excitation. *Periodica Polytechnica. Civil Engineering*, 59(3), 433, 2015.

[9] Mortazavi, S. M. R., Ghassemieh, M., and Motahari, S. A. Seismic Control of Steel Structures with Shape Memory Alloys. *International Journal of Automation and Control Engineering*, 2013.

[10] McCormick, J., DesRoches, R., Fugazza, D., and Auricchio, F. Seismic Vibration Control Using Superelastic Shape Memory Alloys. *Journal of engineering materials and technology*, 128.3, 294-301, 2006.

[11] Omar, M. Seismic Response of Braced Steel Frames with Shape Memory Alloy and Mega Bracing Systems. *International Journal of Civil, Architectural Science and Engineering*, 8(2), 131-138, 2014.

[12] Han, Y. L., Li, Q. S., Li, A. Q., Leung, A. Y. T., and Lin, P. H. Structural Vibration Control by Shape Memory Alloy Damper. *Earthquake engineering and structural dynamics*, 32.3, 483-494, 2003.

[13] Khan, M. M., and Lagoudas, D. C. Modeling of Shape Memory Alloy Pseudoelastic Spring Elements Using Preisach Model for Passive Vibration Isolation. *SPIE's 9th Annual International Symposium on Smart Structures and Materials*, International Society for Optics and Photonics, 2002.

[14] Hanahara, K., and Tada, Y. Vibration Suppression by means of SMA-Wire Truss. *The National Congress of Theoretical and Applied Mechanics*, 62.0, 158, 2013.

[15] Song, G., Ma, N., and Li, H. N. Applications of Shape Memory Alloys in Civil Structures. *Engineering Structures*, 28(9), 1266-1274, 2006.

[16] De Lima, A. M. G., Guaraldo-Neto, B., Sales, T. P., and Rade, D. A. A Time-Domain Modeling of Systems Containing Viscoelastic Materials and Shape Memory Alloys as Applied to the Problem of Vibration. *Engineering Structures*, 68, 85-95, 2014.

[17] Yang, C. S. W., DesRoches, R., and Leon, R. T. Design and Analysis of Braced Frames with Shape Memory Alloy and Energy-Absorbing Hybrid Devices. *Engineering Structures*, 32(2), 498-507, 2010.

[18] Parulekar, Y. M., and Reddy, G. R. Nonlinear Model of Pseudoelastic Shape Memory Alloy Damper Considering Residual Martensite Strain Effect. *Advances in Acoustics and Vibration*, vol. 2012, Article ID 261896, 11 pages, 2012.

[19] Qian, H., Li, H. N., Song, G. B., and Guo, W. Recentering Shape Memory Alloy Passive Damper for Structural Vibration Control. *Mathematical Problems in Engineering*, vol. 2013, Article ID 963530, 13 pages, 2013.

[20] Fosdick, R., and Ketema, Y. Shape Memory Alloys for Passive Vibration Damping. *Journal of Intelligent Material Systems and Structures*, 9(10), 854-870, 1998.

[21] Tamai, H., and Kitagawa, Y. Pseudoelastic Behavior of Shape Memory Alloy Wire and Its Application to Seismic Resistance Member for Building. *Computational Materials Science*, 25(1), 218-227, 2002.

[22] McCormick, J., DesRoches, R., Fugazza, D., and Auricchio, F. Seismic Vibration Control Using Superelastic Shape Memory Alloys. *Journal of Engineering Materials and Technology*, 128(3), 294-301, 2010.

[23] Cismasiu, C., and dos Santos, F. P. A. Numerical Simulation of Superelastic Shape Memory Alloys Subjected to Dynamic Loads. *Smart Materials and Structures*, 17(2), 025036, 2008.

[24] Jose, S., Chakraborty, G., and Bhattacharyya, R. Coupled Thermo-Mechanical Analysis of a Vibration Isolator Made of Shape Memory Alloy. *International Journal of Solids and Structures*, 115, 87-103, 2017.

[25] Ghodke, S., and Jangid, R. S. Influence of High Austenite Stiffness of Shape Memory Alloy on the Response of Base-Isolated Benchmark Building. *Structural Control and Health Monitoring*, 24(2), 2017.

[26] Lu, P. Z., Zhan, X. L., Tang, F., and Shao, H. Fundamentals of Shape Memory Alloy-Rubber Bearing Seismic Design and Assessment. *Journal of Materials in Civil Engineering*, 29(8), 04017081, 2017.

[27] Mekki, O. B., and Auricchio, F. Performance Evaluation of Shape-Memory-Alloy Superelastic Behavior to Control a Stay Cable in Cable-Stayed Bridges. *International Journal of Non-Linear Mechanics*, 46(2), 470-477, 2011.

[28] Müller, I., and Xu, H. On the Pseudo-Elastic Hysteresis. *Acta metallurgica et materialia*, 39(3), 263-271, 1991.

[29] Thomson, P., Balas, G. J., and Leo, P. H. Analysis of Trigger Line Models for Shape Memory Hysteresis based on Dynamic Testing. *Journal of intelligent material systems and structures*, 8(3), 193-201, 1997.

[30] Huo, Y., and Müller, I. Nonequilibrium Thermodynamics of Pseudoelasticity. *Continuum Mechanics and Thermodynamics*, 5(3), 163-204, 1993.

[31] Tanaka, K., Nishimura, F., and Tobushi, H. Phenomenological Analysis on Subloops in Shape Memory Alloys Due to Incomplete Transformations. *Journal of intelligent material systems and structures*, 5(4), 487-493, 1994.

[32] Trochu, F., and Qian, Y. Y. Nonlinear Finite Element Simulation of Superelastic Shape Memory Alloy Parts. *Computers and Structures*, 62(5), 799-810, 1997.

[33] Ikeda, T., Nae, F. A., Naito, H., and Matsuzaki, Y. Constitutive Model of Shape Memory Alloys for Unidirectional Loading Considering Inner Hysteresis Loops. *Smart materials and Structures*, 13(4), 916, 2004.

[34] Savi, M. A., and Paiva, A. Describing Internal Subloops Due to Incomplete Phase Transformations in Shape Memory Alloys. *Archive of Applied Mechanics*, 74, 637-647, 2005.

[35] Zhao, J. P., and Wang, C. J. A New Method for Maximum Dynamic Response Topology Optimization in the Time Domain. *11th World Congress on Structural and Multidisciplinary Optimization*, 2015.

[36] Choi, S. W., Park, S. W., and Park, H. S. Multi-Objective Design Model for Retrofit of Reinforced Concrete Frames with Infilled Walls Using FRP Bracings. *Construction and Building Materials*, 140, 454-467, 2017.

[37] Kirsch, U., Bogomolni, M., and Sheinman, I. Efficient Structural Optimization Using Reanalysis and Sensitive Reanalysis. *7th World Congress on Structural and Multidisciplinary Optimization*, 1111-1120, 2007.

[38] Senba, A., Oka, K., Takahama, M., and Furuya, H. Vibration Reduction by Natural Frequency Optimization for Manipulation of a Variable Geometry Truss. *8th World Congress on Structural and Multidisciplinary Optimization*, 2009.

[39] Jang, H. H., Lee, H. A., and Park, G. J. Dynamic Response Topology Optimization Using Equivalent Static Loads. *8th World Congress on Structural and Multidisciplinary Optimization*, 2009.

[40] Hanahara, K., Zhang, X., and Tada, Y. Dynamic Simulation of Adaptive Truss Consisting of Various Types of Truss Members. *Mechanical Engineering Research*, 6(1), 75-87, 2016.

[41] Abdollahzadeh, G., and Abbasi, M. Response Modification Factor of Suspended Zipper Braced Frames. *Steel and Composite Structures*, 18(1), 165-185, 2015.

[42] Deb, K., Pratap, A., Agarwal, S., and Meyarivan, T. A Fast and Elitist Multiobjective Genetic Agorithm: NSGA-II. *IEEE transactions on evolutionary computation*, 6(2), 182-197, 2002.

[43] Hu, J. W. Numerical Simulation for the Behavior of Superelastic Shape Memory Alloys. *Journal of Mechanics Science and Technology*, 27(2), 381-386, 2013.

[44] Tamai, H., and Kitagawa, Y. Pseudoelastic Behavior of Shape Memory Alloy Wire and Its Application to Seismic Resistance Member for Building. *Computational Materials Science*, 25, 218-227, 2002.

[45] Lagoudas, D. C. eds. *Shape Memory Alloys (Modeling and Engineering Applications)*, Springer.

[46] Wijst, van der, M. W. M. Shape Control of Structures and Materials with Shape Memory Alloys. *Eindhoven: Technische Universiteit Eindhoven*, 1998.

[47] Li, L., Li, Q. B., and Zhang, F. One-Dimensional Constitutive Model of Shape Memory Alloy with an Empirical Kinetics Equation. *Journal of Metallurgy*, vol. 2011, Article ID 563413, 14 pages, 2011.

[48] Jia, H. Y., Lalande, F., and Rogers, C. A. Modeling of Strain Energy Absorption in Superelastic Shape Memory Alloys. *Proc. SPIE 3039, Smart Structures and Materials 1997: Mathematics and Control in Smart Structures*, 1997.

[49] Liang, C., and Rogers, C. A. One-Dimensional Thermomechanical Constitutive Relations for Shape Memory Materials. *Journal of Intelligent Material Systems and Structures*, 1(2), 207-234, 1990.

[50] Lubliner, J., and Auricchio, F. Generalized Plasticity and Shape Memory Alloys. *International Journal of Solids and Structures*, 33(7), 991-1003, 1996.

[51] Auricchio, F., and Sacco, E. A One-Dimensional Model for Superelastic Shape-Memory Alloys with Different Elastic Properties between Austenite and Martensite. *International Journal of Non-linear Mechanics*, 32(6), 1101-1114, 1997.

[52] Lagoudas, D. C., Mayes, J. J., and Khan, M. M. Simplified Shape Memory Alloy (SMA) Material Model for Vibration Isolation. *Smart Structures and Materials 2001: Modeling, Signal Processing, and Control in Smart Structures*, 2001.

[53] Tanaka, K., and Nagaki, S. A Thermomechanical Description of Materials with Internal Variables in the Process of Phase Transformation. *Ingenieur-Archiv*, 51, 287-299, 1982.

[54] Zhang, X., Hanahara, K., and Tada, Y. Dynamic Characteristics of Hanging Truss Having Shape Memory Alloy Wires. *Mechanical Engineering Research*, 7(2), 6-17, 2017.

[55] Bathe, K. J. *Finite Element Procedures*, Prentice Hall, Pearson Education. Inc.

[56] Liu, C. C., Jing, X. J., Daley, S., and Li, F. M. Recent Advances in Micro-Vibration Isolation. *Mechanical Systems and Signal Processing*, Volumes 56-57, 55-80, 2015.

[57] Richardson, J. N., Nordenson, G., Laberenne, R., Coelho, R. F., and Adriaenssens, S. Flexible Optimum Design of a Bracing System for Facade Design Using Multiobjective Genetic Algorithms. *Automation in Construction*, 32, 80-87, 2013.

[58] Witold, B., and Tadeusz, B. Multi-Objective Optimization of Composite Structures by means of the Evolutionary Computations. *8th World Congress on Structural and Multidisciplinary Optimization*, 2009.

[59] Murata, T., Ishibuchi, H., and Tanaka, H. Multi-Objective Genetic Algorithm and Its Applications to Flowshop Scheduling. *Computers and Industrial Engineering*, 30(4), 957-968, 1996.

[60] Liang, C., and Rogers, C. A. Design of Shape Memory Alloy Springs with Applications in Vibration Control. *Journal of Vibration and Acoustics*, 115, 129-135, 1993.

Doctor Thesis, Kobe University
”Dynamic Model Construction and Optimization of Hanging Truss Structural System Having Shape Memory Alloy Wires”, 94 pages
Submitted on January, 26, 2018
The date of publication is printed in cover of repository version published in Kobe University Repository Kernel.